博士論文

In-process Measurement in Micro/nano-Stereolithography Using Optical Response from Near-Substrate Resin with Refractive Index Variation

(光近接場領域における樹脂屈折率変化応答に基づく

ナノ光造形のインプロセス計測)

指導教員　高橋　哲　教授

東京大学大学院工学系研究科 先端学際工学専攻

学籍番号 37-167169

孔　徳卿

ACKNOWLEDGEMENTS

I would like to express my special thanks of gratitude to my Ph.D. advisor Prof. Takahashi who provides me with such intriguing research to work on, and guides me through it. I thank him for his understanding, support, patience, inspiration, and permit for trying a new research topic.

I would also like to thank Dr. Michihata for directly giving me academic advising and providing his valuable guidance during the course of my Ph.D. research. I thank him for his tolerance on my arguments when we made discussions, especially on the research purpose and progress.

I thank my committee members, Prof. Takamasu, Prof. Kondo, Prof. Shimura and Prof. Kajihara for providing their insightful comments and suggestions for my Ph.D. thesis.

I was fortunate to have had the opportunity to work with smart and interesting members in Takahashi laboratory. Mr. Masui gave me a lot of guidance and suggestions on my experiments, as well as Mr. Kume helped me a lot on the spelling of Japanese. Mr. Zhao was my best friend in recent years, we entered the University of Tokyo in the same year and both of us had terrible procrastination. Hope we can overcome this problem. I would also like to thank other students in our laboratory, Mr. Ye, Mr, Tachibana, Mr. Suzuki, Mr. Matsumoto, Mr. Chu, Mr, Kobayashi, Mr. Hayashi, Mr. Furuya, and Mr. Yukei, who shared the happiness with me during.

I would especially like to thank my parents for supporting me to finish my Ph.D. program, although they strongly hope me go back to China and get married to someone as soon as possible.

I have to thank my girlfriend who did not break up with me even in conditions that I did not take shower for several days when I struggled with deadlines.

At last, I need to thank my incurable procrastination for never leaving me alone no matter how serious the situation was.

TABLE OF CONTENTS

LIST OF FIGURES

LIST OF TABLES

LIST OF ABBREVIATIONS

SL	Sterelithography
MSL	Micro-sterelithography
NSL	Nano-stereolithography
EWNSL	Evanescent-wave-based nano-stereolithography
FTIR	Fourier Transform infrared spectroscopy
DSC	Differential Scanning Calorimeter
UV	Ultraviolet
CMOS	Complementary metal–oxide–semiconductor
SPR	Surface plasmon resonance
PLZT	$(Pbl_{1-x}\ La_x)\ (Zr_y\ Til_{-y})\ 1_{1-x}/4\ O_3$
LCD	Liquid Crystal Display
DMD	Digital Micromirror Device
SEM	Scanning Electron Microscope
PDE	Partial Differential Equation
ODE	Ordinary Differential Equation

CHAPTER 1. MOTIVATION OF IN-PROCESS MEASUREMENT IN MICRO/NANO-STEREOLITHOGRAPHY

This chapter makes an introduction and a classification of existing micro/nano-stereolithography (MSL/NSL) techniques. This chapter also presents a novel MSL technique that can flexibly adjust the thickness of each single layer by applying the in-process measurement to determine proper exposure energy of each layer. In addition, this chapter introduces a strong demand for the in-process measurement of the thickness of each layer in an evanescent-wave-based nano-stereolithography (EWNSL). The specific research objectives of this thesis that focus on the in-process measurement in MSL and EWNSL is clarified in this chapter. At the end of this chapter, an organization of the whole dissertation is illustrated.

1.1 Classifications of micro/nano-stereolithography techniques

Stereolithography (SL) is one of the most important additive manufacturing technologies for fabricating structures with three-dimensional (3D) complex geometries [1-3]. The SL techniques utilize a feature of curing (photo-polymerization) of the photo curable resin in an exposure of light in a particular range of wavelength, which provides the energy for inducing a chemical reaction (polymerization reaction) connecting a large number of small monomers, and developing a highly cross-linked polymer (the photo-polymerization process in the SL will be detailed discussed in the chapter 3) [4-6]. Micro/Nano-stereolithography (MSL/NSL) techniques are on the basis of the conventional SL but reach micron or sub-micron fabrication resolution by applying precious instruments

for movement control and using photosensitive resin that can confine polymerization in a very small area. In order to fine control the exposure area of the irradiation, different strategies of the exposure are proposed, including using a focused laser spot with a scanning process, projection-based exposure, an interference pattern of multi-beam that provides a sub-wavelength periodically changed pattern, the two-photon polymerization or evanescent-field-based exposure [7-21]. With a great deal of research progresses in the related fields, fabrication accuracy of the MSL has a huge upgrade and been improved from microscale to nanoscale since MSL was proposed in the early 1980s, as a result, some MSL techniques that reach a submicron fabrication resolution can also be named as Nano-stereolithography (NSL) [20,21 24-27]. To date, there are wide investigations on the MSL/NSL techniques in different apparatuses. **Figure 1-1** identifies different stereolithographic ways and makes a classification of the existing MSL/NSL techniques.

As shown in **Figure 1-1**, first of all, due to the photosensitive resin is cured by optical energy, according to the difference of irradiation ways, the MSL/NSL techniques can be simply classified into two major categories: the point exposure and the surface exposure. Both of two categories have been widely investigated for many years and supported by corresponding mature technologies. They will be discussed in the following contents from an aspect of technical principles. Due to difficulties of generation of the stereo exposure in arbitrary shapes by one-shot exposure, for most of the MSL/NSL techniques, the resin is cured using a strategy of layer-by-layer, and three-dimensional structures can be generated by stacking the layers that are in the same patterns with cross-sections of the three-dimensional structures. The pattern of each layer is controlled by the lateral distribution of exposure after scanning or projection.

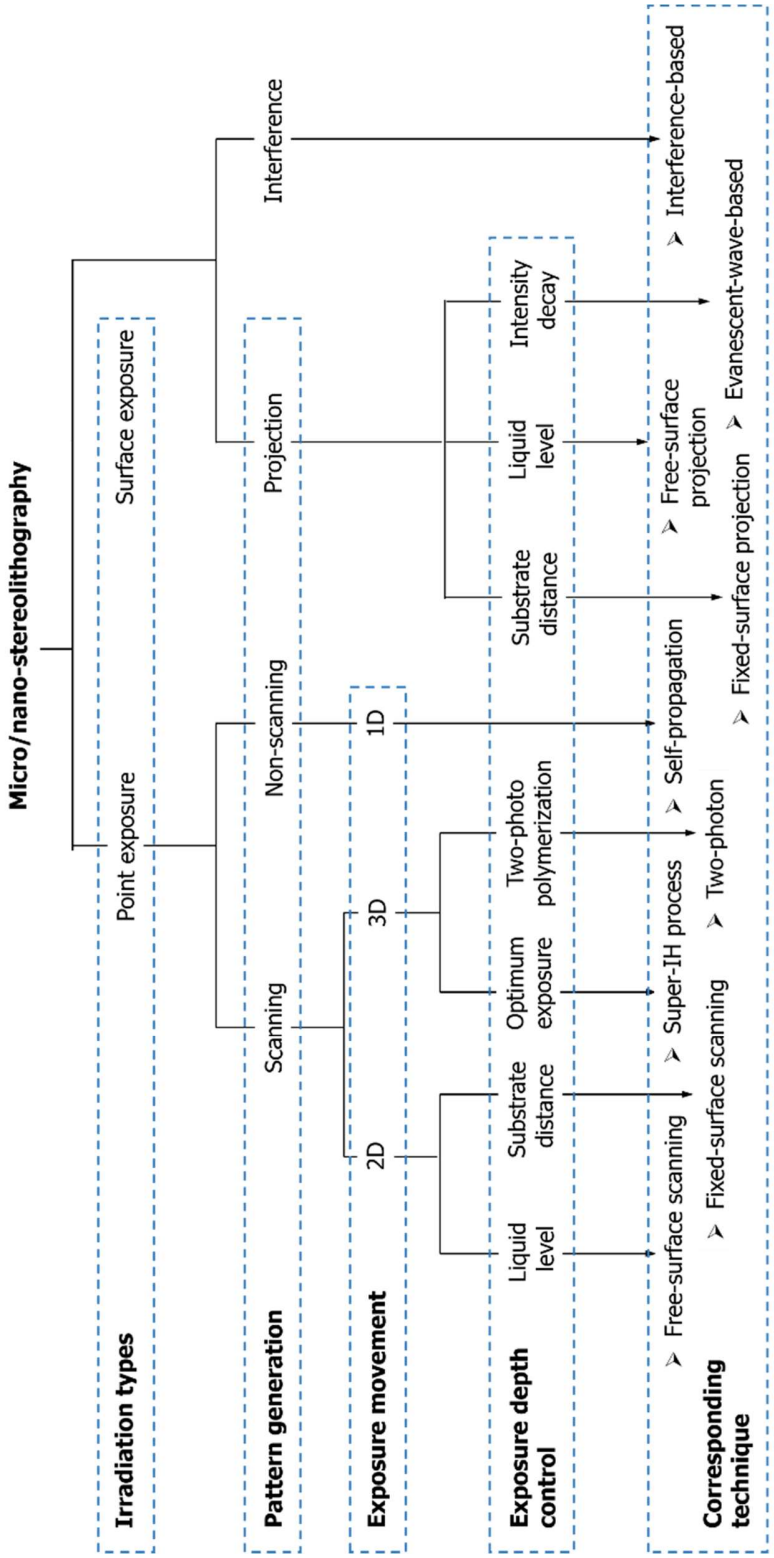

Figure 1-1 Classification of existing MSL/NSL techniques

For the point exposure, a two-dimensional pattern is generated by making a scanning process in a horizontal plane. For the surface exposure, the mask or projection is used to control the exposure patterns. In some special cases, the resin is cured by one-shot exposure with three-dimensional distribution rather than in the strategy of layer-by-layer. One of a typical three-dimensional exposure is based on the interference. Standing waves generated by the interference makes the exposure energy periodically change in a sub-wavelength scale [40-43].

In the transverse direction of the irradiation, the pattern is well controlled by scanning the exposure point or the projection; however, in the propagation direction, the optical energy that can solidify resin has a long span due to the propagation of the exposure beam. In order to limit the exposure depth or thickness of the cured resin, conventional way is to restrict the exposure area. Especially, the exposure field can be controlled by the distance from the cured resin to a movable substrate or the height of the liquid-state uncured resin. These two methods are called fixed-surface MSL and free-surface MSL, respectively. The basic mechanism of them that combines with the scanning-point method are shown in Figure 2 (a) and (b).

Fixed-surface-scanning MSL was firstly proposed by Ikuta and Hirowatari in 1993 [22]. In this method, curing of the resin occurs on the fixed space between the substrate and the already cured resin, as shown in **Figure 1-2 (a)**. A movable substrate is used to persist the uncured resins to avoid the problem of unwanted curing on the propagation path of the exposure beam. The main disadvantage of this method is that the cured resin always sticks to the substrate; therefore, an operation of separation is needs between the cured

resin and the substrate when moving the substrate, which might lead to partial or total destruction of the cured resin during the manufacturing process.

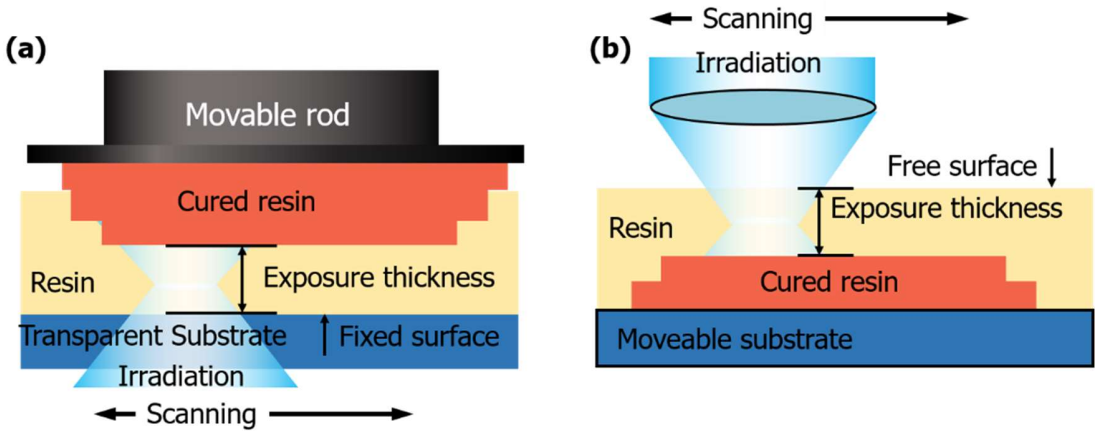

Figure 1-2 Diagrammatic explanations of scanning MSL that restrict the exposure area layer-by-layer using (a) fixed surface (b) free surface methods.

Free-surface-scanning method bypasses the problem of separation. It is firstly proposed by Takagi and Nakajima in 1993 [23]. They also called this technique as "vector-by-vector" MSL, as the resin is solidified in a point-by-point and line-by-line style in each layer. In this method, the exposure range along the propagation direction of the exposure beam is limited by the height of the uncured resin between the air and the already cured resin, as shown in **Figure 1-2 (b)**. Due to the top surface of the cured layers is exposed to the air, which makes it always feasible to fabricate a new layer of liquid resin over the previously-cured layer without the separation between the resin and the substrate. The problem is when a very thin layer is required, the curing of the new layer becomes really challenging and even impossible due to the liquid viscosity and surface tension.

For both of the fixed-surface and the free-surface type MSL, the transverse (spatial) resolution is mainly determined by the spot size of the focused beam limited by the optical

diffraction limit. For the exposure using ultra-violet light, a submicron spatial resolution can be achieved. The resolution in the vertical direction (minimum thickness of each layer) is mainly determined by the movement resolution of the rod or the substrate; however, the surface tension influences the flatness of the cured layer especially when a thin layer is cured. As a result, for fixed surface scanning, the recorded minimum thickness is 4 μm; while for free surface scanning, a recorded minimum thickness of each layer is larger than 10 μm, since the resin on the top surface directly connects with the air making the problem of surface tension worse.

For some MSL/NSL techniques, the thickness of each can be well confined without limiting the exposure space. In this case, three-dimensional structures can be fabricated by directly making a three-dimensional scanning of the exposure point rather than making the two-dimensional scanning of each layer and then move the substrate/rod to make space for the next layer. Supper-HI process and two-photon-polymerization method are two famous methods to achieve this goal.

Supper-IH process MSL does not use the strategy of the layer-by-layer process that restricts the exposure area to control the thickness of each layer. It utilizes the threshold feature of photo-polymerization [38]. The curing process is a continue process and the degree of curing of the resin sustainable growths under the exposure condition. The reaction rate of polymerization is largely influenced by the exposure intensity; therefore the resin exposed in a higher intensity will earlier reach the threshold that determines the resin remind or not after the etching and drying process. In the super-HI process, the exposure beam is highly focused and the exposure intensity and duration is optimized in a

proper condition to make sure that only the resin in the center of the exposure reaches the threshold, as shown in **Figure 1-3 (a)**. By this way, both of the lateral and the vertical resolutions are determined by the size of the focused spot. Results in reference [38] proved that the resolution of this method was 180 nm in the horizontal direction and around 500 nm in the veridical direction.

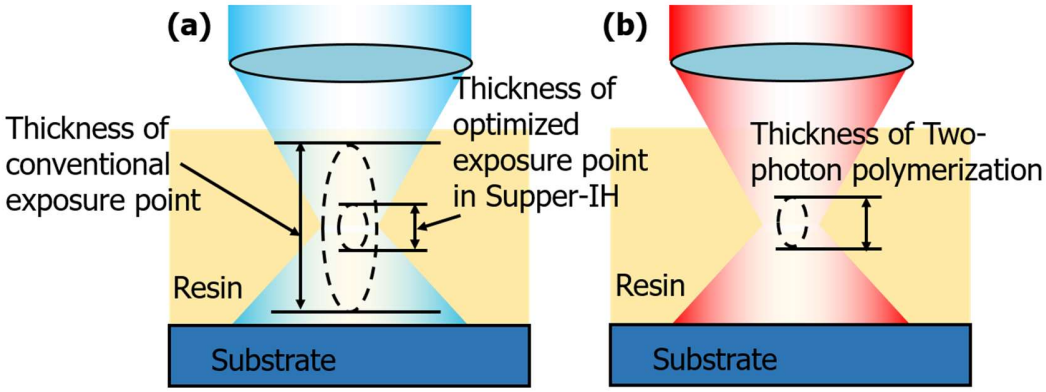

Figure 1-3 Diagrammatic explanations of scanning MSL with shot exposure thickness using (a) optimum exposure in Super-IH process and (b) two-photon polymerization.

Two-photon MSL with the high central curing field can also overcome the problem of long curing thickness without using the resist, and further improve the fabrication resolution to a submicron scale, as shown in **Figure 1-3 (b)** [24-25]. In the two-photon polymerization process, the photoinitiator needs to absorb two photons for releasing a free radical that can initiate polymerization. Therefore, the resolution of the photo-polymerization process improves considerably because only the resin in the center of the exposure has a high-enough energy ensuring that two photons strike to the same molecule of photoinitiator. Maruo firstly developed MSL based on two–photo polymerization [26] in 1998, and Kawata proposed a two-photon exposure system with a femtosecond laser and achieved 120 nm fabrication resolution [27].

Non-scanning point exposure can also generate three-dimensional polymer architecture by using some clever tricks like self-propagation. However, non-scanning and non-projection mean the exposure field cannot be flexibly controlled; therefore polymer in arbitrary shape cannot be fabricated by this strategy. The self-propagation effect occurs in a single point exposure of light in the photosensitive resin, which can generate polymer structure in a form of waveguide or micro-rod with a high aspect ratio (length is hundreds of times larger than diameter) and approximately constant cross-section [28-30]. This phenomenon is a result of self-focusing of the exposure light, which is caused by the increase of refractive index of the cured resin. When the diameter of exposure spot and the wavelength of exposure are in a match condition, the incident light is trapped in the cured resin from the point of exposure due to the total internal reflection (as in optical fiber). The effect delivers exposure energy towards the end of already-cured resin and increases the polymerization length. The limitation of this method is apparent: only columnar structures can be fabricated. In some research [30, 31], self-propagation polymerization with multi-beam or masks has been proposed to fabricated periodic lattice structures. The mechanism of it and corresponding products observed by using SEM is illustrated in **Figure 1-4**.

Surface exposure means the irradiation directly provides a two-dimensional pattern; therefore, it is possible to omit the scanning process and significantly save the build time of each layer. For most of the conventional methods, the projection is applied to control the exposure distribution. Moreover, the projection based MSL can dynamically change the pattern of exposure by using a Liquid Crystal Display (LCD) or a Digital Micromirror Device (DMD), which further improves the flexibility of MSL to fabricate three-dimensional polymer architecture in arbitrary structures [17-19, 32-37].

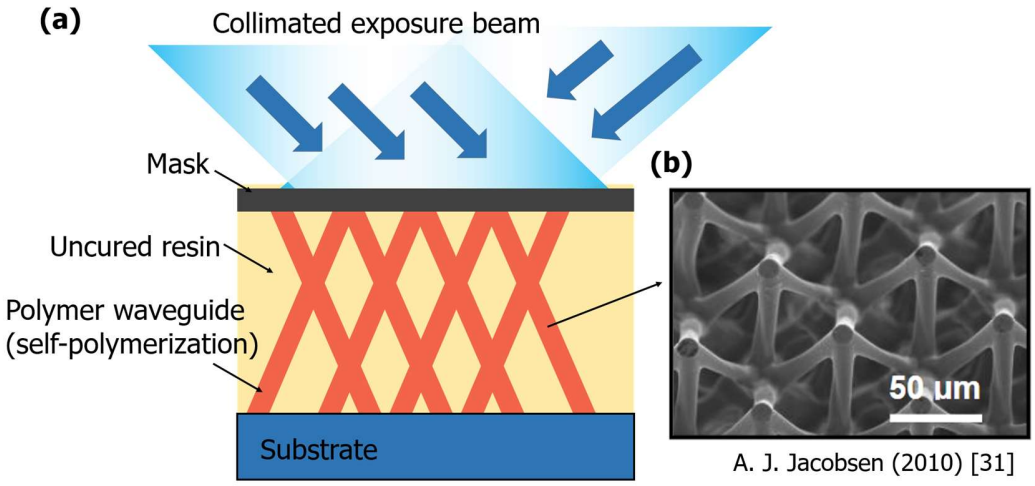

Figure 1-4 MSL based on self-propagation polymerization with multi beam and mask; (a) Diagrammatic explanations; (b) Products observed by SEM.

It is notable that the mask or the projection can only control the transverse optical field and a three-dimensional structure still needs to be cured in the way of layer-by-layer. The same problem comes here: how does the thickness of each layer be limited? Conventional strategies to overcome this problem are based on fixed surface and free surface two types of methods, just as in point-scanning MSL. Fixed-surface-projection MSL is also named as "bottom-up typed" in some literatures [35-37], since light transmits through the substrate to the bottom of the resin; and free-surface projection method is also called "top-down type" as the exposure beam propagates from the air to the top surface of the cured resin, as shown in **Figure 1-5**. Problems of these two exposure types are similar with what I discussed in the scanning-point MSL, including the damages on the cured resin caused by separation process in fixed-surface type and the deformation due to the surface tension of the resin in the free-surface type.

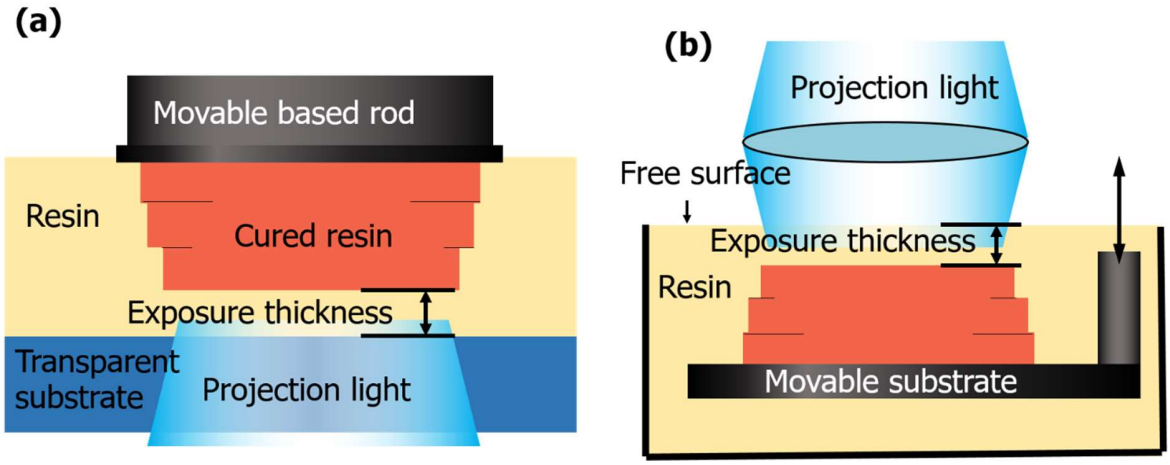

Figure 1-5 Diagrammatic explanations of projection MSL using (a) fixed surface and (b) free surface.

Evanescent-wave-based nano-stereolithography (EWNSL) utilizes the high confined energy field of evanescent waves to provide polymerization energy and restrict the exposure thickness [20, 21]. Therefore, by this way, the thickness of each layer is limited by the intensity decay of the exposure intensity rather than restricting the distance of movable substrate or the height of the liquid level. It can produce each layer of the resin in the sub-micrometer thickness because of the ultra-thin electric-field distribution of the evanescent waves, as shown in **Figure 1-6**. When the exposure light incident from the high-refractive-index substrate to the resin and the incident angle is large enough to develop the total internal reflection, localized light in the resin is generated near the interface between the substrate and the resin. The localized energy is used to provide curing energy of the resin, the intensity of which decreases exponentially as depth increases. Therefore, the thickness each layer can be limited to several hundred nanometers due to the intensity decrease of exposure. In order to develop the total internal reflection, the resin has to be cured on the high refractive index substrate. Therefore, the exposure system of EWNSL should be similar to the fixed surface MSL, but it requires a high-refractive-index substrate

and a large incident angle of the exposure beam. It is notable the thicknesses of each cured layer mainly depend on exposure energy rather than the space limited by movable substrate or rod. The problem of this method is obvious, the thickness of each layer is hard to be controlled since it is influenced largely by the exposure energy. Therefore, there is a strong demand on the in-process measurement of the thickness of cured resin. Regarding the motivations of in-process measurement, a detailed discussion will be shown in the next sections.

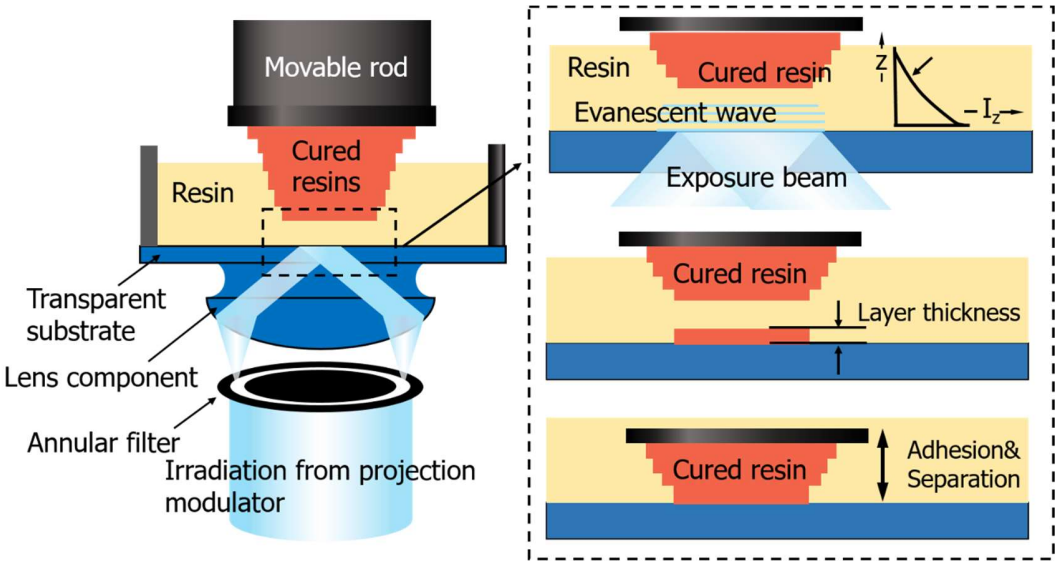

Figure 1-6 Diagrammatic explanations of EWNSL. The large incident angle is achieved by applying immersion lens and annular filter. Left figures show magnification images of photo-polymerization. Fabrication of three dimensional architectures is achieved by repeating exposure, adhesion and separation process.

For most of the projection or the mask based MSL, only one projector or mask is used. In some researches, double masks have been used to generate exposure in special distribution. When two masks are coaxial, the resin in different depth is cured by different patterns; As a result, three-dimensional architecture in a double order structure can be cured in one shot [44]. When masks in different axials, combing with the self-propagation

polymer, periodic lattice structure can be fabricated, which is similar with MSL using multi-beam in different incident angles.

Interference MSL has been proposed to cure resins by using the interference fringe generated by multi-beam of the exposure light in the same wavelength [40-43]. Since the interference patterns are in the same size with or smaller than the wavelength, submicron periodic structures like grating can be fabricated in one shot. Moreover, by combining evanescent-wave-MSL and interference, products in a submicron thickness with a submicron periodic pattern can be achieved. However, the problem is that it cannot meet the requirement of fabrication polymer architecture arbitrary structures and only periodic lattice structures can be fabricated. One of its application is the fabrication of the biomimetic surface with submicron structures.

1.2 Motivations and targets for developing in-process measurement

"In-process measurement" makes it possible to obtain real-time conditions of products during the fabrication process. Based on this, a feedback loop can be developed and the fabrication system can be real-time controlled or adjusted according to the fabrication conditions. For the MSL/NSL, the curing process of the resin is totally unknown in the fabrication process until the whole products are fabricated and the uncured resin is removed by etching and drying treatment (like etching process). An in-process

measurement of resin before etching and drying treatment makes it possible to dynamically control the exposure distribution and determine the exposure duration.

Combining with the background that there are several different types of the MSL/NSL techniques with different mechanisms and fabrication process, the applications of the in-process measurement in the MSL/NSL should base on specific types. In other words, for different types of MSL/NSL, the exact demands for the in-process measurement are different. In the thesis, there are two main research topics:

1.2.1 In-process measurement of the curing degree distribution of cured resin in conventional projection MSL (fixed-surface type).

1.2.2 In-process measurement of the thickness of cured resin in evanescent-wave-based nano stereolithography.

In these two topics, in-process measurement is applied in fixed-surface MSL and EWNSL. The motivations of these two topics are explained in 1.2.1 and 1.2.2., respectively

1.2.1 In-process measurement of the distribution of curing degree of the cured resin in MSL

In both fixed- and free-surface type MSL, the thickness of each layer is pre-set by the height of the liquid-state uncured resin or the substrate distance from cured resin to the movable substrate. In the practical fabrication process, the thickness of each layer, even though it can be flexibly controlled by the movable stage, has to be fixed to the same value. This is because different exposure energy is required for the resin layer in different

thickness. If the thickness of each layer dynamically changes in the fabrication process, the corresponding exposure energy for each layer should also be changed. This is hard to be achieved since it is hard to know the proper exposure energy for each layer in an arbitrary thickness especially when a thick sample is required.

As shown in **Figure 1-7**. In conventional MSL, due to the fact mentioned above, the thickness of each layer should be in the same value (**Figure 1-7** (a)). The flexible thickness of each layer (as shown in **Figure 1-7** (b)) is highly expected. It has some obvious advantages including saving the fabrication time when large thickness layer is fabricated and higher vertical resolution of the fabrication. For an example, when a product in a thickness of 7 μm is required, the conventional method with fixed thickness of each layer in 4 μm can only fabrication products in 8 μm after stacking two layers, while a flexible thickness system can directly fabricate the cured resin in a thickness of 7 μm in one layer.

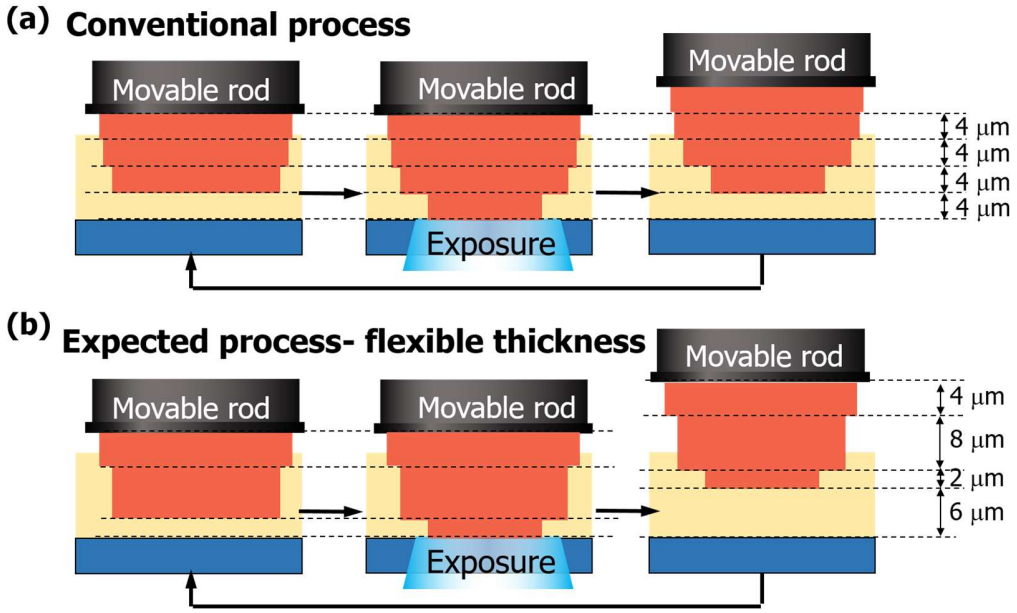

Figure 1-7 Diagrammatic explanations of thickness problem in MSL; (a) Conventional MSL with same thickness of each layer; (b) Expected MSL with flexible thickness

In order to achieve the flexible thickness of each layer in MSL, it is necessary to know the proper exposure energy for the different thickness. The problem is that scattering and diffraction occur at the bottom surface of the cured resin, accompanied with the multi-reflection between two surfaces, which largely influences the intensity distribution of exposure and results in that proper exposure energy is hard to be pre-determined. Therefore, I proposed to apply in-process measurement in MSL to obtain the curing condition of each layer. By this way, it is possible to cut the exposure in time for each layer in any thickness. The strategy of in-process measurement can be simply explained by **Figure 1-8**. With the exposure energy (exposure time) increase, the width of the new layer is widened. In the condition of insufficient exposure, the width of the cured resin is smaller than the expected width, while in the condition of excessive exposure the width of cured resin is larger than the expected width due to scatting and reflection of light from the cured resin makes the resin in the surrounding area be cured. If the width of the cured resin is in-process measured, and once it reaches the expected width, the exposure can be stopped and I can make sure the proper exposure energy is provided.

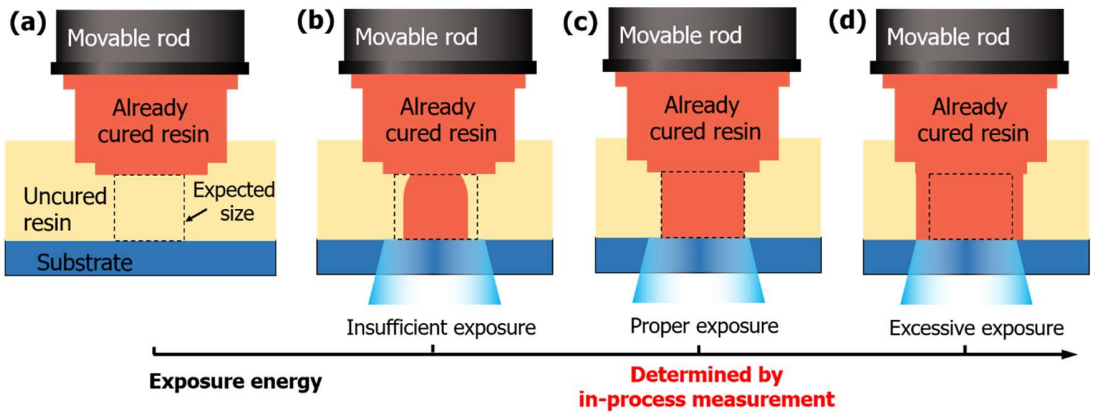

Figure 1-8 In-process measurement in MSL for determination of proper exposure energy

In order to determine the proper exposure duration, the most important thing is to solve the problem of in-process measurement of width in MSL. In the thesis, the exact measurement method will be explained and experiment results that confirm the feasibility of the proposed method will be illustrated.

It is notable that in the curing process, the cured resin is always submerged in the uncured resin. Between the cured and the uncured resin, there is gradient boundary made up by the resin in a half-cured state. Therefore, there is no clear boundary between the cured and the uncured resin and it is impossible to directly measure the width of the cured resin. Based on the fact that clear boundary or shape of the cured resin appears after etching and drying treatment, it is possible to predict the width of the cured resin according to the conversion degree of the resin and critical conversion degree of etching (washing) process. During the curing process, the degree of conversion of the resin keeps increasing. Only the resin in a conversion degree that is larger than the critical conversion degree of etching will be remained after washing and drying process. The degree of conversion especially means the reaction of the carbon double bond in the resin, which will be explained in the next chapter in detail. Therefore, in the fabrication process, what I measure is the distribution of the degree of conversion. The potential width of cured resin can be predicted according to the distribution of the degree of conversion.

1.2.2 In-process measurement of the thickness of the cured resin in EWNSL

Evanescent-wave-based nano-stereolithography (EWNSL) also has a strong requirement of in-process measurement of the thickness of cured resin due to the inevitable fact that the thickness of resin cured by evanescent-wave-based MSL is hard to be

controlled. This is because that in EWNSL thickness of each layer is mainly determined by the exposure intensity and duration, which is different from conventional MSL that directly limits the exposure area by the moveable rod or substrate to control the thickness of the resin. As shown in **Figure 1-9**. The exposure beam is incident in an incident angle that is much larger than the critical angle. Therefore total internal reflection occurs and evanescent wave in a form of intensity decay is generated on the substrate. In the near substrate area, the resin is cured in a larger intensity and resin near the substrate has a higher curing rate. As a result, the thickness of cured resin increase with exposure energy.

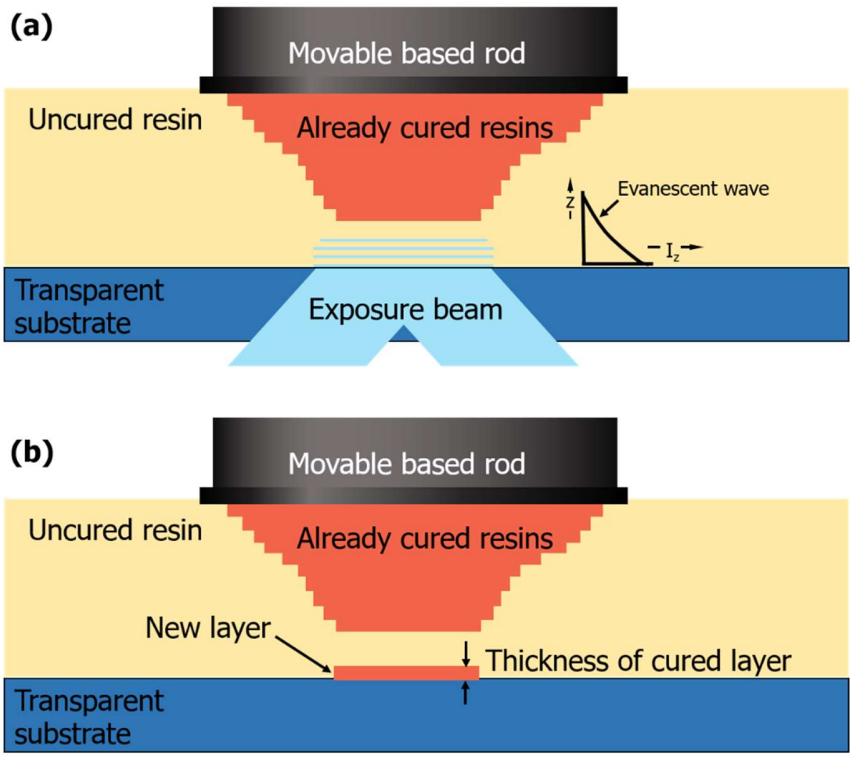

Figure 1-9 Curing process of EWNSL.

In the consideration of that one of the most important applications of EWNSL is to fabricate photonic crystal structures which have a strict requirement of the accuracy of

thickness of each layer, it is necessary to precious control the thickness in EWNSL. Even in normal structures without the high requirement of the thickness of each layer, after stacking of all the layers, a slight distinction of each layer leads the final products to distort largely. Although it is possible to achieve the thickness control by repeating the fabrication process many times to determine the optimum exposure intensity and duration, it is hard to achieve in real production since optimization should be done for each layer and a whole structure might be stacked over hundred layers.

In order to determine the proper exposure energy and make sure each layer in the expected thickness, in-process measurement is strongly required in EWNSL as well. By this way, once the thickness reaches the expecting value, the exposure can be cut in time and the thickness of each layer can be previously controlled.

The final target of this research topic is to improve the thickness control of EWNSL. In my research, same with the previous topic in MSL, what I focused is the in-process measurement. Different thing is that the measurement target is the thickness rather than the width of the cured resin. In addition, due to the thickness of the cured layer is in a submicron meter. The special measurement method is required. I proposed the measurement method that can indirectly obtain the thickness information and did the experiment to confirm it. Therefore, the objective of this thesis regarding this topic is the in-process measurement in EWNSL.

1.3 Research purpose and originality

In order to improve the flexibility of existing MSL/NSL techniques and provide the possibility for next generation of MSL/NSL, I count on the in-process measurement and attempt to intelligentize the existing MSL/NSL techniques with feedbacks from the in-process measurement. With the ambition of this target, I specifically explored in two directions. These two direction as two research topics are demonstrated in this thesis

In the first topic, the in-process measurement is applied in MSL. The research purpose is to make MSL be able to fabricate each layer of resin in an arbitrary thickness. In MSL, the thickness of each layer can be adjusted by changing the height of moveable rod or substrate; however, for cured resin in different thickness, the required exposure energy (exposure duration) is different as well. When the resin is exposed insufficient or overexposure, the width or pattern of the resin will be incomplete or out of shape. In order to determine the proper exposure energy for the resin layer in different thickness, the in-process measurement is used to determine the proper exposure energy by measuring the curing condition of the resin. In MSL, the distribution of conversion degree of the resin near substrate can directly present curing condition of a whole layer and determine the width of each layer after etching and drying. Therefore, I carried out the topic of in-process measurement of the conversion degree in MSL.

In the second topic, the in-process measurement is applied in EWNSL. The research purpose is to control the thickness of the cured resin by using the in-process measurement. It is based on a requirement that the thickness of the cured resin keeps growing with the exposure energy and the thickness need to be in-process measured to determine the perfect

time for cutting the exposure. Compared with the first research in MSL, the resin cured by the evanescent wave in EWNSL is much thinner and normally in submicron thicknesses. In this case, when the critical-angle reflection is applied as the in-process measurement method, the resin cured in such ultra-thin thickness generates the optical response of measurement light in a form of reflection-phase-contrast interference. The interference condition is sensitive to the thickness increase of the cured resin. Therefore, I proposed to directly measure the thickness of the cured resin by detecting the interference intensity using the critical-angle reflection method in EWNSL.

Originality: There are seldom researches about the in-process measurement of the resin in MSL/EWNSL. As far as I am aware, the visualization of the curing process in MSL/EWNSL was achieved for the first time in the world. In addition, the measurement method based on the critical-angle reflection in MSL/EWNSL has never been reported. There are somewhat similar measurement methods based on total internal reflection microscopy, reflection-phase-contrast interference or frustrated total internal reflection; but these methods did not use the high sensitivity feature of reflection at the critical angle. I also optimized a novel multi-layer SPR substrate with PLZT that can change the highly sensitive measurement range by load voltage, even though it is not my main research direction.

1.4 Organization of this dissertation

The organization of this thesis is shown in **Figure 1-10**. This research is based on the topic of in-process measurement in the MSL and EWNSL. In order to clarify the measurement target and find the suitable parameters that show the curing conditions of the

resin and can be efficiently in-process measured, I investigated the existing MSL/NSL techniques. Summary and classification works have been done and demonstrated in the chapter 1. In addition, I talked about my motivations of in-process measurement in MSL and EWNSL, respectively. The parameters that need to be in-process measured is clarified. There are two topics in this research: one is the is the in-process measurement of the conversion degree in convention fixed-surface type micro-stereolithography (MSL) another is the in-process measurement of the thickness of the cured layer in evanescent-wave based nano-stereolithography (EWNSL),.

In chapter 2, some potential methods that might be suitable for in-process measurement and their limitation will be discussed in this chapter. At last, I will briefly talk about my measurement strategies that utilize the refractive-index variation of the resin in the curing process and optical response from the near-substrate resin.

In chapter 3, the photo-polymerization process in the MSL/EWNSL will be introduced. The investigation of this process benefits for us to understand the curing process of the resin in the MSL/EWNSL, and more important, help us to determine which parameter should be measured in the curing process. My measurement method is based on the change of the refractive index of the resin in the curing process since the refractive index can indirectly show the curing condition of the resin and can be simply measured by the optical method.

In chapter 4, the proposed measurement method that uses total internal reflection at the critical angle will be explained. In this method, the refractive index of the resin or the thickness of the cured resin directly influence the optical response and are reflected in

the form of variation of the reflection distribution. Therefore, in-process measurement can be measured by detecting the reflection. I will discuss the optical response when the cured layer is in large thickness that is in the same condition with the in-process measurement in MSL; and when the cured layer is thin (submicron scale) which is in the same condition with the in-process measurement in EWNSL.

In chapter 5, the in-process measurement of the conversion degree of the resin in the MSL will be discussed. There will be detailed investigation progress about this research topic including the experiment setup, and the verification experiment. The relationship of conversion degree and refractive index is also experimentally measured. Based on measured relationship, the in-process measurement of conversion degree is achieved by detecting the variation of the refractive index of the near-substrate resin.

In chapter 6, the in-process measurement of the thickness of cured resin in EWNSL will be demonstrated in the similar layout, including the detailed analyzation of optical response, the experiment setup, and the verification experiment. I experimentally measured the relationship between the thickness of cured layer after etching and drying process with the reflectivity and used this relationship to predict the thickness of the cured resin, making the in-process measurement in EWNSL be realized.

In chapter 7, I will illustrate another measurement method based on the Surface Plasmon Resonance measurement. This method is similar to the critical-angle-reflection method that utilizes the variation of refractive index of the cured resin. This method uses the high-refractive-index sensitivity of SPR and required a coating on the substrate. The principle and theoretical investigation of multi-layer SPR substrate will be demonstrated.

In chapter 8, I will make a conclusion of my work according to the results in the previous chapters. Besides of the main research progress, I also did some related investigations on the absorption constant of the resin. This work will be demonstrated in the appendix.

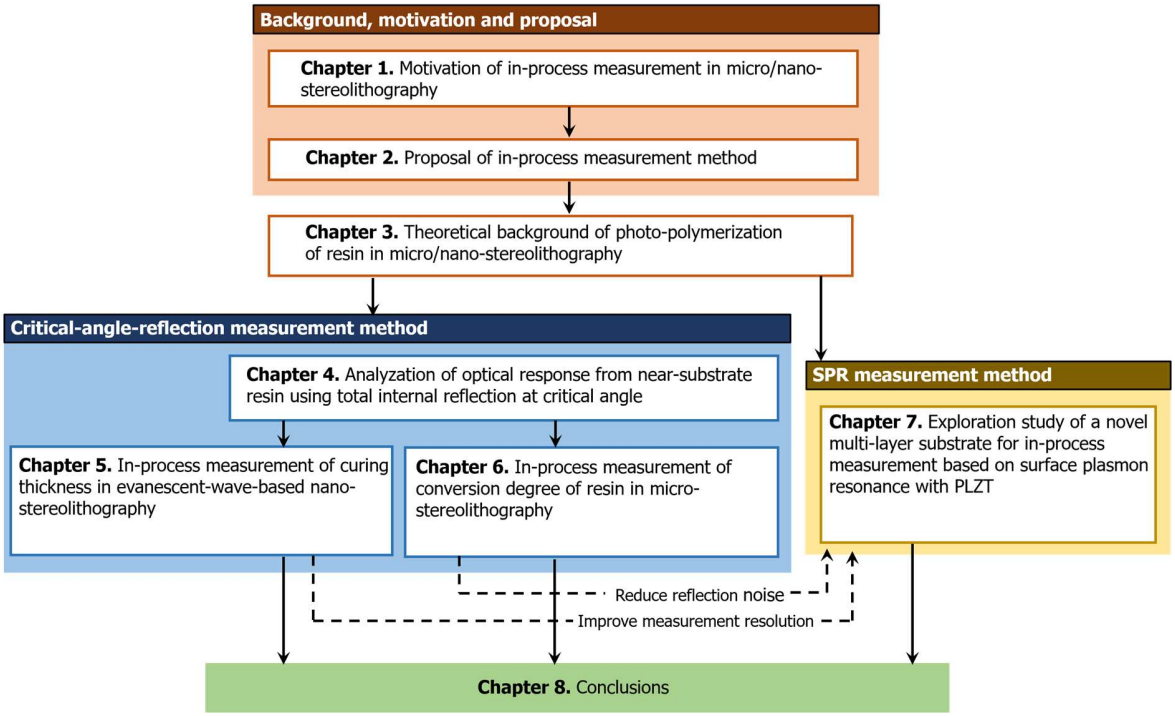

Figure 1-10 Structure of organization of this dissertation

CHAPTER 2. PROPOSAL OF IN-PROCESS MEASUREMENT METHOD

This chapter presents the difficulties of the in-process measurement in MSL/EWNSL. Particularly, this chapter summarizes the existing in-process measurement methods which are used in the in-process measurement in the polymerization process of the resin. The measurement methods have the potential to be applied in the MSL and EWNSL since they directly measure the states or the curing conditions of the resin in the curing process. This chapter also explains the basic principle of each method and illustrates the limitations of them when applied as the in-process measurement. The limitations of the commonly used measurement methods are the primary reason for proposing my own measurement method for in-process measurement. At last, my measurement method based on refractive-index detection using the optical response from near-substrate resin will be briefly introduced in this chapter.

2.1 Difficulties of in-process measurement

There is seldom research about the in-process measurement in MSL/EWNSL, however, a lot of investigations have been done to study the polymerization process of the cured resin [47-56]. The requirements of in-process measurement in the MSL/EWNSL is totally different with the in-process measurement in the photo-polymerization process. For in-process measurement in the polymerization process, it is no problem to just measure a point of resin sample or measure the average state of resin; however, for the in-process measurement in the MSL/EWNSL, the measurement on the single point or average state

of the resin cannot obtain the whole fabrication conditions, in the other world, a distribution information of the resin should be measured for achieving the curing condition of a whole resin layer. Most importantly, the horizontal shape (pattern) of each layer should be in-process measured to make sure each layer is cured in an expected pattern.

For in-process measurement in the MSL, my target is to measure the distribution of conversion degree of the resin, which contains the information of the horizontal shape of the resin since the conversion degree directly determines that the resin will remind or not after the etching and the drying process. The difficulty of this work is mainly on that measurement of the distribution of conversion degree of the resin in the whole exposure area is required. For conventional measurement methods used for detecting conversion degree like Raman spectroscopy and Fourier Transform Infrared Spectroscopy (FTIR), only a point of the sample or the average conversion degree of the sample can be measured, and long detecting time is required [58-62]. Therefore, it is hard to achieve the in-process measurement in the MSL by directly measure the conversion degree of resin using the conventional measurement methods.

For in-process measurement in EWNSL, as I explained above, the measurement of the thickness of each layer is highly expected; therefore, I should find or propose a measurement method that can measure not only the horizontal shape but also the thickness of the cured layer, which is like a three-dimensional measurement but allow to lose some detail of surface. In addition, the thickness of the cured resin is in the submicron scale, and the cured resin is submerged in the uncured resin. There are gradient boundaries made up by the half-cured resin between the cured and uncured resin. In addition, high sampling rate is required since the curing process is finished in several seconds. Based on the above

facts the in-process measurement in EWNSL becomes extremely difficult and special measurement method is required.

2.2 Potential methods overview

In this section, I investigated the existing methods for the in-process measurement in the polymerization process and tried to find a suitable method that can be applied in MSL/EWNSL. These methods can be classified into following types according to their basic principle: spectroscopy, calorimetry, thermometry, dielectrometry, rheometry, acoustics method and interferometry [45-56]. The basic principle and properties of each type of method are shown in **Table 2-1**. Unfortunately, for all the method listing below, none of them can totally meet the requirement of the in-process measurement in the MSL/EWNSL.

Table 2-1 Principle and properties of existing methods for in-process measurement in photo-polymerization process

Classification	Basic principle	Typical techniques	Measurement target	References
Spectroscopy	Measuring the vibration energy of molecules, Identifying and quantifying molecules by light spectrum	FTIR Raman spectroscopy	Conversion degree of a point	[46][47]
Calorimetry	Measuring heat transfer associated with chemical reactions or physical changes	Differential scanning calorimetry (DSC)	Averaged conversion degree of whole field	[48][49]
Thermometry	Measuring temperature changes caused by photopolymerization process	Optical pyrometer	Conversion degree of a point	[50]
Dielectrometry	Adding external electric field, measuring the amplitude and the phase shift of the current response caused by orientation changes of polar molecules	Interdigitated comb electrode sensor	Averaged conversion degree of whole field	[51]
Rheometry	Measuring the change in mechanical properties	Particle tracking microrheology	Viscosity	[52]
Acoustics method	Measuring the change of wave propagation characteristics	Ultrasonic cure monitoring	Averaged conversion degree of whole field	[53] [54]
Interferometry	Measuring changes of optical path lengths	Interferometry	Refractive index change of a point; Shrinkage	[55][56]

For spectroscopy and thermometry, only conversion degree of a point can be measured, while for calorimetry, dielectrometry and acoustics methods, what can be measured by them is averaged condition of a bulk sample. Therefore, it is hard to use these methods to get distribution information of the cured resin like distribution of conversion degree.

The spectroscopy method including FTIR and Raman spectroscopy can directly measure the degree of conversion of the resin by identifying and quantifying molecules of the resin in the curing process. For FTIR-based spectroscopy, the most conventional way of measurement is to deliver a beam of inferred light in a wide-wavelength band into a bulk sample and analyzing the spectrum of light penetrating through the sample. In this way, the average state (conversion degree) of the resin in the path of measurement beam will be measured rather than the distribution of conversion degree. I considered applying FTIR imaging or total-internal-reflection-based FTIR imaging technique to make FITR suitable for in-process measurement in the MSL. However, the absorption light used to analyze the conversion degree of the resin is in a wavelength around 6.12 μm (1643 cm^{-1} in wavenumber), which is the absorption peak of carbon double bond (C=C) in the spectrum [63,64]. It is worth notable that the wavelength of fabrication light (405 nm) is significantly smaller than the wavelength of the measurement light, which results in the resolution of the measurement is much worse than the resolution of fabrication and the in-process measurement will lose distribution or spatial information of the products.

Raman spectroscopy can use a laser in a visible range as the measurement light; the wavelength of it can be approximated to the fabrication light. By selecting an appropriate wavelength used in Raman spectroscopy, it is possible to avoid the influence on curing

state of the resin caused by the measurement light and also make sure a high-enough spatial resolution of measurement that approaches to that of fabrication. However, Raman spectroscopy requires an accumulation time of measurement, there is an apparent trade-off between detection time and intensity of measurement beam. In one hand, short measurement time means high sampling frequency, which is highly expected for the in-process measurement since the curing of a single layer can be finished within several seconds. In the other hand, the large intensity of the measurement beam will directly increase the curing degree of the resin by providing optical energy, and indirectly change curing rate by increasing temperatures of the resin in the irradiation area. In the worst condition, the resin is burned by the measurement light in high intensity. As a result, on the premise of reduction of the intensity of measurement beam, the limitation of Raman spectroscopy when applied in the in-process measurement is mainly on the low sampling frequency.

Calorimetry and thermometry method measure the heat transfer and temperature change of the resin determined by the polymerization reaction. Differential scanning calorimetry (DSC) is one of the typical calorimetry methods [48-50]. In order to avoid the environmental disturbance, the resin must be heat insulation, which is an inconvenience for the in-process measurement in the MSL/EWNSL. In addition, the most serious limitation is the measurement of averaged conversion degree of all the resin in an insulated container without any spatial information, which cannot meet the requirement of measuring the distribution of conversion degree.

Other measurement methods based on current detection (dielectrometry), partial tracking (rheometry) or intensity detection using ultrasonic (acoustics method) can

indirectly obtain the conditions of the resin in the curing process [52-54]. The same limitation comes again: they can only measure the average condition of the resin without any lateral information.

Interferometry methods show a large potential to make the in-process measurement in the MSL/EWNSL since it utilizes the refractive index increase of resin in the curing process and refractive index variation can be simply measured by optical methods using interferometry. However, according to the investigations in the references [55] [56], the researches stopped at measuring the refractive index change or detecting the shrinkage of the cured resin, and of course, they did not study on the in-process measurement of the distribution of conversion degree or thickness of the cured resin. In addition, in the curing process, the existence of gradient boundary largely reduced the reflection between the cured and uncured resin due to the gradient-changed refractive index. Therefore, even utilizing the refractive index change of the resin, an optical method with special tricks is required. That is why I proposed my own in-process measurement method.

2.3 Brief introductions of proposed method

The measurement is based on the fact that the refractive index of cured resin increase in the curing process, and resin in higher conversion degree has a higher refractive index. The relation between refractive index and conversion will be introduced in the next chapter and I also measured this relationship in an experiment that will be discussed in chapter 5. For both MSL and EWNSL, the resin is cured over the transparent substrate. Therefore, I try to measure the refractive-index distribution of resin near the substrate using an optical method and calculate other expected information. In MSL, once the refractive-

index distribution of the resin near the substrate is measured, the distribution of conversion degree in the bottom of the cured resin can be calculated according to the relationship between conversion degree and refractive index. In case of EWNSL, since the resin is in submicron thickness, the thickness of cured resin influences the optical response and therefore, the thickness can be derived by detecting the variation of effective refractive index of resin near the substrate. In the other word, even though I have two individual research topics that apply in-process measurement in two kinds of MSL/EWNSL, I can still use similar measurement method that detects the refractive index of resin near the substrate, as shown in **Figure 2-1**.

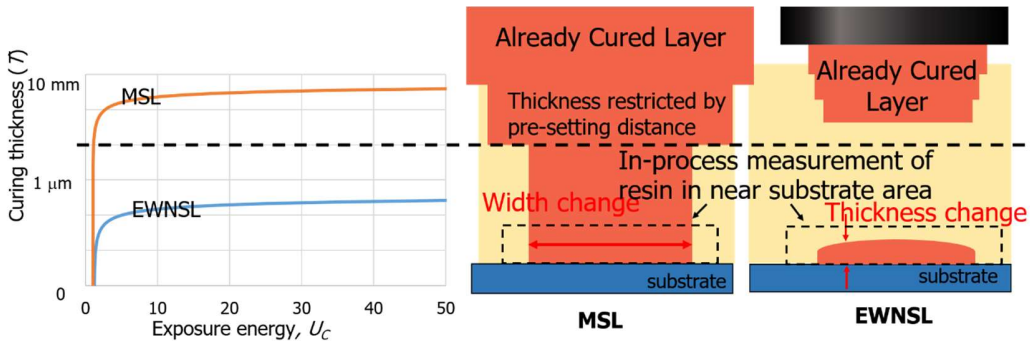

Figure 2-1 Brief introduction of proposed method, by which refractive index of near-substrate resin is measured to derive distribution of conversion degree in fixed-surface-type MSL and thickness of the cured resin in EWNSL.

As a result, the problem comes how to make an in-process measurement of refractive index of near-substrate resin. Actually, based on this problem, I proposed two measurement method, one is using total internal reflection at the critical angle, which is the main part of this research and will be clearly explained in from chapter 4 to chapter 6; another one is using Surface Plasmon Resonance measurement method, which is still under investigation and the progress results will be demonstrated in chapter 7.

CHAPTER 3. THEORETICAL BACKGOUND OF PHOTO-POLYMERIZATION OF RESIN IN MICRO/NANO-STEREOLITHOGRAPHY

This chapter presents the reaction principle of photo-polymerization. The chemical reaction mechanism of the resin in the curing process is demonstrated step-by-step. In addition, some notable phenomena including the oxygen inhibition and gradient boundary are explained in this chapter as well. The definition of conversion degree of carbon double bond that used to directly evaluate the curing degree is clarified in this chapter. At the end of this chapter, the refractive index change of resin in the curing process will be discussed, which is an important section as my in-process measurement method is essentially based on the increase of refractive index of the resin.

3.1 Polymer formation

Essentially, photo-polymerization of the resin is one of the polymerization process, which is a process of connecting small monomer or molecules together by covalent bonds (carbon bond for the resin) to develop high-molecular-weight polymers. Photo-polymerization with the optical sensitive initiator is a polymerization process initiated by optical energy [65-67]. The resin used for photo-polymerization generally consists of monomer, photo-initiator and some other fillers or additives like reactive diluents, stabilizers and small ceramic particles.

Two kinds of the resin that are widely used including acrylates and epoxy with vinylether. The corresponding mechanisms of curing are free-radical polymerization and

cationic polymerization, respectively [68]. The resin used in our experiment is acrylates type, and therefore photo-polymerization kinetics is free-radical. The most common acrylic monomer is methyl methacrylate and its corresponding reaction product is polymethyl methacrylate, as shown in the following formula [69]:

Figure 3-1 Methyl methacrylate

Some more complex acrylate-type resin with a multi-reaction-functional group and particular radical group are used to fabrication polymer in different features. For an example, a typical tetrafunctional acrylate monomer is shown in **Figure 3-2** [69 70]:

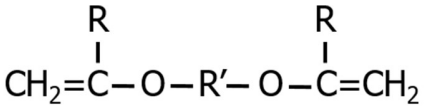

Figure 3-2 Tetrafunctional acrylate monomer

where R can be H or CH3 and R' can be short chain alkylene, arylene, polyester, polyurethane or polydioxane.

The photo-polymerization process of the resin has been widely investigated for many years. This thesis does not focus on the curing reaction itself, and therefore, my study on the photo-polymerization process is mainly based on the bibliographic survey. According to the conclusions of the comprehensive references in related fields, briefly

speaking, the whole curing (photo-polymerization) process can be divided into the following four steps [70,76], as shown in **Figure 3-3**.

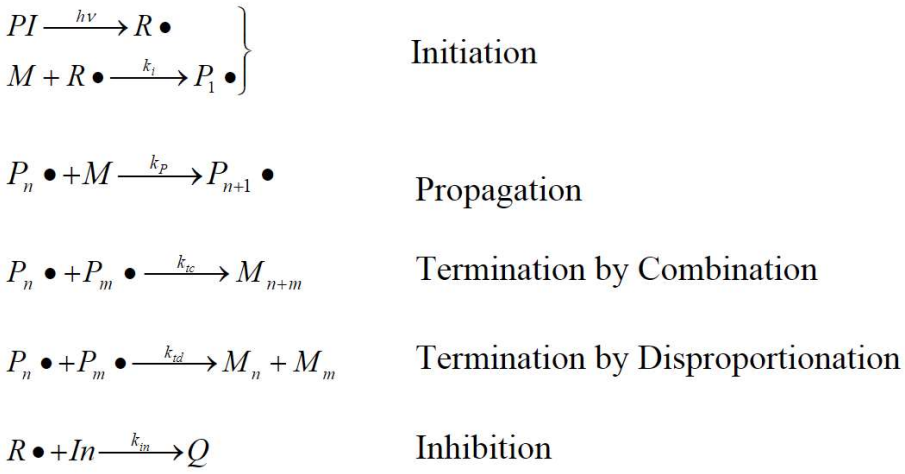

Figure 3-3 Curing process of resin

Initiation is the formation of an active center that can start the polymerization of the monomer. The active center that can be a free radical, a carbanion or a carbonium ion. In the initiation process, the photo-initiator is photodecomposition after absorption of photons in the exposure condition. Then the radicals generated from photo-initiator react with the monomer to form an active center that can start the propagation process.

Figure 3-4 shows the reaction of chromatic carbonyl compound as the photo-initiator which breaks its homolytic carbon bond in the exposure condition. There are also some special initiators (iodonium, sulphonium salts, and arene complexes) can generate radical and cationic active centers at the same time [69]. The initiators normally take less than 1% in total amount of the resin but critically determine the polymer properties including curing rate, continuity of development of high molecular and maximum conversion degree.

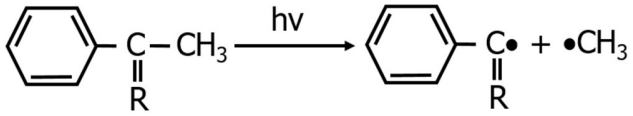

Figure 3-4 reaction of chromatic carbonyl compound

Propagation involves the connection of more monomer to the reactive site (active center) at the growing chain end, which makes molecular weight increase rapidly. In this process, the chain polymer with the active centers at one side keeps growing by adding monomer with the reactive site. The propagation reaction is the main reaction that consumes the monomer in the resin.

Termination is the disappearance of the active center. In this step, the polymer chains stop growing because of combination or disproportionation of two active centers. It is known that the weight of the polymer is determined by the termination process. For termination by combination, the final weight of polymer chain is twice of termination by disproportionation.

Inhibition is the reaction of inhibitor like oxygen with the free radical. The reduction of free radical will limit the reaction to some extent. In one hand, the inhibition slows down the reaction and decreases the maximum conversion degree, which is strived to avoid for most of the conditions. In the other hand, the existence of the inhibition makes it possible to stop the initiation once the stimulation for initiation is stopped, which makes it possible to limit the polymerization in expected range or time, improving the accuracy of products, especially in photo-polymerization.

3.2 Rate equations

For each curing step, the rate of each step explained above can be expressed as Equations (3-1), (3-2), and (3-3), respectively [69,70,76].

$$R_i = \phi_i I_a \tag{3-1}$$

$$R_p = k_p[P\bullet][M] \tag{3-2}$$

$$R_t = k_t[P\bullet]^2 \tag{3-3}$$

where k_i k_p and k_t is the reaction constant for each step, [M] is the concentration of monomer and [P•] is the concentration of reactive center.

For the whole photo-polymerization process, according to the general equation for polymerization, the reaction rate can be expressed by:

$$R = \frac{k_P}{k_t^{0.5}}[\mathrm{M}](\phi I_a)^{0.5} \tag{3-4}$$

In the consideration of absorption when light propagates deeply into the resin, the exposure intensity decrease exponentially with exposure depth in the resin. According to the Beer-Lambert law, the reaction rate can be expressed by:

$$R = \frac{k_P}{k_t^{0.5}}[\mathrm{M}](\phi I_0(1-e^{-\varepsilon[In]t}))^{0.5} \tag{3-5}$$

These equations are obtained by setting up conservation laws for mass and energy, using the kinetic rate constants. They can simply express the reactions; however, these constant k_i k_p and k_t are influenced with the temperature and the conversion degree of the monomer, and therefore, keep changing during the curing process. In addition, the species balance and the heat transfer can be used in calculation of the concentrations of components and reaction rate in a higher accuracy. Base on this point, photo-polymerization process models that simulates the curing process of the resin were developed in the references [54-59]. I also did the similar work to simulate the curing process in EWNSL which will be shown in the chapter.6

3.3 Conversion degree

The extent of reaction of photo-polymerization or curing process is generally expressed by the degree of monomer conversion, is also referred to as the degree of conversion, the degree of curing and degree of polymerization. In addition, based on the fact that every monomer has only one carbon double bond and the carbon double bond will break after polymerization, the degree of monomer conversion also means the degree of carbon double bond (C=C) conversion. Due to the variation of C=C can be directly measured by infrared absorption or Raman spectroscopy, in chemical field degree of C=C conversion is widely used. In the following contest of this thesis, conversion degree and degree of conversion are the same meaning with the degree of C=C conversion. It can be simply expressed by calculating the reduction of monomer compared with its initial concentration before the polymerization reaction [71-73]:

$$\alpha = \frac{[M_0] - [M]}{[M_0]} \tag{3-6}$$

Figure 3-5 shows the conversion degree increase as a function of exposure energy in photo-polymerization. It is known that, before the reaction, the resin mainly consisted of small molecules is in a state of liquid. With polymerization progresses, the average weight of molecules, as well as the viscosity of the resin keep increasing, and the state of the resin changes from liquid to gel and approach to solid gradually until the exposure is cut down or the resin is fully cured [70,76]. The conversion degree also increases with the exposure successively. It is obvious that a larger conversion degree of the resin means a higher solidification or reaction level of the resin.

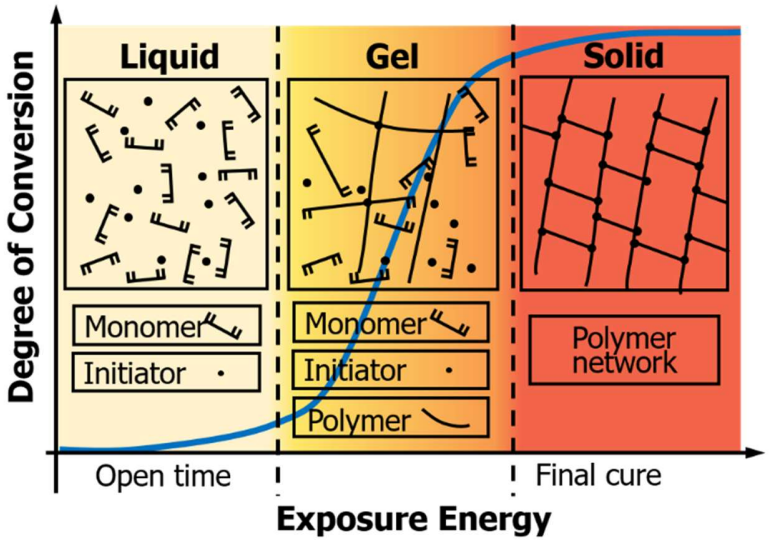

Figure 3-5 Degree of conversion and variation of resin in an increasing exposure energy

It is known that after the curing process and before products are totally finished, there is a process to remove the uncured resin. It includes the etching and drying treatment, and in some cases, post curing is also required to further solidify the resin [74 75]. The

conversion degree directly determines the resin be removed or not after etching and drying process. It can approximately treat gel point as the critical etching degree that once the resin reaches this critical etching degree it will not be removed after the etching and drying process. Tang proposed a more complex threshold model of curing [77] rather than simply using gel point as an exposure threshold. In his model, both species balances and mass transfer effects are involved into the calculation of curing rate. Also in his model, the degree of conversion reaches an asymptote lower than 100%. This is because the solidified resin decreases the dissociation of initiator and largely reduced the mobility of monomer in the resin, as a result, some monomer might be sealed among the dead polymers and cannot be excited without the active species nearby [69,70,76].

Apart from the reaction rate model according to the species balances in three reaction steps, a phenomenological model was proposed to calculate the reaction rate (dα/dt) with the influence of temperature and the mass transfer, as shown in following equation [78-80]:

$$\frac{d\alpha}{dt} = k_c(T) f(\alpha) \tag{3-7}$$

where a is the degree of conversion, $d\alpha/dt$ the reaction rate of whole reaction containing initiation, propagation and termination three steps, $f(\alpha)$ a function related with conversion degree that expresses the influence of variation of mass transfer with conversion degree increases, and $k_c(T)$ the temperature-dependent rate function that was given by the Arrhenius law [70]:

$$k_c(T) = k_0 e^{\frac{-E}{RT_{abs}}} \tag{3-8}$$

where k_0 is a factor should be experimental measured, E the activation energy required for initiator, R the gas constant, and T_{abs} the absolute temperature (Kelvins temperature).

In case of ignoring the auto-calytic (auto-acceleration) of polymerization, $f(\alpha)$ can be express by equation (3-9). If the auto- calytic is included, $f(\alpha)$ should be expressed by function (3-10), proposed by Yebi [61].

$$f(\alpha) = (1 - \alpha)^n \tag{3-9}$$

$$f(\alpha) = (1 - \alpha)^p \alpha^q \tag{3-10}$$

where the parameter n, p and q are the reaction orders of these fitting equations. Thus the reaction rate expressed by conversion of degree is given by[70,79-80]:

$$\frac{d\alpha}{dt} = k_0 e^{\frac{-E}{RT_{abs}}}(1 - \alpha)^n \tag{3-11}$$

or

$$\frac{d\alpha}{dt} = k_0 e^{\frac{-E}{RT_{abs}}}(1 - \alpha)^p \alpha^q \tag{3-12}$$

3.4 Heat transfer

Based on the fact that photo-polymerization is accompanied by an exothermic phenomenon, in the curing process, heat is generated and delivered to the surrounding area

where the resin is not being curing. Due to the heat (temperature) influences the curing rate largely, it is necessary to discuss the distribution of heat in the curing process. The heat transfer in the resin is in a balance among heat storage, conducting and generation, which can be expressed by a general heat transfer equation [77-80]:

$$\frac{\partial \rho c_p T}{\partial t} = k\nabla^2 T + \Delta H_p R_p \tag{3-13}$$

where ρ is the density of the resin (the density of the cured resin is slightly larger than the uncured resin, but same density value was used for simplifying calculation; the same problem of following characteristic parameters), c_p the specific heat of the resin, T the temperature, and k the thermal conductivity of the resin. Heat generation caused by polymerization itself is $\Delta HpRp$, where ΔHp is the heat generation constant in a certain reaction rate, and Rp the rate of the curing process. Generated heat will increase the reaction rate and the speed up of the curing process will produce more heat, which is one of the reasons for auto-acceleration of the curing process. Some heat equations also involve the heat from the absorption of the exposure, which is necessary to be considered when the bulk sample is cured but can be ignored in MSL/EWNSL since the absorption in such small size products can be neglected.

When I developed the simulation model using both reaction rate (3-12) and heat transfer (3-13), the thermal boundary condition should also be considered carefully as exemplified by Yebi' explanations [79,80]. In a one-dimensional simulation (only the curing depth is considered), one of the simulation boundaries should be the interface between the resin and the substrate or the air (corresponding to the fixed- and free- surface

type MSL, respectively), another boundary should be the natural heat convection boundary [79] which means that out of this boundary, the material is still the resin. Another problem is about the variation of the parameter of materials caused by the increase of temperature and the state change of the resin. For some parameters, the influence from temperate can be calculated according to Arrhenius law [78]. Other parameters including density and conductivity can be treated as temperature- and state- dependent.

3.5 Oxygen inhibition

In the polymerization process, the oxygen as one of the inhibitors exerts a detrimental effect of the photoinitiators by reacting with the free radical generated by initiators [69,76,81]. Moreover, it is known that the oxygen reacts with the carbon-based active center at the end of the polymer forming peroxy radical which shows much lower activity compared with the carbon double bond, as a result, the oxygen indirectly decreases the reaction rate [81]. To involve the oxygen inhibition into the calculation of reaction rate, the simulation equations should be expanded with species balance including the oxygen and the inhibition on initiators.

The undesirable reactions mainly caused by the oxygen that dissolves into the resin. For two typical types of MSL (fixed surface and free surface), the concentration and distribution of oxygen are totally different in the curing process. In the fixed-surface system, the oxygen is replenished from the surrounding area with a higher concentration of oxygen, as a result, the oxygen inhibition occurs at two sides of the cured resin [70]. In free-surface MSL, the top surface of the resin directly contacts with the oxygen in the curing process

and once the oxygen is consumed, it can be absorbed and supplemented from the air. Therefore, the inhibition becomes worse in this case.

Normally oxygen inhibition is treated as the undesirable reaction and be avoided; however, it can be well applied in the fixed-surface MSL to prevent tight adherence of the resin to the substrate [84].

One of the simplest solutions of oxygen inhibition is to prevent diffusion of oxygen from the atmosphere by sealing the resin in inert gas during the curing process, and nitrogen is always used. This strategy can be easily achieved in a laboratory condition but becomes difficult and expensive in an industrial scale [70,82,83].

3.6 Gradient boundary

The curing process of the resin is a continue polymerization process. During the curing process, the degree of conversion keeps increasing. Therefore, the intermediate product – half-cured resin is unavoidable. The half-cured resin between the fully cured resin and the uncured resin forms the gradient boundary, as shown in the left figure in **Figure 3-6**. A part of gradient boundary made by the resin in a conversion degree lower than the critical etching degree will be removed after the etching process.

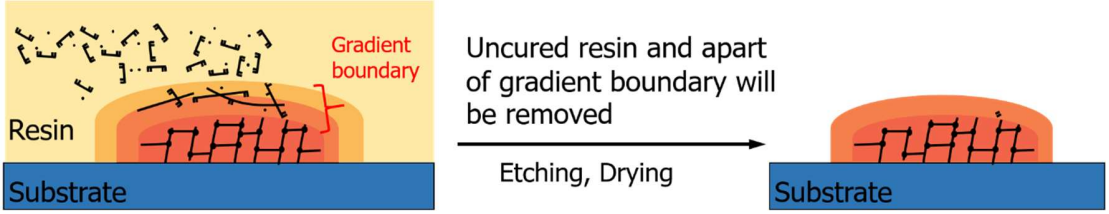

Figure 3-6 Explanation diagram of gradient boundary

The existence of the gradient boundary makes it impossible to measure the absolute shape of the cured resin during the curing process. Therefore, my strategy is to measure the distribution of conversion and predict the shape in prerequisite that critical etching degree is known.

For MSL as shown in **Figure 3-7**, in the depth direction, the conversion degree slowly decreases due to exposure beam that is absorbed by the resin and its intensity decreases with the curing depth. In the near-substrate area, the degree of conversion is treated as constant since the absorption can be ignored in a short propagation distance. Because the in-process measurement of the width of cured resin is expected, the spatial distribution of cured resin near substrate is more important. In the spatial direction, the predicting of (etching) width can be achieved by measuring the spatial distribution of the conversion degree and find the width of critical etching degree.

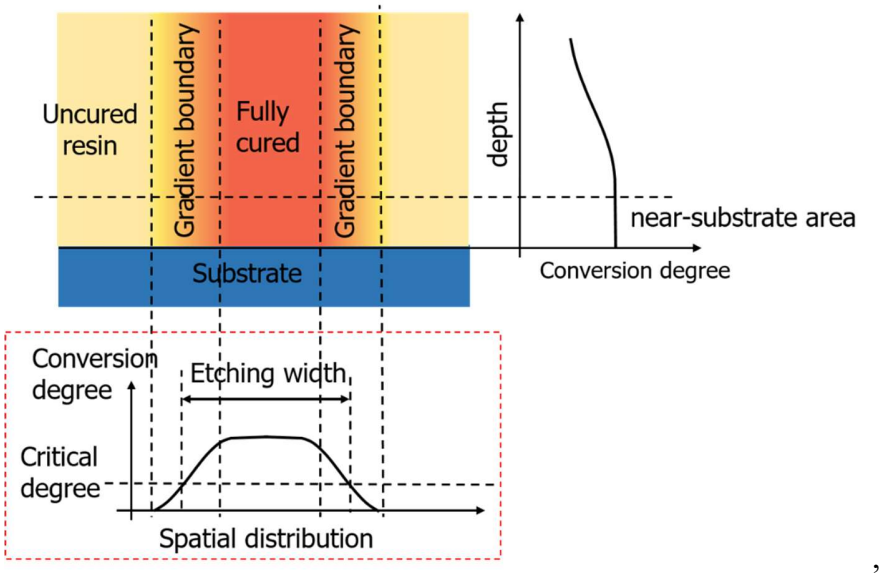

Figure 3-7 Curing condition and gradient boundary in MSL

For EWNSL as shown in **Figure 3-8**, due to the intensity of exposure beam decrease largely in the depth direction, the gradient boundary appears within the near-substrate range. My target, as explained above, is the in-process measurement of the thickness of the cured resin. Based on the difficulties that the range of gradient boundary is in submicron scale, a degree-of-conversion profile in nanoscale resolution is required. Actually, no exiting technique has been found that can achieve this measurement. Therefore, in EWNSL, I do not use the strategy of measurement degree of conversion. An alternative approach is directly measure the curing or etching thickness by detecting the reflection and using the relationship between the thickness and reflectivity.

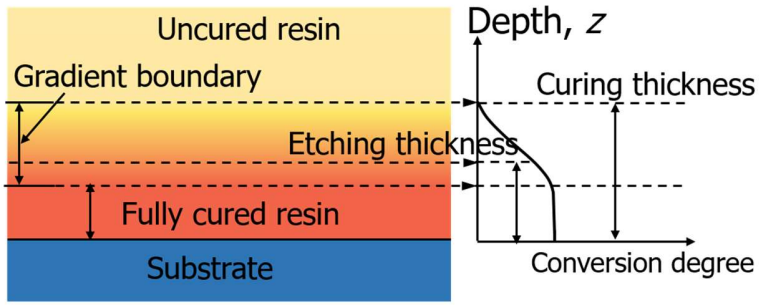

Figure 3-8 Curing condition and gradient boundary in EWNSL

3.7 Refractive index increase

It is known that the conversion degree can directly indicate the conversion degree; however, the difficulties of measurement of conversion degree make it hard to achieve the in-process measurement of the conversion degree. Therefore, some other characteristic change of the resin in the curing process should be utilized to evaluate the curing level of the resin. In the curing process, there are two apparent accompanying phenomena:

shrinkage and increase of refractive index of the cured resin. Shrinkage is hard to detect and analyze due to it starts from the beginning of the curing process when the resin is still in the liquid state. The variation of refractive index, as a change of optical characteristics, is an ideal measurement parameter since optical measurement normally has the advantage of non-contact, high sampling rate and low damage of sample. Therefore, my measurement method is just based on this point, I utilize the refractive index increase of the cured resin and detect the optical response from the resin.

The refractive index change of the resin after the photo-polymerization is surely a proven fact and claimed by many researchers. In Fujita's research [85], the refractive index of several types of resin has been measured. His results show that all of the resin he measured has a refractive index increase after the polymerization, but the increment of refractive index differs with the types of resin, as shown in **Figure 3-9**.

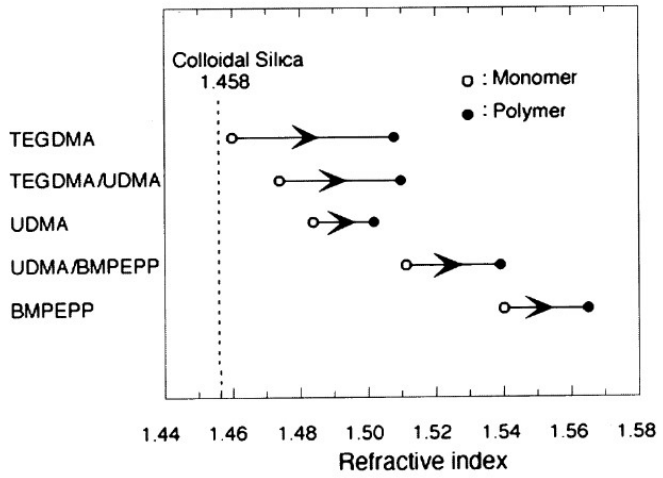

Figure 3-9 Variation of monomer's refractive index after polymerization [70]

In Howard's work, the relation between the refractive index and the conversion degree was measured and a linear relationship was proved, as shown in the **Figure 3-10** [86].

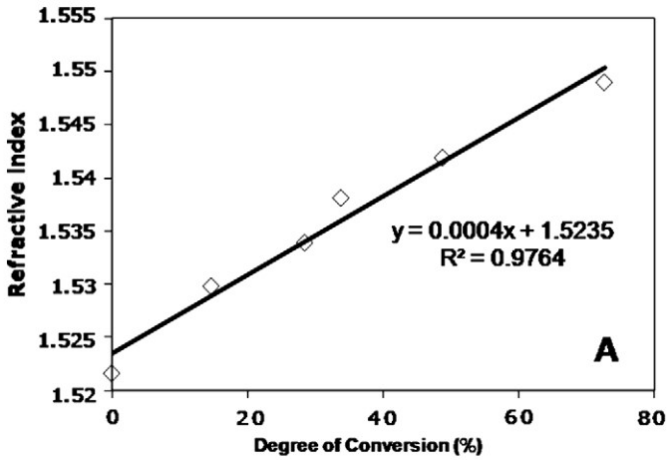

Figure 3-10 Relationship between refractive index and conversion degree measured by Howard [86]

The numerical relationship between the refractive index and the conversion degree differs from the types and concentration of the resin used in the experiment, therefore, in my investigations, I measured their relationship by applying refractometer and Raman spectroscopy in the same time. This experimental work will be demonstrated in chapter 5. Based on this measurement results, once the refractive index of the cured resin is measured, the corresponding conversion degree is able to be obtained.

3.8 Definitions of noun phrases

Definitions of noun phrases used in this thesis were summarized and listed in the following contexts:

- **The degree of conversion** is defined as the percentage of reacted carbon double bonds (C=C) from the monomers present in their polymeric matrices. The extent of reaction of photo-polymerization or curing process is generally expressed by the degree of conversion, is also referred to as conversion degree, the degree of monomer conversion, the degree of curing and degree of polymerization. The physical and mechanical properties of resin composites are strongly influenced by the degree of conversion.

- **Gradient boundary** means a range where resin in half-cured state with a gradient changed conversion degree and refractive index.

- **Critical etching degree** is the maximum conversion degree of the resin can be removed by the etching process. In the etching and drying process, resin with a conversion degree smaller than critical etching degree will be removed.

- **Etching width:** the width of cured resin after etching and drying.

- **Etching thickness:** the thickness of the cured resin after etching and drying.

- **Curing thickness:** The thickness of the cured resin whose conversion degree is not zero

CHAPTER 4. ANALYZATION OF OPTICAL RESPONSE FROM NEAR-SUBSTRATE RESIN USING THE TOTAL INTERNAL REFLECTION AT THE CRITICAL ANGLE

This chapter presents the basic principle of my measurement method. The proposed measurement method is on the basis of the refractive index increase of resin in the curing process.

It is known that the refractive index influences the optical response, therefore, the in-process measurement can be achieved by optical measurement method. Optical measurement is a wide measurement field. There are a lot of methods that can directly or indirectly measure the variation of the refractive index. In my investigation, in order to meet the requirements of detection in a high sampling rate, it requires a measurement of the whole bottom surface of the cured resin. Also, a compact measurement system is expected to be integrated into the measurement systems.

Based on the above requirements, I proposed the in-process measurement using the refractive-index-sensitive feature of total internal reflection at the critical angle. In this case, once the refractive index of the resin increase, the condition of total internal reflection will be destroyed. As a result, the reflection from the cured resin will decrease drastically, which means the cured resin can be easily distinguished with the uncured resins according to the reflection.

The basic knowledge about the total internal reflection and Fresnel equation is introduced in this section, and then how I applied total internal reflection at a critical angle

into in-process measurement will be demonstrated. At last, I will explain the difference when critical-angle reflection method is applied into the in-process measurement in MSL and EWNSL. Even I used the similar measurement method in both fabrication systems, they are totally different in the optical response, since the resin cured by evanescent wave is in the thickness of sub-micron meters and the reflection from the top and the bottom surface of the cured resin have a strong interference, as well as the influence of multi-reflection. While optical response from the thick layer is much simpler since most of the light that propagates into cured resin will transmit away for the sides of the cured resin due to large refractive angle.

4.1 Fresnel equations and total internal reflection

Fresnel explains the simplest reflection that light transmits towards an interference of two medium with refractive index contrast. Here I talk about the internal reflection that light transmits from a high-refractive-index medium to a low-refractive-index medium as shown in **Figure 4-1**.

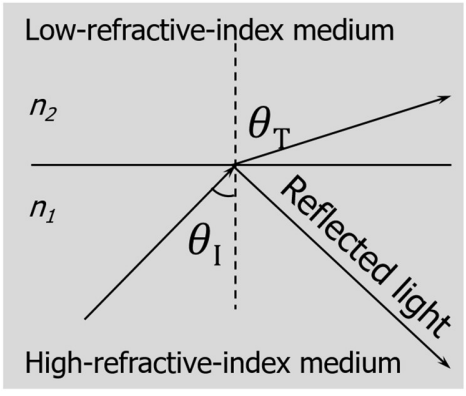

Figure 4-1 Diagram of internal reflection

When light strikes to the interface of a medium in a high-refractive-index n_1, and a second medium with low refractive index n_2, both reflection and refraction of the light will occur in case of the incident angle is not lager than the critical angle. The Fresnel equations describe the ratio of the reflected and transmitted light to that of the incident light. As we can see in **Figure 4-1**, the angles of the incident, refracted light are given as θ_I and θ_T, respectively. The relationship between incident and refraction angles is given by the Snell's law:

$$n_1 \sin\theta_I = n_2 \sin\theta_T \tag{4-1}$$

The reflection coefficient (reflectivity) r is the ratio of the reflected light's electric field amplitude to that of the incident light. The transmission coefficient (transitivity) t is the ratio of the transmitted light's electric field amplitude to that of the incident light. For s- and p- polarization, the calculation equations of r are different. In each case that an incident light at an angle of θ_I and refracted in at an angle of θ_T, corresponding to the above **Figure 4-1**. In case that ignores the absorption (n is complex), the reflectivity in each polarization can be calculated as the following equations:

$$r_P = \frac{n_2 \cos\theta_I - n_1 \cos\theta_T}{n_2 \cos\theta_I + n_1 \cos\theta_T} \tag{4-2}$$

$$r_S = \frac{n_1 \cos\theta_I - n_2 \cos\theta_T}{n_1 \cos\theta_I + n_2 \cos\theta_T} \tag{4-3}$$

According to these equations, the reflectivity is determined by the refractive index of both mediums and the incident angle. Therefore, the variation of the refractive index

must directly influence the reflectivity. In addition, the expression of reflectivity is not in a linear relationship with the incident angle and refractive index, therefore, there must be a particular incident angle where reflectivity shows the highest sensitivity to the variation of refractive index.

4.2 Optical response of total internal reflection at the critical angle

In order to clearly understand the optical response in the MSL/EWNSL, the refractive index of resin (1.47 for the uncured resin and 1.51 for the cured resin) and a high-refractive-index transparent substrate (1.78) is brought into the Fresnel equations. The reflectivity as a function of incident angle in both of the cured and the uncured resin when the incident light is in p- and s- polarization, respectively, are shown in **Figure 4-2**.

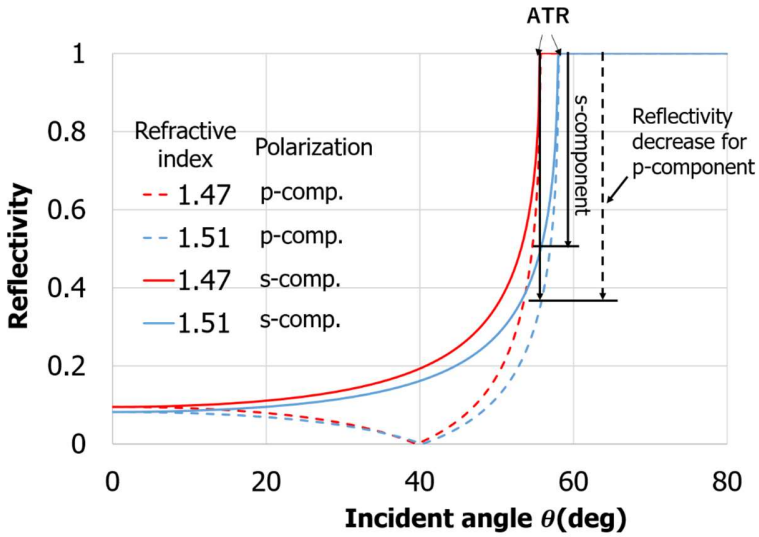

Figure 4-2 Reflectivity of s- and p- component as a function of incident angle

It is shown that the angular spectrum of reflectivity positively shifts after the resin is cured. More importantly, at the critical angle of the uncured resin, the reflectivity between the uncured and the cured resin differs greatly, which means it is possible to directly observe the horizontal shape of the cured resin by detecting reflection distribution at the critical angle. In this case, light reflected from the cured resin shows much lower intensity than the uncured resin. The reason that I use total internal reflection at the critical angle is obvious: highest sensitivity of refractive variation is obtained at the critical angle.

Comparing the reflectivity of s- and p- component in **Figure 4-2**, it is apparent that reflectivity of p-component shows larger decrease at the critical angle when the resin is cured, which means p-component has higher sensitivity than the s-component when applying proposed measurement method. In addition, for p-component, the existence of Brewster's angle can be applied to reduce the reflection from two sides of the prism as shown in **Figure 4-3**. In order to generate the total internal reflection, light is incident from one side into the prism, when the incident angle is near to Brewster's angle the reflection from the interface between air and prism can be reduced largely. This does not just provide a higher intensity of measurement light, but also reduce the interference and noise generated by the reflection when the light propagates out of the prism, which is a really serious problem especially when a laser is used as the measurement light.

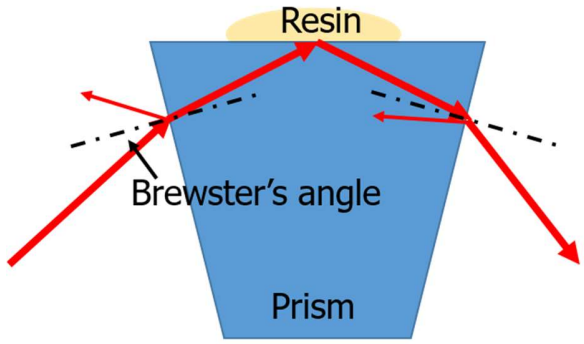

Figure 4-3 Illustration of light incident into the prism. Reflection in two sides of the prism can be reduced largely, if p-polarization light is incident at Brewster' angle.

The reflectivity contrast between uncured and cured resin in p-component is plotted in **Figure 4-4**. It is obvious that maximum reflectivity contrast is obtained at the critical angle of the uncured resin; while at the critical angle of the cured resin, there is no reflectivity contrast which means I cannot distinguish the cured and the uncured resin in the critical angle of the cured resin. In the following context, all the critical angle means the critical of the uncured resin, where the maximum reflectivity contrast is obtained.

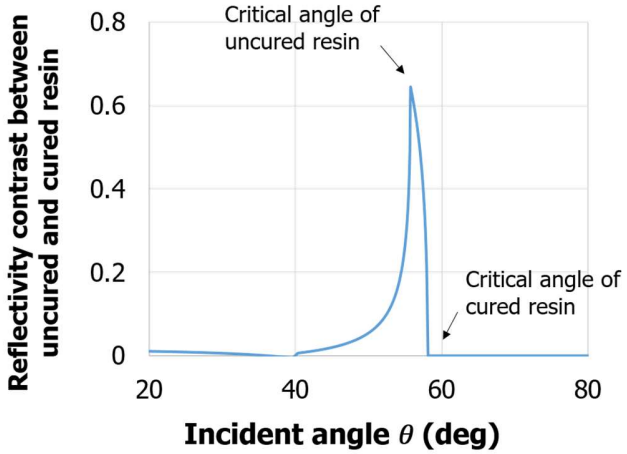

Figure 4-4 Reflectivity contrast as a function of incident angle between uncured and cured resin

Above results prove that it is possible to directly distinguish the uncured resin with the cured resin by detecting the reflectivity from the interface between the resin and the high-refractive-index substrate. In addition, it also shows that the maximum sensitivity is obtained when the incident angle is at the critical angle of the uncured resin. Actually, in this incident condition, the measurement lights transmit into the bottom of the uncured resin will be totally reflected, and therefore, there will no light propagate into the uncured resin and generate reflection from the top surface of the resin, which reduces the noise to a great extent.

What I discussed here is just the reflection contrast between the cured and the uncured resin. It helps us directly distinguish the uncured and the cured resin. However, this is not enough for my target. In the MSL, I want to measure the distribution of the conversion degree of the near-substrate resin, while in EWNSL, my measurement target is the thickness of the cured layer. Therefore, it necessary to study the relation between the measurement targets with reflectivity and clarify how I get the required parameters from the reflectivity. For two research topics, the diffidence of optical response analyses will be discussed in the following section and the detailed measurement method will be explained in chapter 5 and chapter 6, respectively.

4.3 Different models for optical response in different thicknesses

I proved that the cured resin can be directly distinguished with the uncured resin by detecting the reflection distribution from the measurement light incident at the critical angle; however, my target is no just observe the cured resin from the bottom. Other

information like conversion degree or thickness of the cured resin should be derived from the reflectivity, which needs a more detailed analyzation of the optical response in case of total internal reflection at the critical angle.

Firstly of all, let us consider the topic where the in-process measurement in applied in the MSL. In this case, the ultra-thin layer cannot be fabricated, and the minimum thickness of each is in several micron meter scale and a new layer is directly cured on the previously cured layer; therefore, there is not top surface of the cured resin to generate the reflection. The optical response model becomes simple in this case, which is like the most simple reflection model from the interface of the medium, as shown in **Figure 4-5**.

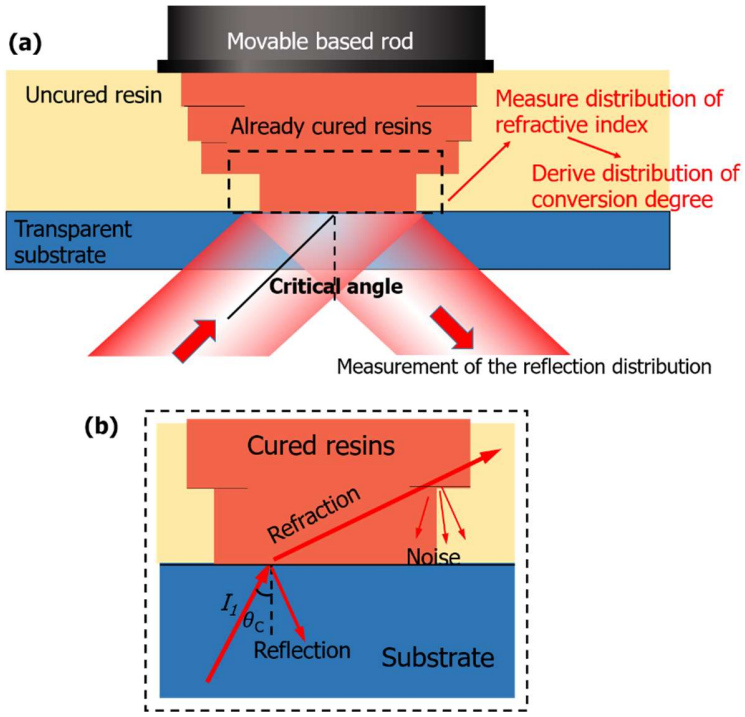

Figure 4-5 Optical response using total internal reflection at the critical angle, when cured layer is in large thickness and stacked together, for resin cured by fixed-surface type MSL.

According to the Fresnel equations, the refractive index of resin in the bottom can be directly calculated from the reflectivity. As I discussed in chapter 3, the relationship between conversion degree and the refractive index has been measured before and the linear relationship has been proved. Therefore, if this numerical relationship of the resin used in my experiments is measured, the in-process measurement of the conversion degree distribution of the near-substrate resin can be simply achieved by measuring the refractive index distribution near the substrate.

Then for in-process measurement in EWNSL, in this case, the thickness of the cured resin is in submicron scale, due to the resin is cured by evanescent waves, as shown in **Figure 4-6**. In this case, each new layer is not coated on the previous layer and the cured resin is located on the substrate individually. As a result, the part of the light that propagates into the cured resin will be totally internally reflected from the top surface between the cured and the uncured resin.

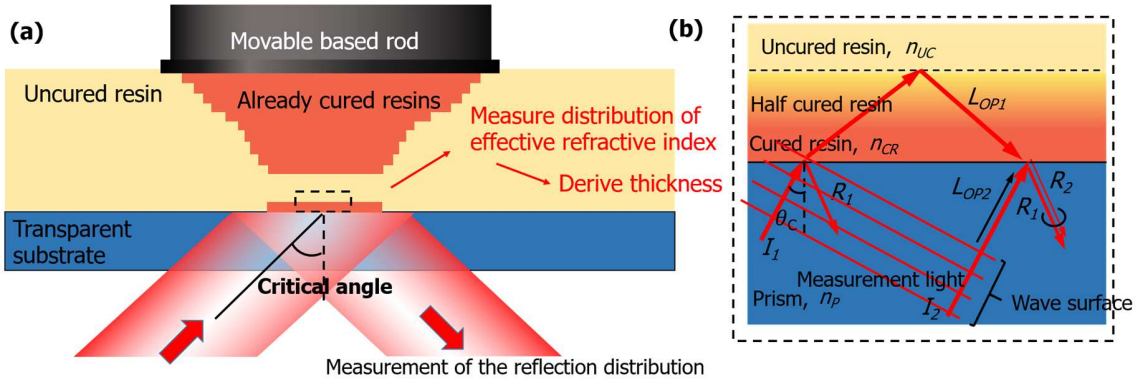

Figure 4-6 Optical response using total internal reflection at the critical angle, when thickness of cured resin is in submicron scale, for resin cured by EWNSL.

Due to a part of light is reflected from the bottom of the cured resin and another part of light will transmit into the cured resin. This part of the light sticks on the top surface

of the cured resin and is totally reflected from the interface between cured and uncured resin. The reflection from the bottom and top surfaces will generate interference and this interference is mainly determined by the thickness of the cured resin which directly influences the difference of optical path. As a result, the variation of the thickness of cured resin can be measured in a form of change of reflection intensity after interference. Therefore, it is possible to obtain the thickness information of the whole surface by detection the reflection distribution, which will be applied in the in-process measurement of thickness in EWNSL.

Above models are the ideal conditions that ignore the gradient boundary. Actually, the development of the gradient boundary is totally different when the resin is cured by the propagating light and the evanescent wave, especially in the normal direction of the substrate.

For conventional MSL using propagating light, when the exposure light transmits deeply into the resin, there is an intensity decrease due to the absorption of the resin according to Beer-Lambert's law, as shown in **Figure 4-7**. For a certain exposure time, the exposure beam with the intensity decrease leads the resin being cured in a different rate. The resin near the substrate is exposed by a higher intensity and therefore has higher conversion degree compared with the resin far from the substrate, as shown in **Figure 4−7**. However, due to the absorption of the resin is really weak when the curing depth is in a micron scale (I measured the absorption of the resin, which will be demonstrated in the Appendix), in the practical production of MSL before reaching the depth where the conversion degree decrease to an obvious value light will be blocked by the previous layer.

Therefore, for MSL we can treat the conversion degree of each layer is constant in the normal direction of the substrate. This means once conversion degree of the resin in the bottom is measured, this conversion of the whole layer is known.

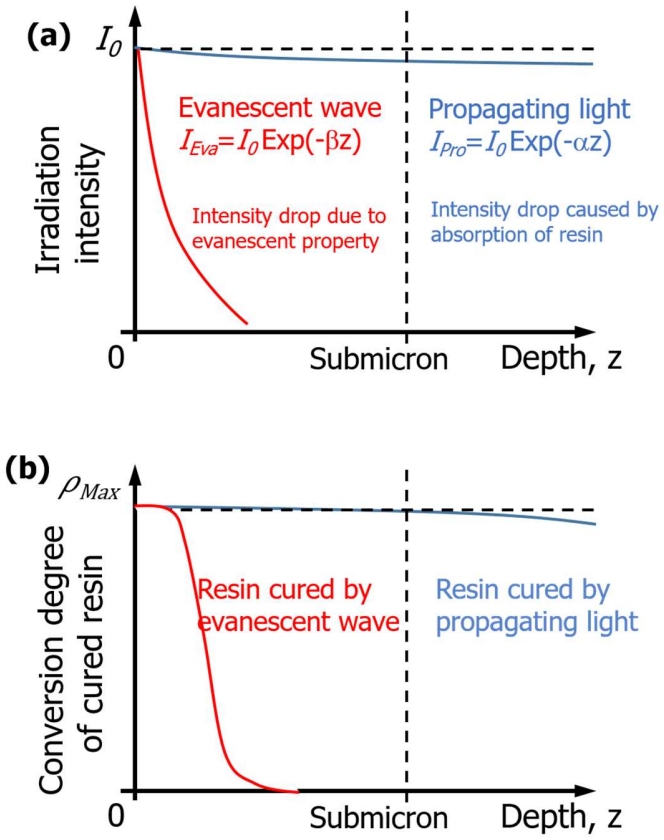

Figure 4-7 Difference of exposure using evanescent wave and propagating wave in case of (a) irradiation intensity and (b) conversion degree of cured resin in the normal direction of the substrate.

For EWNSL, each layer is even in a smaller thickness than the resin cured in MSL and therefore, the intensity drop caused by absorption can be ignored as well. However, the intensity decrease caused by the feature of the evanescent wave is quick. The drastic decrease of evanescent wave means the obvious variation of conversion degree in the normal direction of the substrate, as shown by the red line in **Figure 4−7**. Therefore, there

is a gradient boundary of the cured resin in EWNSL that is not negligible. Based on the fact that the refractive index increase with the conversion degree in a linear relationship, the gradient boundary has a feature of gradient-change refractive index, which influences the reflection from the top of the cured resin and makes the reflection more complex (the propagation path of the light in the cured resin is bent). As a result, it is hard to calculate the relationship between the curing thickness (or the etching thickness) with the reflectivity, and the calibration work of this relation is necessary. Regarding this topic, a detailed explanation is in chapter 6.

In summary, the critical-angle-reflection method can be applied in both of MSL and EWNSL, and the curing process of the resin generates the influence on reflectivity which can be in-process measured; however, the optical response in MSL and EWNSL is totally different was analyzed respectively.

CHAPTER 5. IN-PROCESS MEASUREMENT OF CONVERSION DEGREE OF RESINS IN THE MICRO- STEREOLITHOGRAPHY

This chapter presents how I make an in-process measurement in MSL to indirectly measure the distribution of the conversion degree of cured resin by detecting the reflection distribution when the incident angle is at the critical angle. First of all, the verification experiment that proves the reflectivity decrease in the curing process is illustrated in this chapter. In order to obtain the relationship between the conversion degree of resin and the reflectivity, both mathematical analysis and calibration experimental has done. In the mathematical analysis, the refractive index distribution of the near-substrate resin is calculated from the reflection. In the calibration experiment, the numerical relationship between the conversion degree and refractive index is measured by using Raman spectroscopy and refractometer at the same time. Finally, the in-process measurement of the distribution of conversion degree is demonstrated in this chapter. The results of conversion degree distribution calculated from reflectivity distribution are plotted and discussed.

5.1 Verification experiments on bulk sample

A verification experiment has been done using a bulk sample to confirm the increase of refractive index and the reflectivity decrease in the fabrication process. **Figure 5-1** depicts the optical configuration of the initial verification experiment for the measurement method using the total internal reflection at the critical angle. An optical fiber was used to deliver light in a wavelength of 638 nm into an illumination section fixed on a

rotating stage. After collimated and polarized, the light struck on the resin and was reflected from the interface between resin and substrate. Then the reflected light propagated into imaging section fixed on another rotating stage and was imaged to CMOS camera after transmitting though the imaging lens.

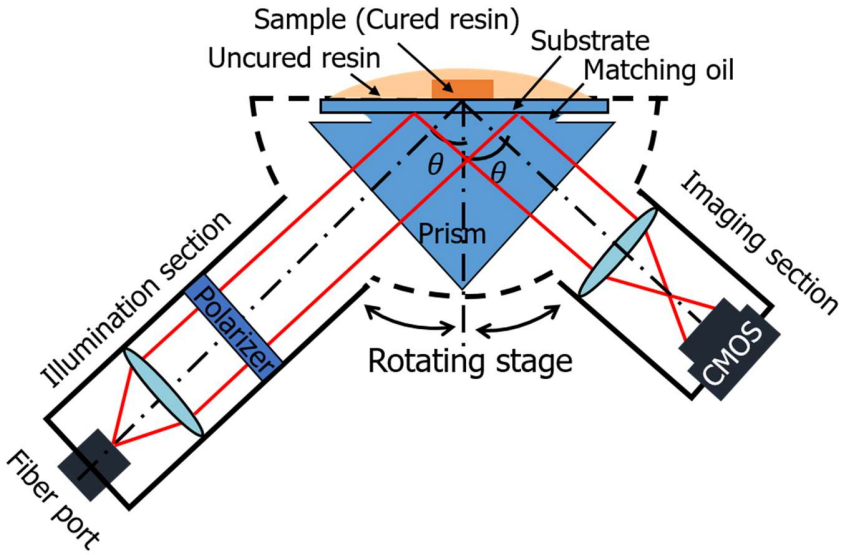

Figure 5-1 Experiment setup of verification experiment on bulk sample

Bulk cured resin that was submerged in the uncured resin was observed in various incident illumination angle (fabrication section was not used in this experiment). **Figure 5-2** (a) to (c) shows the images recorded by a CMOS camera when the incident angle was in 54.1, 55.7 and 61.2 degree. Cured resins were in the center of the image. Around the cured resin, there were some dark spots whose gray value did not change with incident angle. They were background noises caused by the dust. According to the refractive of prism and resin, the critical angle of uncured and cured resin was 55.7 and 58.1 degree respectively. The relationship between the critical angle and incident angle is shown in **Figure 5-2** (d).

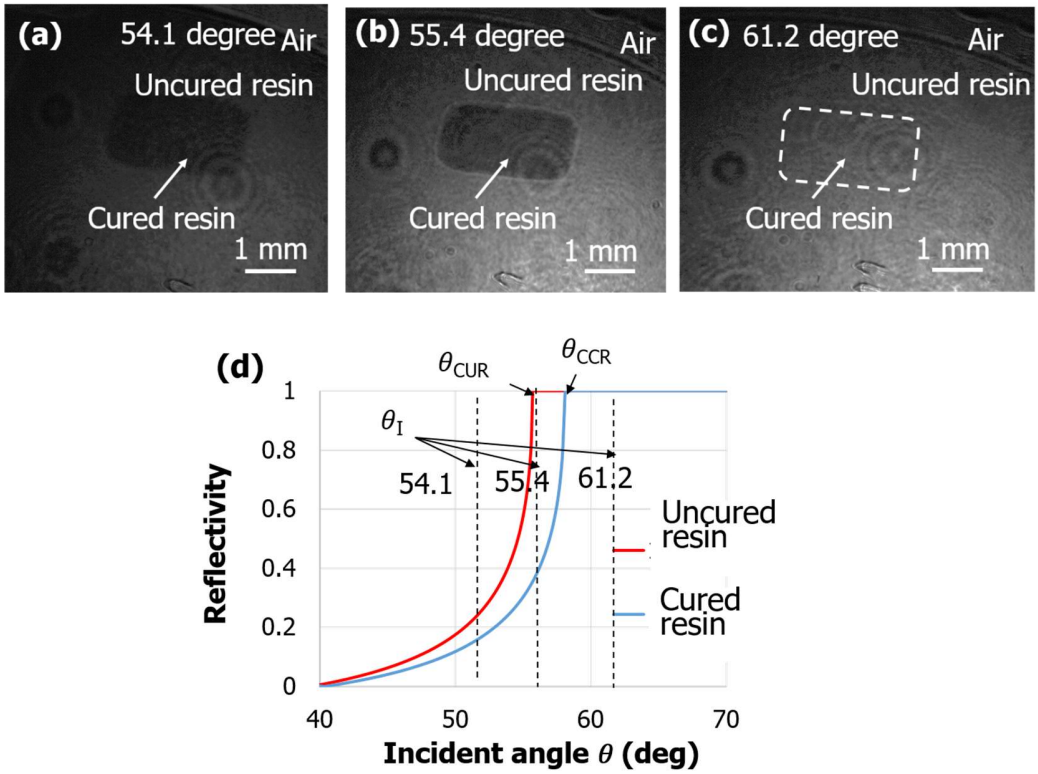

Figure 5-2 Experiment on bulk sample in various incident angle. Intensity distribution of reflected light launched in incident angle of (a) 54.1, (b) 57.1 and (c) 61.2 degrees. Figure (d) shows the relation between incident angle and critical angle

Figure 5-2 (a) shows the image taken in case of θ_I (incident angle) < θ_{CUR} (critical angle of uncured resin) < θ_{CCR} (critical angle of cured resin). Since both uncured resin and the cured resin provided low reflectivity in such an incident angle, the brightness of resin's both states were low, and there was only a slight variation between cured resin and uncured resin shown in this figure. **Figure 5-2** (b) shows the image gained when $\theta_{CUR} < \theta_I < \theta_{CCR}$. In this case, the total internal reflection occurred at the interface between the uncured resin and substrate, which leads the highest intensity of reflected light from uncured resin; while total internal reflection did not occur at the bottom of the cured resin since the current incident angle was smaller than the critical angle of the cured resin. As a result, both the brightness of the uncured and the cured resin vary largely; the position and the shape of the

cured resin can be easily observed. This result confirmed the feasibility of my method when the incident angle is at the critical angle. **Figure 5-2** (c) shows the image when $\theta_{CUR} < \theta_{CCR} < \theta_I$. It is obvious that two states of the cured resin cannot be distinguished as total internal reflection occurred at the bottom of both and insensitivity of reflected light from resin in both states reach maximum.

The cross-section of gray value near the boundary region stretches from the cured to the uncured resin in the various incident angle is plotted in **Figure 5-3**. The grey value of the image that directly indicates the intensity of reflection was used to evaluate the reflectivity. In order to remove the noises in the images, every curves in this figure were averaged from ten lines stretching the same distance. It is obvious that the gray values of the cured resin and uncured resin vary with incident angle. The reflectivity contrast became maximum when the incident light was near the critical angle.

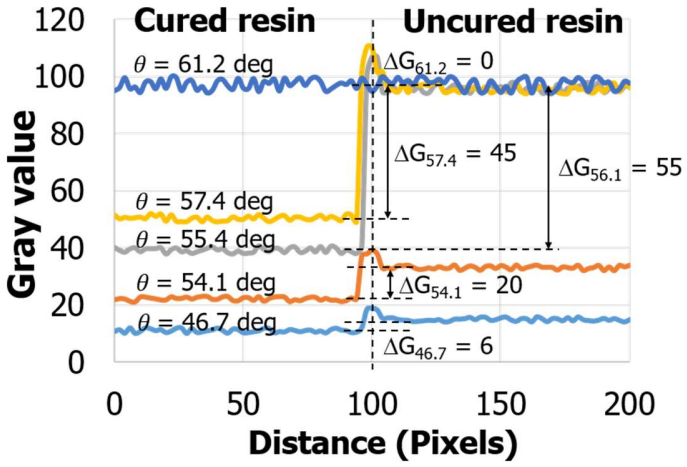

Figure 5-3 Cross-section of averaged grey value near boundary region between cured and uncured resin

At the boundary, there were small peaks that show the increments of reflectivity, which was caused by the scattering at the boundary. The reflectivity drop of cured resin

was calculated by dividing averaged gray value drop by the gray value in the total internal reflection condition (around 96 grey value units).

The reflectivity contrast obtained by experiment was plotted with the theoretical value gained by calculating the reflectivity difference between the cured and the uncured resin, as shown in **Figure 5-4**. It shows that the experiment results are well agree with the theoretical value, which confirms the refractive index increase of resin and also proves my experiment can well control the incident angle of the measurement light.

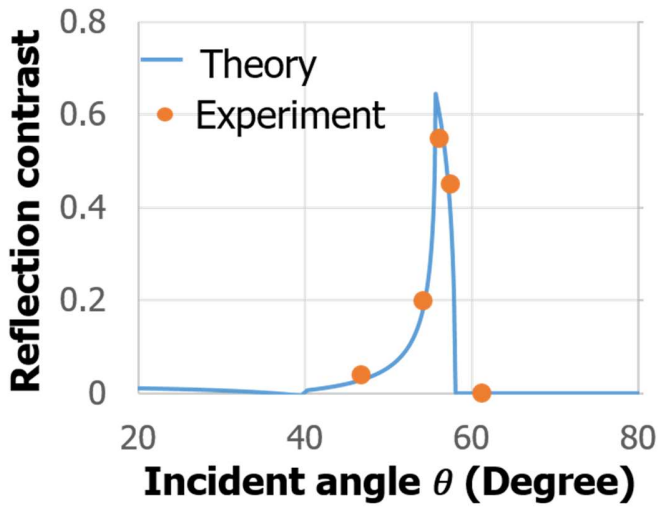

Figure 5-4 Experimental grey contrast and theoretical reflectivity contrast as function of incident angle.

5.2 Verification experiment of in-process measurement

In the first verification experiment, what I measured is the resin sample prepared in advance. The sample was fully cured already and the size of it is in millimeter scale. In this experiment, the dynamically curing process will be measured by the proposed method to

confirm that the reflectivity successively decreases in the curing process. Most important, I want to prove the spatial size (width) of the cured resin will keep increasing in the curing process, which will be used to determine the proper exposure time.

The experiment setup is shown in **Figure 5-5**, the measurement section was similar to that of the previous verification experiment. The measurement light was delivered into the bottom of the cured resin and the reflection was collected by the detection section on the other side. Two arms of measurement section were in the critical angle calculated by the refractive index of the uncured resin and the substrate. In order to clearly observe the cured resin in the micron scale, one more lens was used in the imaging system compared with the previous experiment. The focal distance of the first lens (lens near the prism and sample) was 30 mm and the second lens was 150 mm. Therefore, the magnification of the imaging system is 5 times.

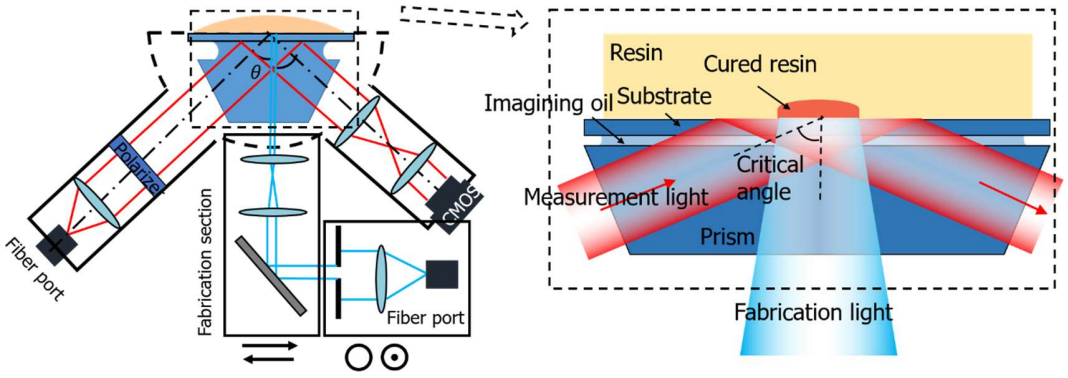

Figure 5-5 Experiment setup of verification experiment of in-process measurement

Besides the measurement section, a simple fabrication section was supplemented into this setup, where the irradiation for fabrication was incident from the bottom to the resin. An x-y movable stage was used to move the exposure beam controlling the position of the curing. In order to limit the spot size of the exposure beam, the aperture was used to

cut apart of collimated light and then two lenses in focal distances of 200 and 20 mm were used to further narrow down the spot size to a micron scale. The intensity of the fabrication light was measured in 1.5 mW before transmitting through the aperture. After propagating through the aperture, the intensity was reduced a lot. Since this was a verification experiment and my target was just to confirm the reflectivity decrease, the exact intensity of fabrication light in the cured resin was not preciously measured.

The left figure in **Figure 5-6** shows the magnified image of the curing area. It is obvious that the measurement light is incident in a large angle while the fabrication light was vertically incident from the bottom. In order to avoid the damage on the prism, the resin was put on the substrate. The substrate is in the same refractive index with the prism (1.78). Between the substrate and prism is the refractive-index-matching oil.

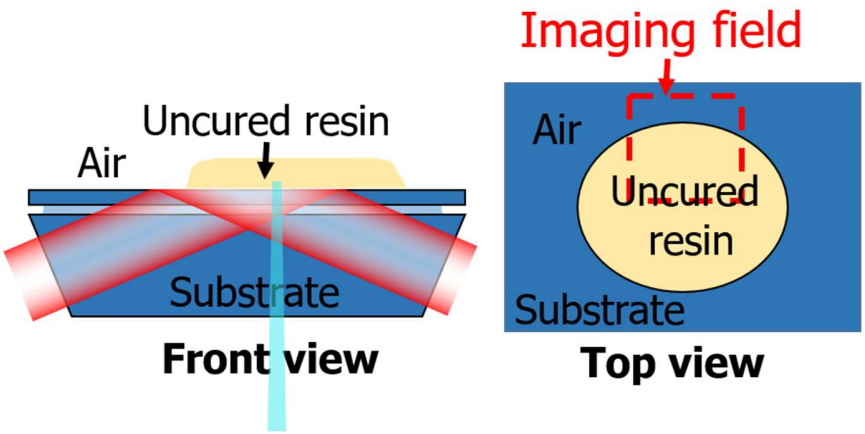

Figure 5-6 Experiment setup and imaging field

It is notable that the fabrication light was in a wavelength of 405 nm while the measurement light was in a wavelength of 638 nm. Measurement light in such wavelength generated a small impact on the curing process, especially when measurement light is weak

enough, and therefore, the influence of measurement light on the conversion degree was neglected.

In the verification experiment, the reflection from the bottom of the resin was recorded by CMOS camera. It is notable the measurement field did not cover the whole field of the resin. Only a part of the resin was in the field of view (imaging field), as shown in the right figure in **Figure 5-6**.

The experiment results were shown in **Figure 5-7**. They were original in a form of the video file and cut into figures in various exposure duration. **Figure 5-7** (a) shows the reflection distribution before the resin was exposed by the fabrication light. It is notable that there is a clear curved black line in the figures. It was the boundary of the liquid drop of the uncured resin and it was visible due to the scattering of at the boundary reducing the reflection of the measurement light. **Figure 5-7** (b) to (h) show the reflection distribution after the resin was exposed in a certain time. By comparing the differences of this series of pictures, the variation of the cured resin can be directly observed due to the increase of the gray value (reflection decrease).

It is obvious that with the exposure time increase, the reflection in the center of the exposure area decreased drastically and the range of the cured resin (the field showed low reflection) was enlarged. These results proved that the reflectivity used to evaluate the conversion degree successively decreases in the curing process, as well as confirmed that spatial size (width) of the cured resin keeps increasing in the curing process, which will be used to determine the proper exposure time.

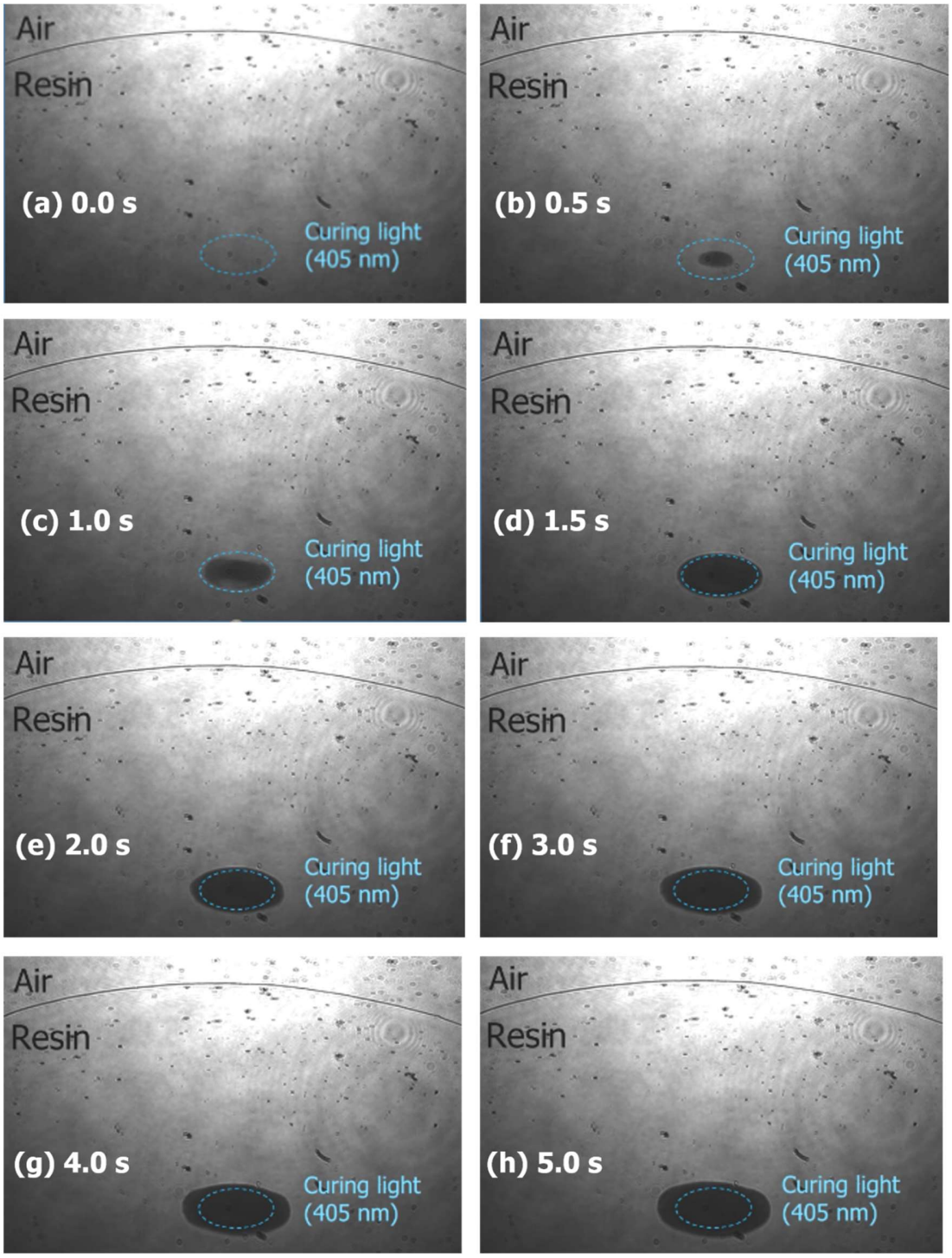

Figure 5-7 The experiment results of verification experiment of in-process measurement when exposure in increasing duration when (a) 0.0 s (b) 0.5 s (c) 1.0 s (d) 1.5 s (e) 2.0 s (f) 3.0 s (g) 4.0 s and (h) 5.0 s.

5.3 Theoritical relation between reflecitivity and refractive index of the cured resi

Two verification experiment effectively proved that the curing process of the resin can clearly observed by the proposed method; however, my measurement target is not just to observe the cured resin, but also measure the distribution of conversion degree. As I explained that my measurement method is based on the refractive index variation of the cured resin. The strategy is to detect the optical response (reflection) from the bottom of the resin, then calculate the refractive index distribution of the near-substrate resin, at last, obtain the distribution of conversion degree of the resin according to the numerical relationship between the refractive index and the conversion degree. Based on this strategy, first of all, it is to calculate the reflectivity in an increase refractive index of the cured resin.

In MSL, as I explained before, due to the new layer is recoated on the previous layer and there is no top surface, the reflection is only from the interface between resin and substrate. In my experiment, the incident angle and the refractive index of the substrate is already known, therefore the distribution of the refractive index of the bottom of the resin can be simply calculated according to the Fresnel's equation.

Figure 5-8 shows the reflectivity decrease in various incident angle when resin's refractive index keeps increasing. As expected, reflectivity simultaneously decreases with the increase of the refractive index. In addition, for a specific refractive range, exist optimal measure angles for the different refractive range. In consideration of the experimental difficulty to change the incident angle during curing process (extremely fast reaction), the

incident light should be fixed and 55.7 degrees was used in my investigation, which is the critical angle of the uncured resin.

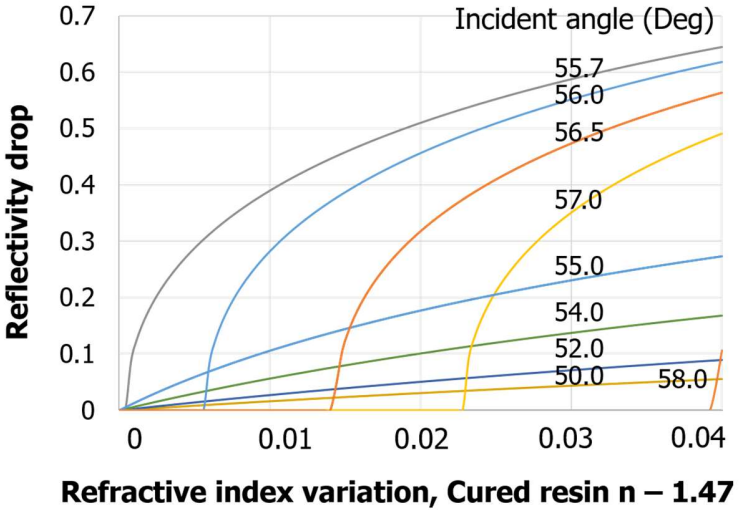

Figure 5-8 Theoretical explanations of reflectivity as a function variation of refractive index in different incident angle

Based on the above calculation, the relationship between reflection and the refractive index of near-substrate resin is obtained. In order to achieve in-process measurement of conversion degree. It necessary to know the exact numerical relationship between conversion degree and the refractive index of the cured resin. This relationship is experimentally measured, the experiment setup and results are shown in the next section.

5.4 Experimental measurement of the relationship between refractive index and conversion degree of cures

In this experiment, we measured the relationship between conversion degree and the refractive index of the cured resin at the same time using Raman spectroscopy and critical angle shift method. During the measurement, the resin was in a condition of

successive exposure to make the conversion degree and refractive index keep increasing. Due to both methods make a point detection, in the experiment, in order to make sure the accuracy, I set the measurement point of two method in the same position.

5.4.1 Experiment setup

The experiment setup is shown in **Figure 5-9** and **Figure 5-10**. It consisted of four sections. The refractive index of substrate and prism was 1.78. Between substrate and prism, immersion oil was used to remove the air gap. The measurement section of conversion degree was based on the Raman spectroscopy. The measurement of the refractive index was based on the fact that the critical angle shifts when the refractive index of resin changes. There was also an exposure section using light in a wavelength of 405 nm to excite the photo-polymerization. Resin (KC1162) was put on the substrate, the measurement point of the Raman spectroscopy and critical-angle-shift based refractometer were in the same position. Due to the conversion degree and refractive index were measured at the same time, for each conversion degree state the corresponding refractive index can be determined, and their relationship can be obtained.

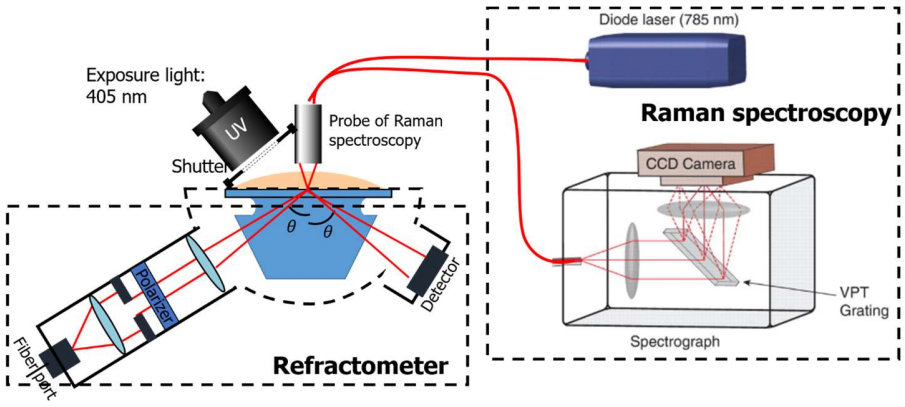

Figure 5-9 Diagram measurement of relationship between conversion degree and refractive index

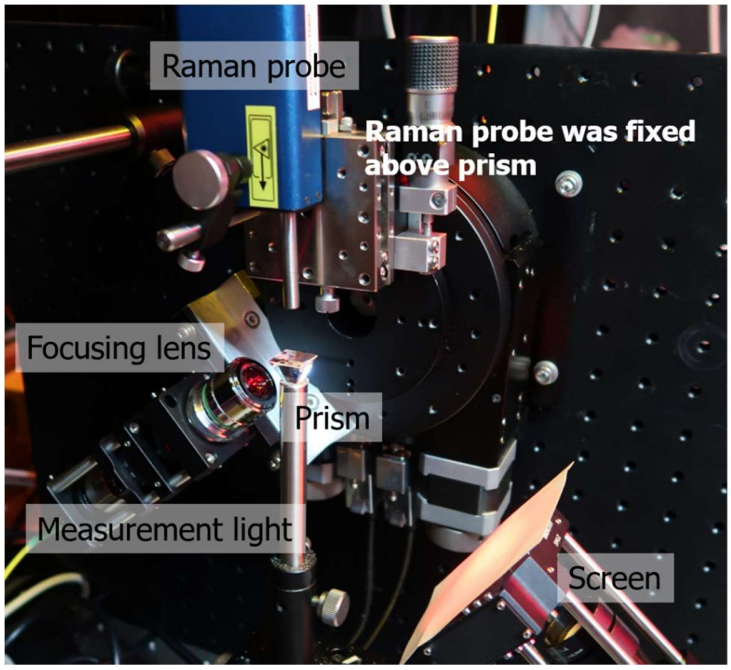

Figure 5-10 Experiment setup of measurement of numerical relationship between conversion degree and refractive index

The probe of Raman spectroscopy was fixed over the cured resin to measure the conversion degree of carbon double bond (C=C) by detecting the intensity variation of the peak of the carbon double bond in the spectrum. The intensity change of the peak of C=C directly express the conversion degree, and C=O bone was used as the reference since C=O does not change in the photo-polymerization process. Therefore, the conversion degree can be calculated by the following equation:

$$\alpha = 1 - \frac{\frac{\text{Cured C=C}}{\text{Cured C=O}}}{\frac{\text{Initial C=C}}{\text{Initial C=O}}} \tag{5-1}$$

According to the above expression, for an example, the spectrum in **Figure 5-11** was used to calculate the conversion degree of the resin in different exposure durations. Results show that resin exposed by 10 seconds and 30 second was in conversion degree of 25% and 54%, respectively.

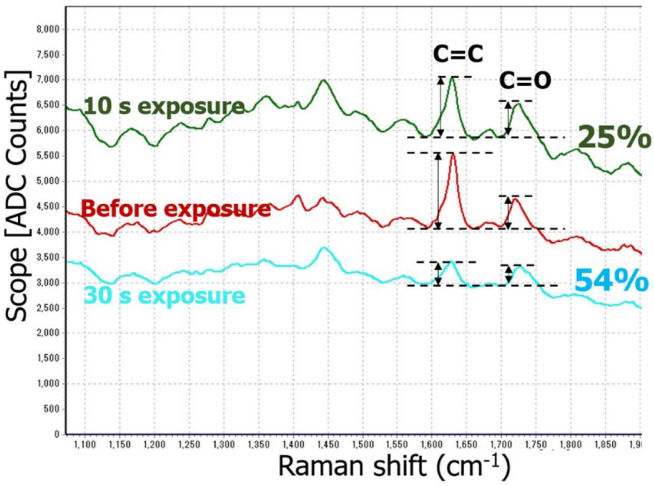

Figure 5-11 Spectrum of measurement of resin using Raman spectroscopy, the intensity change of the peak of C=C directly express the conversion degree, C=O bone was used as the reference since C=O does not change in the photo-polymerization process

The critical-angle-shift method was used to detect the refractive index change of resin in a point. In this method, a focused beam was delivered to the bottom of the cured resin. After reflection, the angle spectrum was plotted on the detector. There was a clear boundary to express the critical angle, as shown in the insert figure in **Figure 5-12**. According to the position of boundary that represents the position of critical angle, the refractive index can be calculated by Snell equation.

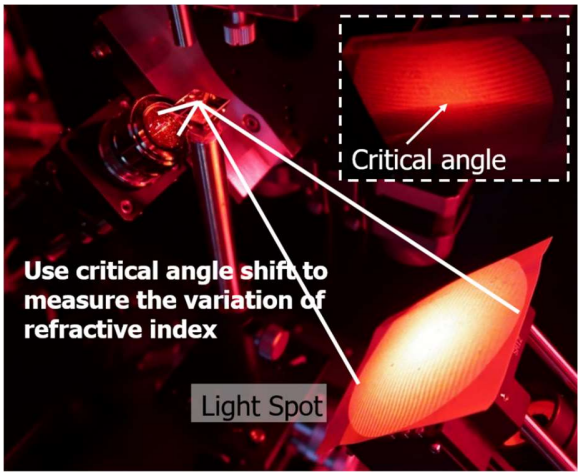

Figure 5-12 Refractive index measured by critical angle shift method. The obvious line in at the critical angle of measured object

5.4.2 Results and discussions

In this experiment, resin KC1162 was used as a sample. In the uncured state, the refractive index of this resin is 1.478 according to the commercial refractometer. Due to the measurement light is well focused and it is in a high intensity, measurement in a long duration will damage or burn the resin, therefore the experiment was stopped before resin reach maximum conversion degree. Since a single point of resin was measured by Raman spectroscopy and refractometer at the same time, one the conversion degree was measured, the corresponding refractive index in that state was detected. The relationship is plotted in **Figure 5-13**. In this figure, a linear relationship within 60% conversion degree was proved. Actually, the linear relationship was also proved by reference [57] in chapter 3. The types of resin were different and therefore the variation range of the refractive index is different between my measurement results and that in the reference, but the linear relationship found by other enhanced the feasibility of my results.

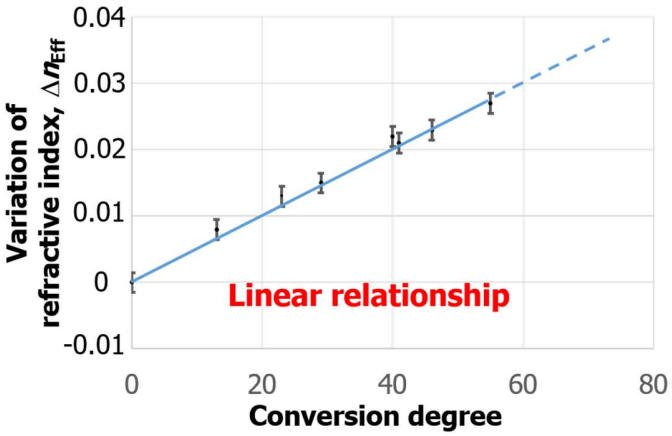

Figure 5-13 Measurement results of relationship between variation of refractive index and conversion degree of cured resin

The linear relationship makes it possible to directly calculate the conversion degree of near-substrate resin from the reflectivity measured by the proposed method. Firstly, the refractive index of near-substrate resin was calculated according to the Fresnel equation, then according to the calculated refractive index, the conversion degree can be obtained using the linear relationship. The conversion degree as a function of refractivity change when the incident light is at the critical angle is plotted in **Figure 5-14**.

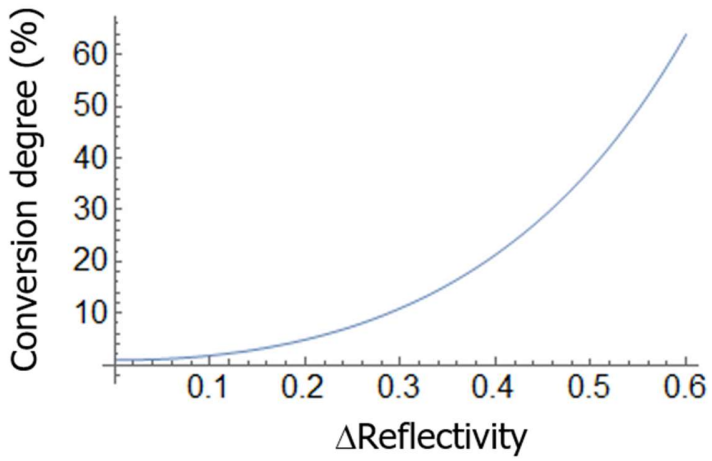

Figure 5-14 Conversion degree as a function of reflectivity change when incident angle is at critical angle

5.5 In-process measurement of conversion degree of the resin

My research target in this section is to experimentally achieve the in-process measurement of the conversion degree of near-substrate resin using the theoretical analyses in 5.3 and the numerical relationship between conversion degree and refractive measured in 5.4. The experiment setup is same with the verification experiment shown in **Figure 5-**

5. After the in-process measurement of the reflection, the distribution of the conversion degree was obtained according to the relation shown in **Figure 5-14**.

5.5.1 Experiment Setup

The whole experiment system (same with **Figure 5-5**) consists of two sections including fabrication and measurement. Two light sources in different wavelengths were used and the light used for measurement does not lead resin to be cured. Fabrication light in a wavelength of 405 nm was used. It was transmitted through an aperture and then narrowed to the small beam width by the lens system. A micro-sized light spot was projected into the resin. In the measurement section, the polarized laser light in the wavelength of 638 nm was launched into the bottom of resin at an incident angle of 55.7 degrees.

5.5.2 Results and discussions

The experiment results were also similar to the verification experiment, but more clear reflection distribution was obtained after I delicately adjusted the experiment setup, as shown in **Figure 5-15**. It is obvious that the noise is less than that of verification experiment and the shape of the cured resin is much clearer.

The curing process was monitored from the beginning of curing irradiation. The distribution of reflection was recorded at 0.00, 0.125, 0.50 and 2.00 s of exposure, as shown in **Figure 5-15**. Since the cured resin shows a lower reflectivity than the uncured resin, the formation of polymerization was apparent shown in this figure. It is noteworthy that the

resin started polymerizing from a small point and gradually increased to a larger size. This is because the center of the spot had largest intensity and resin in this region was at a higher reaction speed. The shape of cured resin approximated to be elliptical rather than perfect round. This is because the measurement light was oblique incidence (55.7 degrees), and inclined projection results in the distortion of the image.

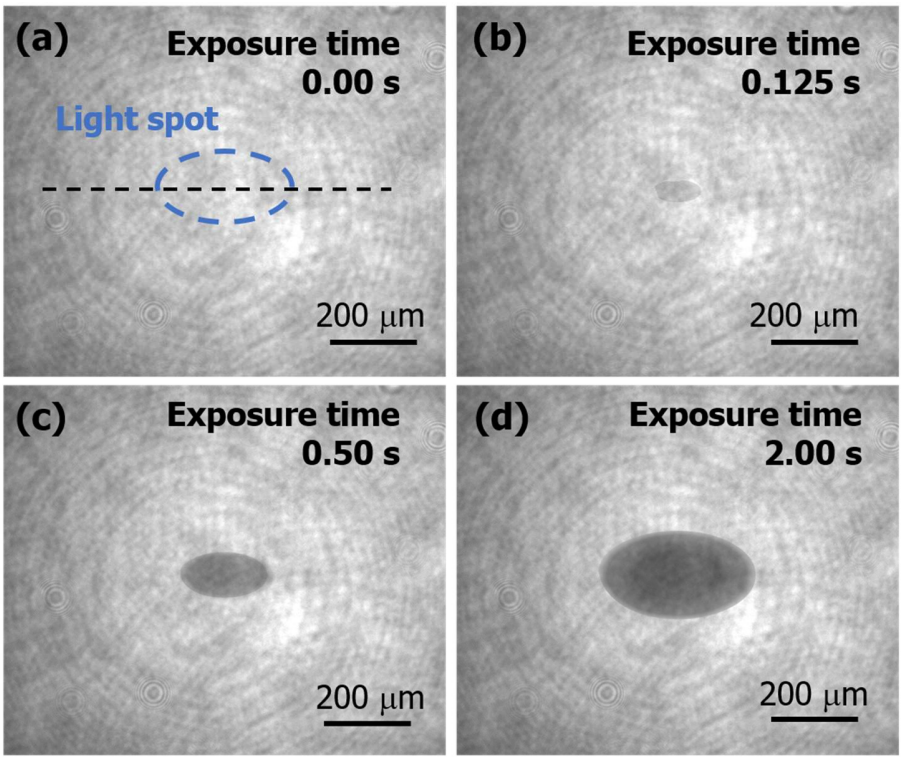

Figure 5-15 Measurement results of reflection distribution in various exposure time

Figure 5-16 (a) shows the grey value of cross-section marked by a black dash line. It is obvious that not only the range of cured resin increased with exposure time but also the grey value in the exposure region kept dropping. This well agrees with the fact that the curing degree continually increases during exposure and higher curing degree shows a higher refractive index and results in a lower reflectivity in my measurement system. In

addition, it is obvious that the width or lateral size of the cured resin enlarged with the increase of the exposure duration.

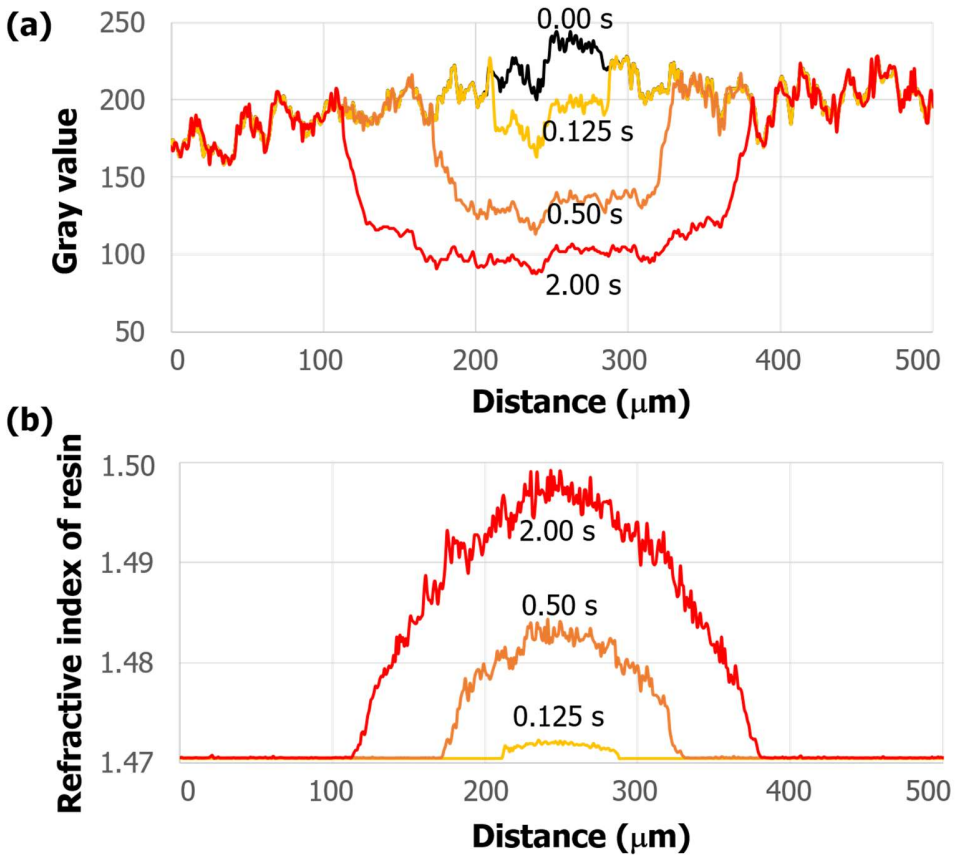

Figure 5-16 Measurement results of cross-section of (a) grey value and (b) reflective index in various exposure time.

It is notable that the reflection was not flat even before the curing process, this is because intensity distribution of measurement light itself was not in the same value and the noise caused oscillation of system or scattering also influence the reflection. This problem can be solved by improving the collimation, cleaning the lens and prism and using LED as the light source rather than a laser. Here I reduced the distribution problem of measurement light by simply making an imaging subtraction. The reflection distribution of the uncured condition was used as the reference and subtracted the reflection distribution obtained after

the exposure. By applying image subtraction, uneven distribution of measurement light was deducted obviously and the reflection contrast was obtained as well. The reflectivity variation was calculated by dividing reflection contrast by the reflection distribution of uncured condition, as shown in the following equation:

$$\Delta\text{Reflectivity} = \left| \frac{\text{Initial Reflection} - \text{Reflection after curing}}{\text{Initial Reflection}} \right| \tag{5-2}$$

Using the reflectivity and the theoretical relationship between reflectivity and refractive index when the incident angle is in 55.7 degrees in Section 5.3, the refractive index distribution corresponding to **Figure 5-16** (a) was calculated and plotted in **Figure 5-16** (b).

The distribution of the conversion degree can be obtained by using the numerical relationship measured in Section 5.4. The distribution of the conversion degree is shown in **Figure 5-17**. In addition, not only the cross-section but also the two-dimensional distribution of the conversion degree was calculated using the reflection distribution, as shown in **Figure 5-18**.

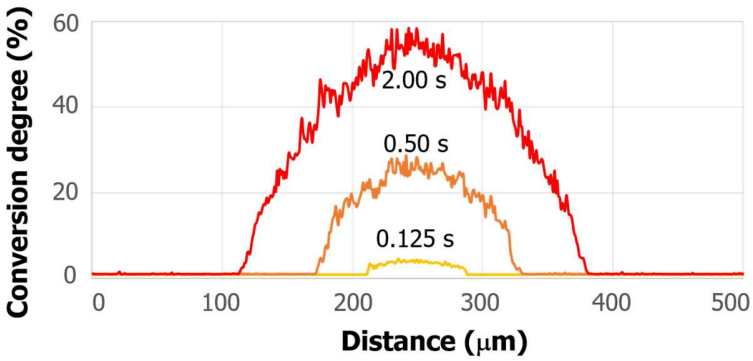

Figure 5-17 Measurement results of cross-section of conversion degree in various exposure time.

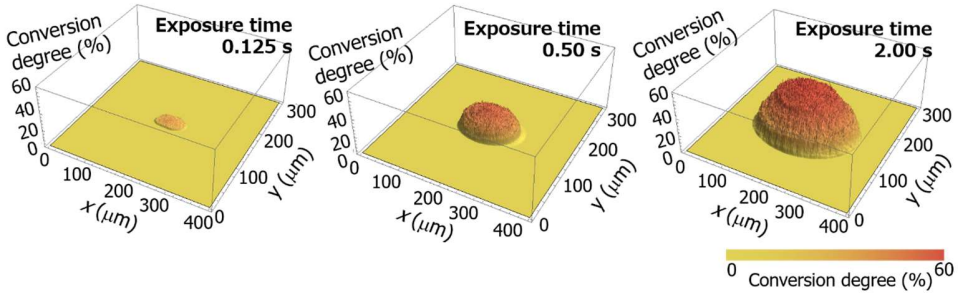

Figure 5-18 Distribution of conversion degree in the exposure time of 0.125, 0.5 and 2.0 second.

It is obvious that the center of the cured resin showed the highest conversion degree. This is because the fabrication light was focused to provide a small exposure spot, and the focused exposure beam showed a Gaussian distribution of the intensity. Therefore, the resin in the center of exposure was exposed by the highest intensity and had the fastest curing rate. The conversion degree in the center of the cured resin increased with the exposure time and reached around 54% degree after 2-second exposure. In addition, the cured resin was also enlarged with the exposure time, which well proves the feasibility that using in-process measurement to determine the proper exposure energy (time) by measuring the distribution of the conversion degree. As I explained before, the width of the resin that not only determines by the conversion degree distribution but also the critical etching degree. Once the critical etching degree is determined, the width of the cured resin is able to be predicted according to the distribution of the conversion degree.

5.6 Conclusions

In this chapter, first of all, by the verification experiment on the bulk sample I proved that the cured resin shows much lower reflectivity than the uncured resin when they are measured by the proposed critical-angle-reflection measurement method. I also

confirmed the reliability of the experiment system by comparing the experimentally measured reflectivity with the theoretical value in the various incident angle.

In the second verification experiment, the dynamic curing process of the resin was in-process measured. Experiment results proved that the curing process of the cured resin directly influences the optical response and the variation of the cured resin can be observed obviously. I also proved that both the size and curing level of the cured resin increase in the curing process according to the enlargement of the low reflection area and the successive decrease of reflectivity.

In order to achieve the in-process measurement of the conversion degree, the relationships between reflectivity, refractive index, and conversion degree were studied step-by-step. I theoretically calculated the relationship between reflectivity and refractive index in a various incident angle by Fresnel's equation. Then I measured the numerical relationship between the refractive index and conversion degree by using Raman spectroscopy and refractometer at the same time. The results showed that the reflectivity linearly decreased 0.03 as the conversion degree increase to 60%.

In the in-process measurement calibrated by above relationship, the distribution of conversion degree was measured in resolutions around 1% with a lateral resolution of 2.6 μm, which can ensure a lateral resolution of width in several micron meters according to the measurement results. In a condition of knowing critical etching degree, my investigations powerfully indicate the feasibility to in-process measure the width of the cured resin, and determine the proper exposure duration in MSL.

Viewing in the research objective, in order to achieve the flexible thickness MSL, I proposed to apply in-process measurement of the resin to determine the proper exposure energy for the resin layer in different thickness. What I want to measure is the width of the cured resin; however, due to the existence of gradient boundary, I can only measure the distribution of the conversion degree and predict the width of the cured resin using the critical etching degree. Until now, I successfully in-process measured distribution of conversion degree. Regarding to the determination of the critical etching degree, it is mainly on the chemical field and requires detailed investigation. It is another step of the final goal that achieves the flexible thickness MSL.

CHAPTER 6. IN-PROCESS MEASUREMENT OF CURING THICKNESS IN EVANESCENT-WAVE-BASED NANO-STEREOLITHOGRAPHY

This chapter presents the investigation of in-process measurement in EWNSL. Two verification experiments have been done. The first one is to compare the differences of the optical responses from the resin sample cured by the evanescent wave and the propagating wave using critical-angle-reflection measurement method. In the second verification experiment, the resin cured by the evanescent wave was in-process measured to confirm the variation of the optical response when the proposed measurement method is applied in EWNSL. In order to achieve the in-process measurement on the thickness of the cured resin, I did a detailed investigation to find the theoretical relationship between the thickness and reflectivity, including a simulation of curing process in EWNSL, the calculation of reflection interference from the ultra-thin cured layer with gradient boundary. This chapter also presents a calibration work that directly measure the numerical relationship between the reflectivity and thickness of the cured resin. In addition, this chapter demonstrates how I use the in-process measurement to determine the exposure time and fabricate the resin layer in the same thickness even the exposure intensity is different.

6.1 Verification experiment on sample cured by evanescent wave

In the first verification experiment, the bulk resin sample was submerged in the uncured resin and observed by detecting the reflection at the critical angle. Both samples cured by the propagation light and the ultra-thin sample cured by the evanescent wave were

observed by the proposed method. **Figure 6-1** (a) and (b) show the sample cured by MSL and EWNSL observed by a convention optical microscopy. Then the sample was submerged in liquid-state uncured resin, and observed by the proposed method. The experiment setup is shown in **Figure 6-2**. The experiment setup and the experiment conditions are same with the previous verification experiment on the bulk sample in 5.1.

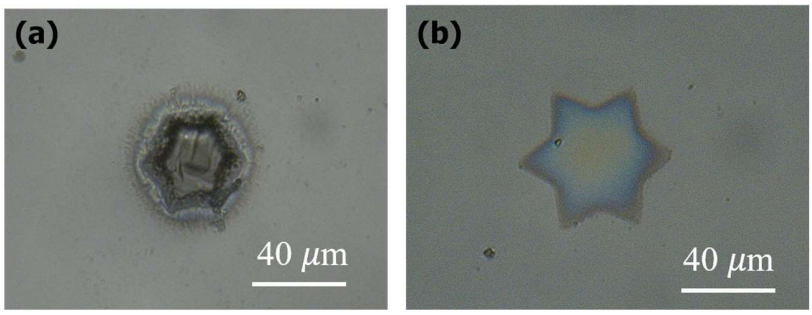

Figure 6-1 Sample cured by (a) MSL and (b) EWNSL observed by convention optical microscopy without uncured resin

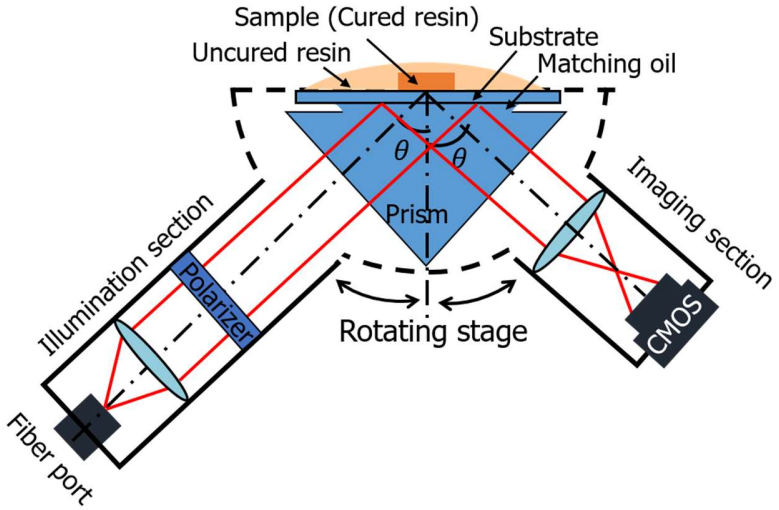

Figure 6-2 Experiment setup of verification. The resin samples (cured by propagating and evanescent light, respectively) were submerged in the uncured resin

The reflection distribution (optical response) from the resin samples when using critical-angle-reflection measurement method is shown in **Figure 6-3**.

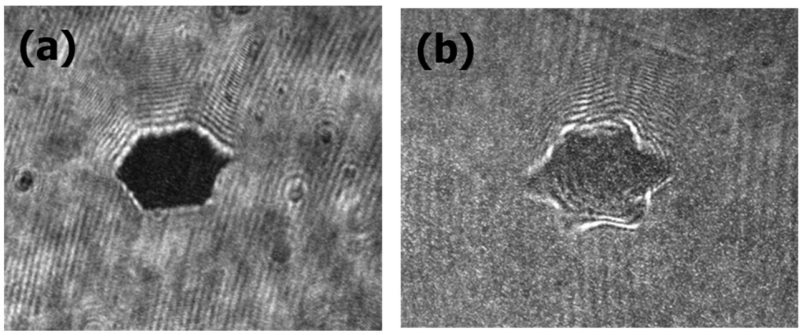

Figure 6-3 Sample cured by (a) MSL and (b) EWNSL observed by proposed method in the submerged state

Figure 6-3 (a) and (b) are the optical response from the resin cured by propagating light and the evanescent light corresponding to **Figure 6-1** (a) and (b), respectively. The results show that even resin cured by evanescent-wave in an ultra-thin thickness can be cleared observed by the proposed method. Moreover, compared with the bulk sample in a large thickness, the reflectivity decrease of sample cured by evanescent wave was relatively weak. This is because that the top surface of cured resin also generated the reflection and the reflection from both the bottom and the top surface of the cured resin were collected by the camera in measurement system. More preciously, the reflection from two surfaces generated interference and determined the total reflection intensity measured by the measurement system.

6.2 Verification experiment of in-process measurement of the resin cured by the evanescent wave

In this verification experiment, the curing process of the resin exposed by evanescent wave rather than the cured sample prepared in advance was measured to

confirm the variation of optical response using the proposed critical-angle-reflection method.

6.2.1 Experiment setup

In this experiment, not only the measurement section but also the fabrication system based on the evanescent wave exposure is required. The experiment setup was developed as shown in **Figure 6-4** (design drawing) and **Figure 6-5** (physical map).

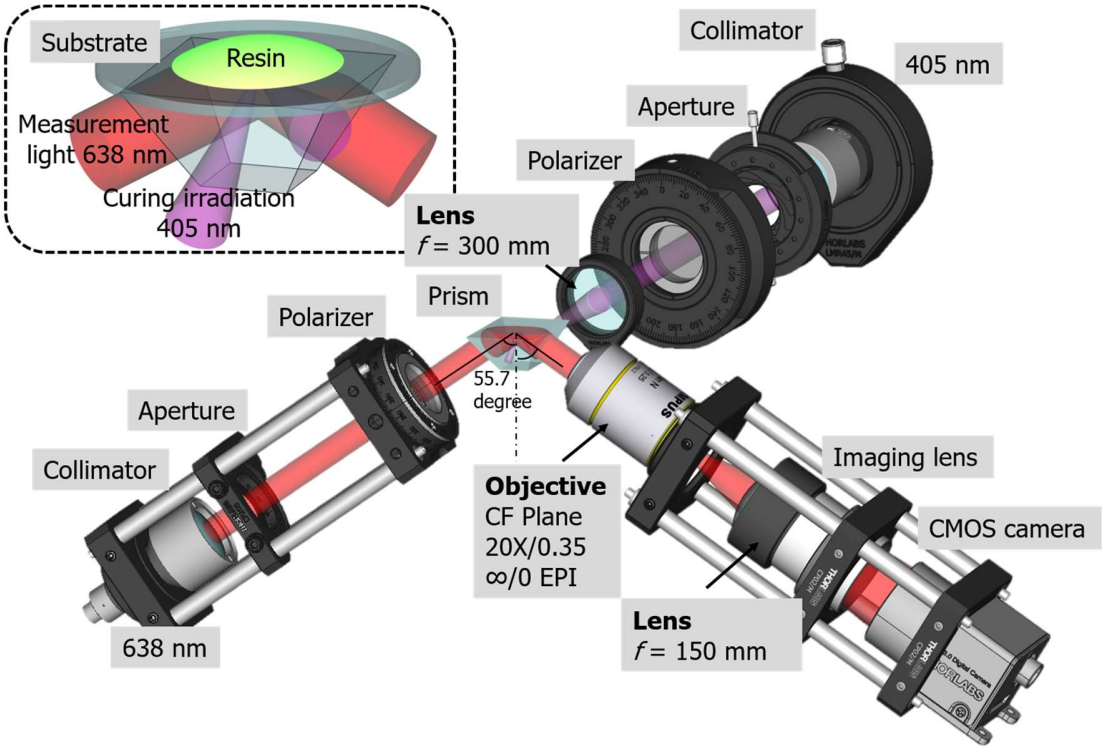

Figure 6-4 Experiment setup for verification experiment of in-process measurement of resin cured by evanescent wave

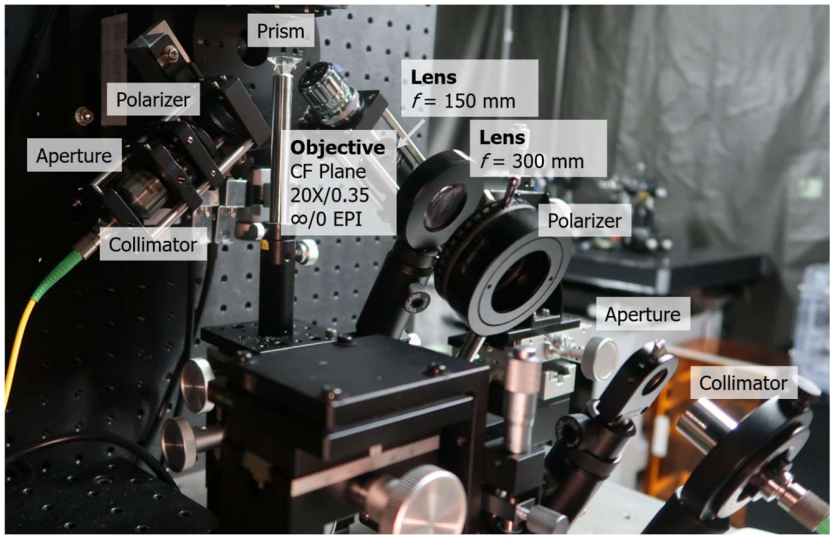

Figure 6-5 Experiment setup for verification experiment of in-process measurement of resin cured by evanescent wave

The measurement section was similar to that of the previous verification and I did some improvement in the imaging system. The first imaging lens near to the prism and the resin was replaced by an objective lens to get better imaging quality. Two beams of light in the wavelength of 405 and 638 nm were used as the curing (fabrication) light and the measurement light, respectively. The commercial laser source was LDM405.55.CW and LBX-S Series 638nm.

In this experiment, the operation of measurement did not impact on the fabrication as the wavelength of the measurement light was out of curing wavelength of the resin. In the fabrication section, the light was delivered by the optical fiber and transmitted through the collimator and the polarizer. A shutter was used to control the exposure time. In order to fabricate the cured resin in a smaller width seeking the real size of production in EWNSL, the curing light was focused by the lens before launched to the prism. In the measurement section, the polarized laser light in the wavelength of 638 nm was delivered by the left arm of and reflected from the interface between resin and substrate. The reflected light

propagated into the imaging section and was collected by an 8-bit CMOS camera (Lt425 from Lumenera). In the experiment operation, the two arms were respectively fixed on the rotation stage centered on the prism. The incident angle of the fabrication light was fixed at 65 degrees and the angle of measurement was fixed at the critical angle. Urethane-acrylate-based resin (KC1162) was used as a sample. In order to avoid the damages on the prism, the resin was put on a substrate that was in a refractive index of 1.78.

6.2.2 Results and discussions

The experiment results, a series of changes of the optical response from the cured resin in increased exposure duration, were recorded by CMOS camera and are shown in **Figure 6-6**. It is obvious that with the exposure duration increase, the reflection distribution changed, and there was a reflectivity decrease in the center of imaging area that corresponding the resin exposed by the fabrication light. These results prove that the curing process shows a successive decrease in the reflection distribution. Therefore, the curing level that also increases with the exposure duration can be evaluated by the successively-decreased reflectivity. In addition, as I explained before, the thickness of the cured resin in EWNSL continuously increase with the exposure duration as well. Combining with my final research target that control the thickness of the cured resin in EWNSL using the in-process measurement to determine the proper exposure energy or duration, this verification experiment well proved that it is possible to measure the thickness of cured resin by detecting the reflection since a lower reflectivity represents a larger thickness of the cured resin.

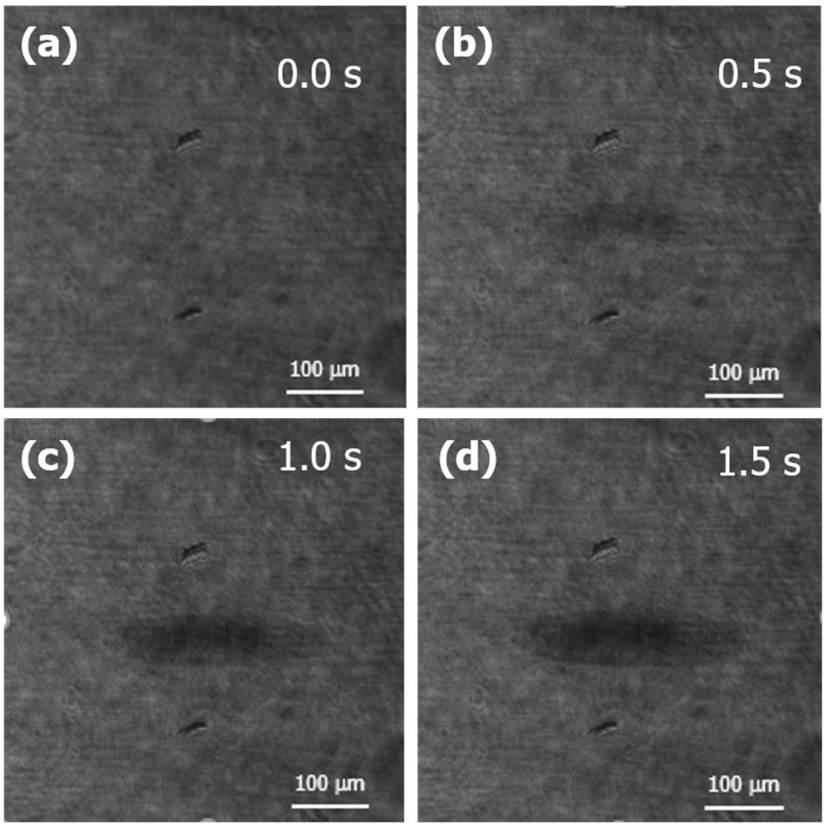

Figure 6-6 Reflection distribution from resin cured by evanescent wave in an increasing exposure time when resin (a) before exposure, and after (b) 0.5 (c) 1.0 (d) 1.5 seconds exposure

The unsolved problem is the relationship between the reflectivity and the thickness is still unknown. It is impossible to determine the thickness from the reflectivity without knowing their relationship. Based on this problem, in one hand, Section 6.3 presents the theoretical relationship between the thickness and the reflectivity obtained by developing a simulation model of the curing process in EWNSL and calculating the optical response based on the reflection interference at the critical angle. On the other hand, Section 6.4 shows the calibration experiment that directly measured the reflectivity decrease in various thickness of the cured resin to find the numerical relationship between them.

6.3 Theoretical relationship between thickness of the cured resin and the reflectivity of critical-angle reflection

I proved that the pattern of cured layer can be directly observed (Section 6.1) and the reflectivity of the cured resin successively decrease in the curing process (Section 6.2). Even resin cured by evanescent-wave in a submicron thickness can be clearly distinguished with the uncured resin using critical-angle reflection, but my objective is not just in-process observation but the in-process measurement of the thickness of each layer. In this experiment, I theoretically analyzed the optical response of the critical-angle-reflection in the curing process to find how reflectivity changes with the increase of the thickness of the cured resin. However, this is not easy work since there will be a gradient boundary between the cured and the uncured resin. The gradient boundary has a gradient-changed refractive index which influences the interference largely and makes the propagation of measurement light be bent in the cured resin, as shown in **Figure 6-7**.

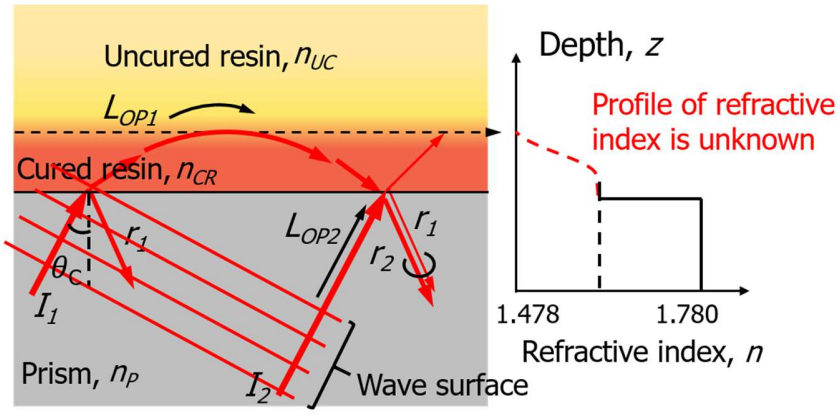

Figure 6-7 Schematic diagram reflection interference from resin with gradient boundary

In order to determine the optical path and calculate the interference, the refractive-index profile of the gradient boundary as a function of depth should be known at first. My strategy is to develop a simulation model of polymerization to obtain the variation of conversion degree of the cured resin in different curing thickness (conversion degree profile in the normal direction of substrate) and then, get the refractive-index profile according to the linear relationship between the conversion degree and the refractive index of the cured resin. After obtaining the refractive index as a function of the depth, the reflectivity can be calculated according to the interference between r_1 and r_2 involving the phase contrast generated by the optical path different L_{OP1} and L_{OP2}.

6.3.1 Simulation of the curing process in the exposure condition of evanescent wave

In order to obtain the refractive index profile, I simulated the curing process of the resin exposed by the evanescent wave. The simulation is based on the phenomenology of the curing process. The curing rate is determined by the exposure intensity and duration, as well as the chemical/physical characteristic of the resin in the exposure condition. Moreover, it cannot be neglected that the curing rate is largely influenced by heat generated by the curing process itself and the transfer of heat. Therefore, the simulation model of the curing process consists kinetics of photo-polymerization and the heat transfer.

Besides applying the general formula of heat transfer and polymerization rate, the PDE-ODE simulation is based on the following considerations and assumptions:

Simulation is based on a one-dimensional model and only the normal direction of the substrate (depth direction) is considered.

- Photo-polymerization process is not classified step-by-step and the conversion rate of the monomer is directly expressed by one formula.
- The oxygen inhibition is ignored.
- Exposure is monochromatic.
- The absorption of the exposure is neglect, and therefore, the intensity decrease of the exposure is only determined by the decreasing feature of the evanescent wave without considering the absorption based on Beer-lambert's law, as well as there will be no heat directly generated from the absorption of exposure.
- The properties of the resin are in the averaged value and the difference between the cured and uncured resin is ignored.

According to above considerations and assumptions and exploratory works in the related field [77-80], simulation of the curing process in the exposure condition of the evanescent wave is expressed by a partial differential equation (PDE) of heat transfer and an ordinary differential equation (ODE) of the curing rate, as shown in **Figure 6-8**. The physical definitions of all the symbols in the equations are explained in **Figure 6-8** as well.

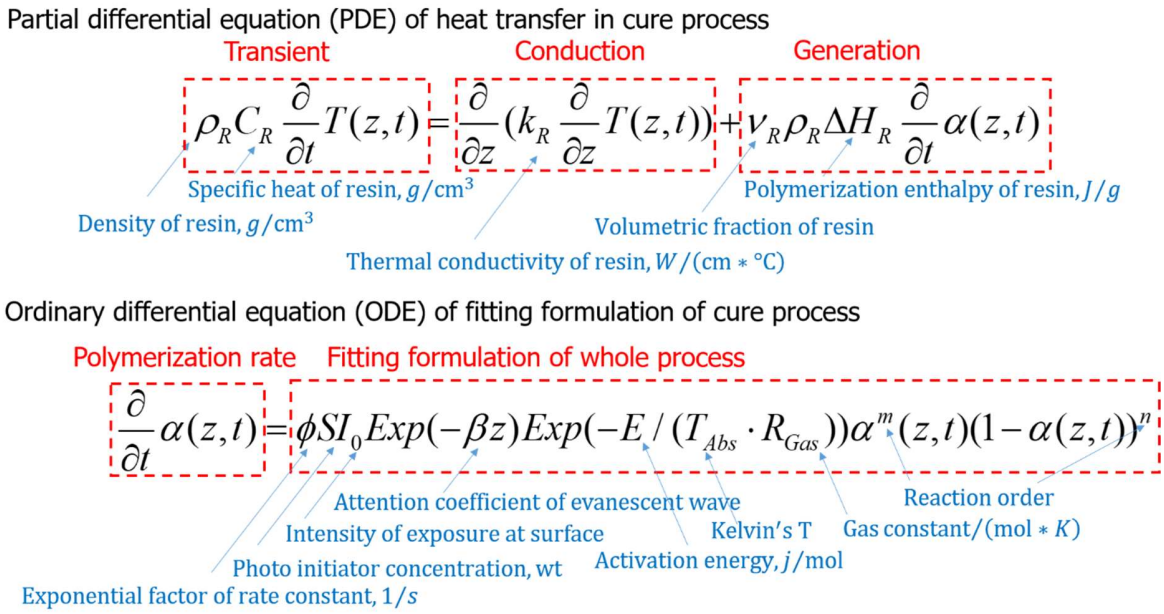

Figure 6-8 Simulation of the curing process expressed by PDE-ODE

It is worthy of note that the attention coefficient of evanescent wave (β) is calculated by following equation:

$$\beta = 2\pi n_1 \sqrt{\sin(\theta_I)^2 - (n_2 / n_1)^2} / \lambda \tag{6-1}$$

where the incident angle (θ_I) is 65 degree, the wavelength of measurement light (β) is 405 nm, and the refractive index of the substrate (n_1) and the resin (n_2) is 1.78 and 1.478 respectively.

In order to simulate the curing process, the PDE-ODE equation set was discretized and supplemented with initiation and boundary conditions. The discretization process and calculation method is shown in Appendix B. The parameters used in the calculation are shown in the **Table 6-1** [78, 87-91].

Table 6-1 Parameters used in simulation of curing process

Parameters	Symbol	Value	Unit
Density of Resin	ρ_R	1.10	g/cm^3
Specific heat of resin	c_R	1.67	J/(g*°C)
Thermal conductivity of resin	k_R	0.0017	W/(cm*°C)
Thermal conductivity of glass	k_G	0.0026	W/(cm*°C)
Convective heat transfer	h	0.002	$W/(cm^2*°C)$
Polymerization enthalpy of resin	ΔH_R	335	J/g
Pre-exponential factor of rate constant	φ	10	1/s
Photoinitiator concentration	S	0.02	wt
Activation energy	E_{Act}	12700	j/mol
Gas constant	R_{Gas}	8.314	1/(mol*K)
Reaction order	m	0.7	
Reaction order	n	1.3	
Temperature	TEnv	25	

It is worth noting that the convective heat transfer (h) appeared in the table was not used in the PDE-ODE equation set. Actually, it was used at the boundary conditions to express a degree of heat transmitting out of the simulation domain.

The simulation results that the conversion degree as a function of curing depth when the exposure time is 0.5, 2, 8 and 32 seconds is shown in **Figure 6-9**. It is obvious that for certain exposure time, the conversion degree of the resin decrease with the exposure depth increase which well agrees with the fact that the intensity of exposure reduces with the depth and the resin near the substrate has a higher curing rate than resin far from the substrate. In addition, I can see that with the exposure duration increase, the conversion degree of the whole field of the resin also increases, which equals to thickness (after etching process) increase with the exposure duration. For example, if the resin in a conversion degree larger than 0.3 (30%) is reminded after etching process (critical etching degree is

30%), the thickness of the cured resin will be around 30, 150 280 and 440 nm corresponding to the exposure duration in 0.5, 2, 8 and 32 seconds. This result also meets my subsection that the thickness of the cured resin increasing with the exposure duration (energy).

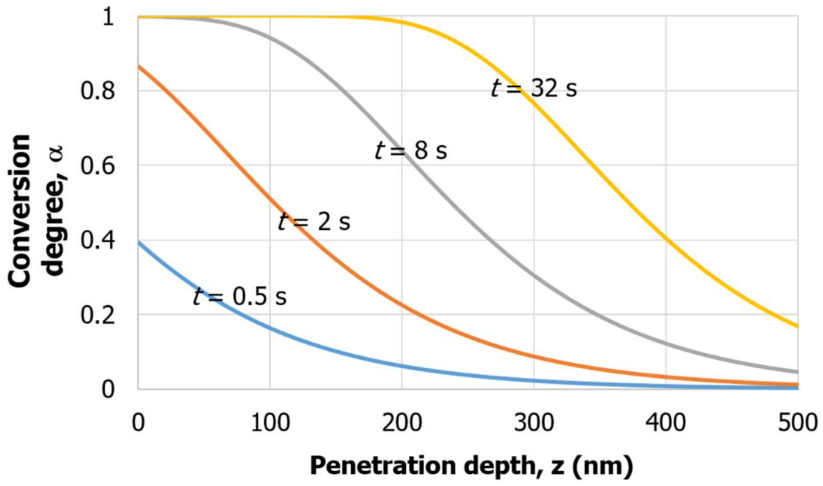

Figure 6-9 Conversion degree as a function of curing thickness in an increasing when exposure time is 0.5, 2, 8 and 32 seconds

From the simulation results, most importantly, it obtained the profile of conversion degree of the resin in the normal direction of the substrate. According to the linear relationship between the conversion degree and refractive index of the cured resin that was demonstrated in Section 5.4, the profile of the refractive index of the cured resin can also be obtained. Based on these results, the optical response using critical-angle-reflection from the cured resin in such refraction index distribution can be calculated, and the reflectivity in an increased exposure time can be obtained, which will be discussed in the following section.

6.3.2 Optical response using critical-angle-reflection based on the simulation results

The optical response of the critical-angle reflection in the cured resin (as shown in **Figure 6-10**) can be analyzed by a model of reflection-phase-contrast interference.

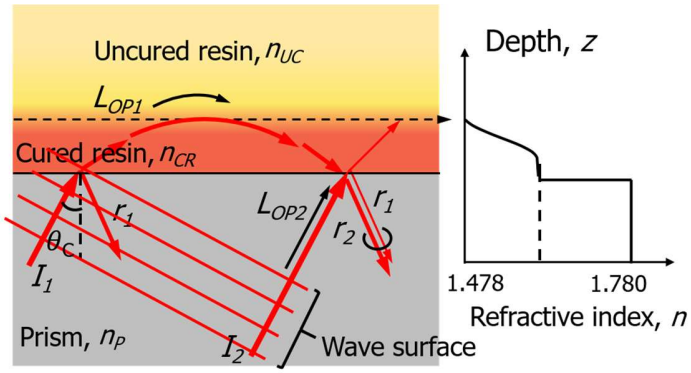

Figure 6-10 Optical response of the critical-angle reflection in the cured resin. Reflection-phase-contrast interference was generated.

In this case, when the measurement light incidents into the bottom of the cured resin, a part of the light is reflected at the interface between the substrate and the cured resin (r_1). The rest of the measurement light that propagates in the cured resin after refracting is totally internal reflected when it reaches to the uncured resin since the incident angle is at the critical angle calculated by the substrate and the uncured resin. The reflection from the uncured resin propagates back to the prism in a reflectivity of r_2. The intensity of the interference between r_1 and r_2 can be calculated by involving the phase contrast caused by the difference of the optical path.

The reflectivity r_1 is calculated by:

$$r_1 = \frac{n_P \cos\theta_T - n_{CR_{z=0}} \cos\theta_I}{n_P \cos\theta_T + n_{CR_{z=0}} \cos\theta_I} \tag{6-2}$$

where n_P is the refractive index of the prism, $n_{CRz=0}$ the refractive index of the cured resin when curing depth is zero, θ_I the incident angle and the θ_T the angle of light transmitted into the cured resin after refraction.

The reflectivity r_2 is calculated by:

$$r_2 = (1 - r_1)^2 \tag{6-3}$$

The interference between r_1 and r_2 according to the phase contrast is expressed by:

$$I_{Interferenc} = r_1^2 + r_2^2 + 2r_1 r_2 \cos(\phi_P) \tag{6-4}$$

The phase contrast is expressed by:

$$\phi_P = 2\pi \frac{L_{OP1} - L_{OP2}}{\lambda} + \frac{\pi}{2} \tag{6-5}$$

where the $\pi/2$ is the phase change of the total internal reflection of r_2; the L_{OP1} and L_{OP2} is the optical path of r_1 and r_2 that can be expressed by (23) and (24), respectively.

$$L_{OP1} = 2\int_0^{z_{tp}} \frac{n^2(z)dz}{(n^2(z) - n^2(z_{tp}))^{1/2}} \tag{6-6}$$

$$L_{OP2} = 2\sin(\theta_I) n_P \int_0^{z_{tp}} \frac{dz}{(n^2(z) - n^2(z_{tp}))^{1/2}} \tag{6-7}$$

where n(z) means the refractive index of the cured resin as a function of the curing thickness (z). and z_{tp} is the depth of the turning point (at the curing thickness) where the total internal reflection occurs and r_2 reverses its direction toward the substrate. The incident angle θ_I is at the critical of the uncured resin. The propagation path of L_{OP1} is bent due to the existence of the gradient refractive index of the cured resin. The length of the optical path is calculated according to optical fiber theory using the profile of refractive index measured in the previous section.

It is notable that the turning point (z_{tp}) is a crucial parameter in the calculation, which directly determines the depth of L_{OP1} directly influences the interference largely. In an ideal condition, the turning point is at the curing thickness where the resin is totally uncured (conversion degree and refractive index variation are zero). According to our simulation, the decease of conversion degree becomes slowly in a larger curing thickness and the curing point can be several hundreds of nanometers or even in micrometer scale. However, it is known that when the conversion degree of the resin is in a low state that much smaller than the gel point, the liquid feature of resin lead the conversion degree in a smaller value cannot be maintained. Therefore, in the practical experiment when conversion degree is low enough, it will drop directly to zero. Due to there is no other investigation on the curing process of the resin exposed by the evanescent wave, the exact conversion degree of the turning point and the curing thickness are still unclear. As a result, I calculated the reflection when the turning point is in a conversion degree of 0.1, 0.01 and 0.001 respectively.

The curing thickness changes with the pre-set value of conversion degree of the turning point. For an example, in **Figure 6-11**, when the conversion degree of turning point

is 0.1, the curing thickness is around 150 and 280 nm for 0.5 and 2 second exposure, respectively; while in case of conversion degree of turning point is set as 0.01, the curing thickness is around 350 nm and 500 nm for 0.5 and 2 second exposure, respectively.

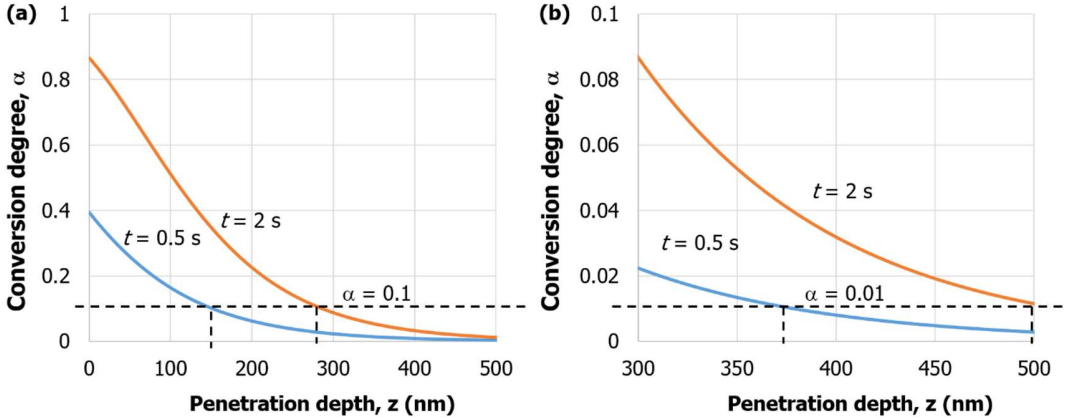

Figure 6-11 Turning thickness is around 150 and 280 nm for 0.5 and 2 second exposure when (a) conversion degree of turning point is 0.1; and is around 350 nm and 500 nm for 0.5 and 2 second exposure when (b) conversion degree of turning point is 0.01.

The curing thickness as a function of exposure duration when the conversion degree of turning point is 0.1, 0.01 and 0.001 respectively are plotted in **Figure 6-12**. It is obvious that the curing thickness increases with the exposure duration. Based on the curing thickness changes and the refractive index profiles obtained from the simulation of the curing process, the reflectivity decrease of the cured resin in an increased exposure time can be obtained by using equations (6-2) to (6-7). The results are shown in **Figure 6-13**.

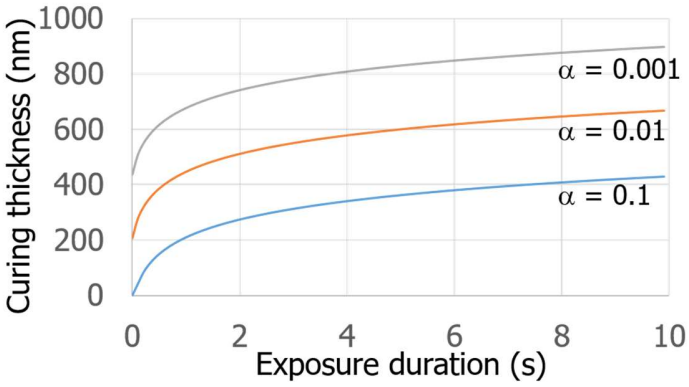

Figure 6-12 Curing thickness as a function of exposure duration when conversion degree of turning point is 0.1, 0.01 and 0.001

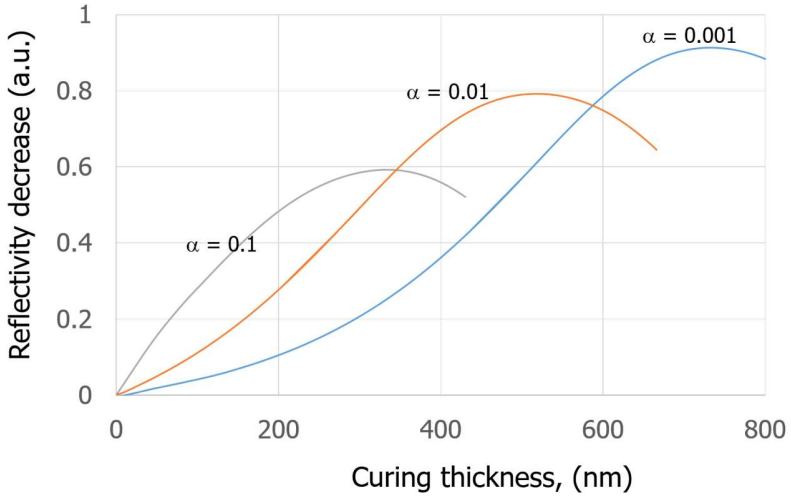

Figure 6-13 Reflectivity decrease as a function of curing thickness when the conversion degree of turning point is in a value of 0.1, 0.01 and 0.001 respectively.

Above results clearly show the theoretical relationship between the curing thickness of the cured resin and the reflectivity of the optical response using critical-angle reflection. It shows that the reflectivity changes apparently with the increase of curing thickness, which proves that it is possible to measure the thickness information by detecting the reflection using the proposed method. However, it is notable that, what I calculated here is the relationship between reflectivity and curing thickness of the cured resin rather than the fabrication thickness (etching thickness) of the cured layer after the etching and washing

process. It can simply understand that the etching thickness increase with the curing thickness of the cured resin, but I cannot obtain the exact numerical relationship between etching thickness and curing thickness without knowing the correct critical etching degree. In addition, based on the facts that the exploratory investigation explained above are based on many assumptions and some calculation procedure are simplified, the obtained theoretical relationship is not accurate enough for us to directly used as a reference to determine the thickness of the cured resin according to the reflectivity. In the other word, these results qualitative analysis the variation of optical response in the curing process of the resin exposed by the evanescent wave, but cannot be directly used to measure the thickness of the cured resin according to the reflectivity change.

6.4 Calibration experiment of the relationship between thickness of the cured resin and the reflectivity of critical-angle reflection

In order to obtain the relationship between the etching thickness of the cured resin and the reflectivity of in-process measurement using critical-angle reflection, in this investigation, I did a calibration experiment to directly measure the relationship between them. More concretely, I measured the reflectivity of the cured resin in the curing process using the proposed method. Then, after the etching process, the thickness of the cured resin was measured by AFM. The numerical relationship can be obtained by developing correspondence of the reflectivity and the thickness.

6.4.1 Experiment setup

A whole experiment system is shown in **Figure 6-14**, which is similar to the verification mentioned in Section 6.2. It includes the fabrication and the measurement two sections. Two beams of light in the wavelength of 405 and 638 nm were used as the curing (fabrication) light and the measurement light, respectively. Urethane-acrylate-based resin (KC1162) was used as a sample.

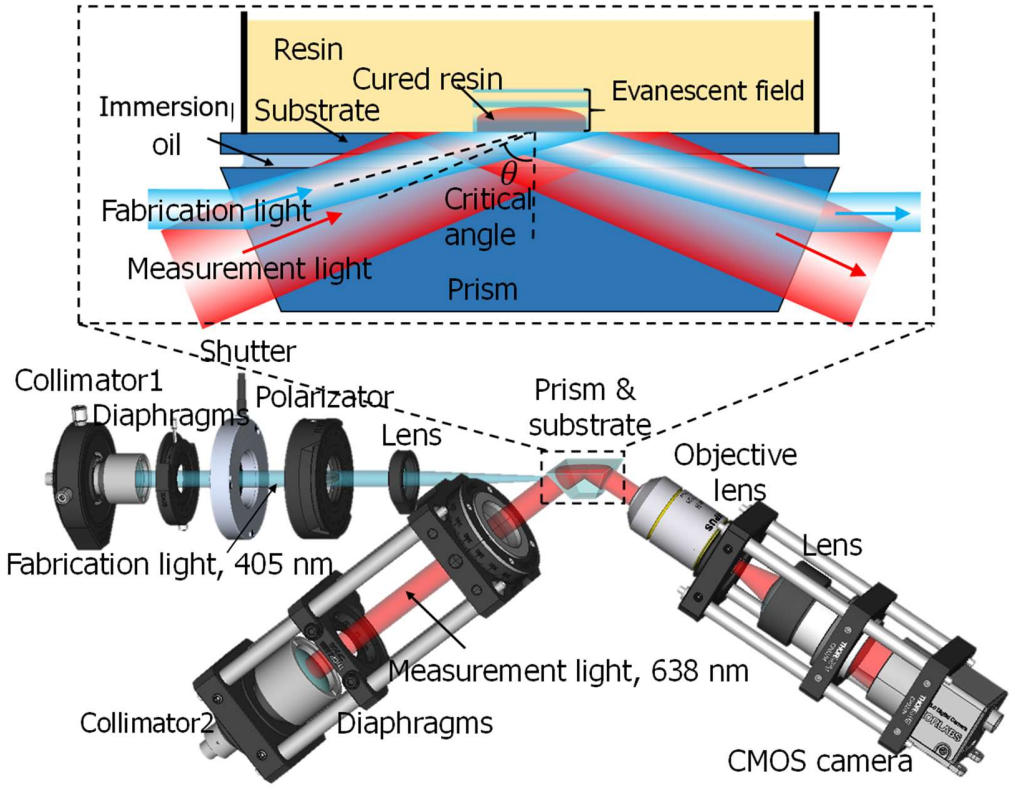

Figure 6-14 Diagram of experiment setup

Regarding performance of the measurement system, there are few points are worth discussing. First of all, the spatial resolution of this system that was mainly determined by the magnification of the imaging system and the pixel-size of the optical sensor in CMOS camera, was around 1.5 μm in my experiment. Regarding the resolution of reflectivity, the

maximum grey value in the experiment was adjusted to around 200 (maximum grey value of the 8-bit camera is 256), which corresponds to the reflectivity of total internal reflection. Therefore, the resolution of reflectivity calculated by 1/200 was 0.005 in the measurement system. In addition, measurement rate (sampling time) of the current system, determined by the CMOS camera and recording rate of a computer. Due to the limitation of recording rate, there is a trade-off between the number of the pixels and the sampling rate in the experiment equipment. A maximum of 90 frames per second (FPS) can be obtained in case of the number of the pixels less than 900 × 900. In the experiments, I used the maximum amount of the pixels of the camera in a value of 2048 × 2048 with the FPS in a value of 30. This sampling rate was sufficient for in my experiments due to the exposure energy that was not too large and an apparent variation of the resin in the curing process continued in several seconds. In the consideration of industry productions, the curing process under a high-intensity exposure can be much faster than that in the experiment, as a result, 30 FPS might be insufficient, but the promotion space of the sampling rate is also large with the assistant of a high-speed camera, high-performance FPGA or integration of high-capacity RAM frame buffers with an imaging sensor. Based on the fact that the measurement is one of the optical methods, the sampling rate is not a big problem.

6.4.2 Experiment results

Figure 6-15 illustrates the experiment results. Three samples exposed in 1.0, 2.0 and 3.0 s was measured, respectively. The reflection distribution of three samples detected by a CMOS camera was shown in **Figure 6-15** (a) to (c), respectively. The shape of cured

resin can be directly observed according to the grey value deduction caused by the reflectivity drop. Besides, it is obvious that the grey value of cured resin in three figures was different; the grey value of cured resin decreases through the exposure time. This is well agreed with my assumption that a longer exposure time leads to a larger thickness of cured resin and finally results in a stronger reflectivity drops.

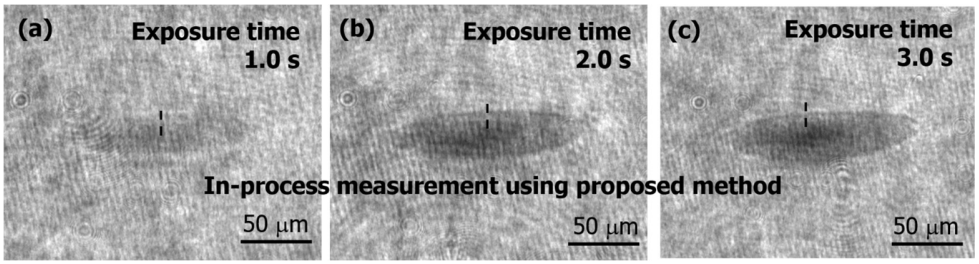

Figure 6-15 Experiment results using proposed method. The distribution of grey value obtained by proposed method when sample were exposed by (a) 1 (b) 2 and (c) 3 seconds.

For comparison, the three samples were observed by optical microscopy after the etching and drying process, as shown in **Figure 6-16**. It is notable that in the proposed method the measurement light was oblique incidence (55.7 degrees), and an inclined projection results in the distortion of the image. Distortion problem will be bypassed in my future work by applying the immersion objective lens to generate the oblique incidence at the critical angle in multi-direction.

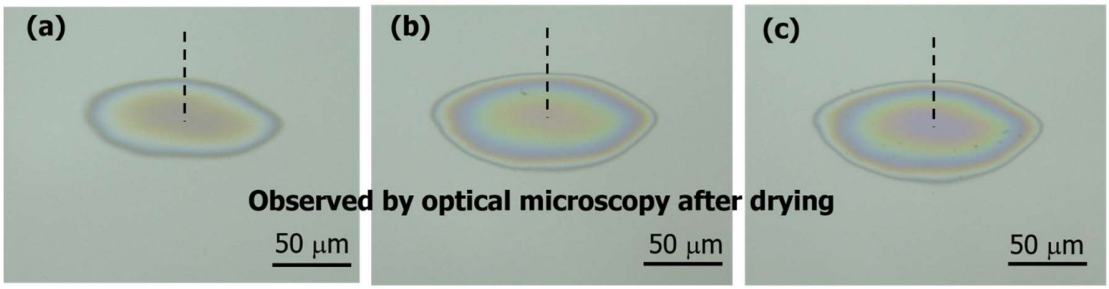

Figure 6-16 Image observed by optical microscopy after drying process when sample were exposed by (a) 1 (b) 2 and (c) 3 seconds..

In order to find the relation between the reflectivity drop in in-process measurement and thickness of cured resin. The thickness of the sample was measured by AFM (atomic force microscope) after the drying process. **Figure 6-17** plots the thickness and the reflectivity drop distribution in the same cross-section of the cured resin. It is obvious that the reflectivity decrease shows the same tendency with the thickness of the cured resin.

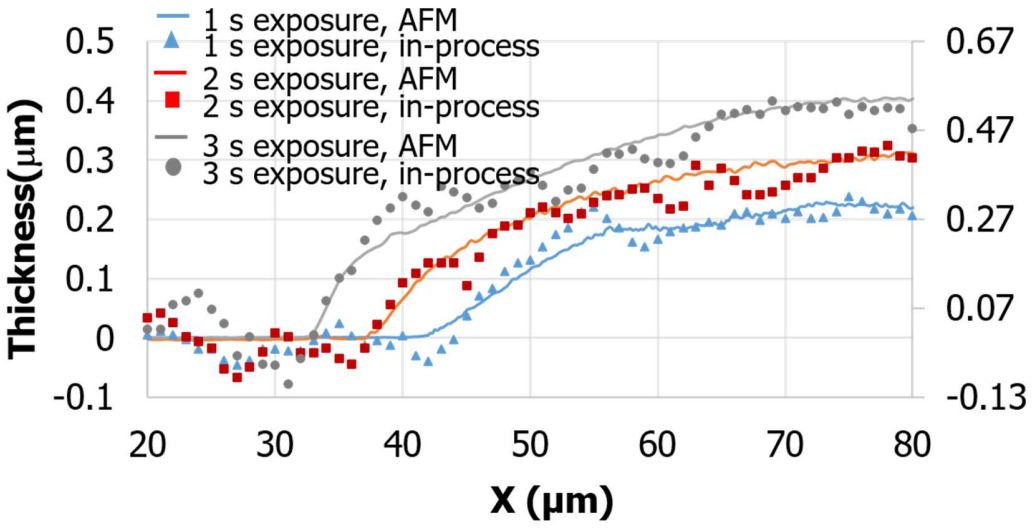

Figure 6-17 Thickness measured by AFM and reflectivity drop obtained by in-process measurement as function of position.

The slope of the reflectivity distribution was not as gentle as the curve of the thickness. This is because in the in-process measurement, interference, and dust caused uneven distribution of measurement light, which directly influenced the measurement results. The uneven distribution can be removed by making subtraction between the grey value distributions obtained before and after curing. The imaging process and its results will be illustrated in the next experiment. In addition, the reflectivity drop varied linearly with the thickness of cured resin according to the measurement results. For this reason, the reflectivity-position curve was coinciding with the thickness position curve after adjusting

the range of the two vertical axes. To confirm this point, the reflectivity drop as a function of the thickness is plotted in **Figure 6-18**.

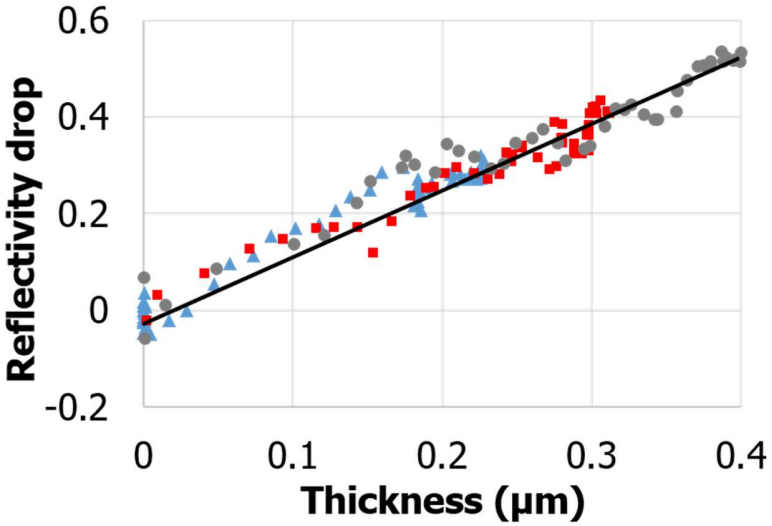

Figure 6-18 Reflectivity drop as function of thickness..

A linear relation between them can be clearly seen. In the experiments, the relation between the reflectivity drop and thickness was caused by many factors including the profile of the gradient boundary, the flatness of the cured layer and the refractive index incensement of resin. The linear relation that was even out of my expectation might not be a standard situation. To explain the linear relation between the reflectivity drop and the thickness, the mathematical relation will be investigated in the future by simulating the curing process and modeling the gradient boundary. Compared with the simulation results, the obvious reflectivity drop on one side of cured resin was not shown in the experiment. This is because the shape of cured resin in the experiment is different from an ideal rectangular shape in the simulation and therefore, multi-interference between the top and bottom boundary of cured resin was largely weakened.

6.5 In-process measurement of resin in continue and discontinues exposure condition

In this experiment, in-process measurement was applied to study the curing process when resins were continuously and discontinuously exposed. **Figure 6-19** (a) shows reflection distribution of resin in an increased exposure time of 0, 1, 2, 3 and 4 seconds respectively. **Figure 6-19** (b) shows a series of reflection distribution of resin cured by discontinues exposure. In this case, the shatter was switched 8 times; resin was given an exposure of 1 second and then rest without exposure for 1 second and repeat. The reflection distribution was measured immediately after each exposure.

Comparing **Figure 6-19** (a) and (b), even the total exposure time of both were same, the resin cured by continues exposure showed lower reflectivity than discontinues exposure, which means resin had a larger thickness when it was cured by continues exposure time. This is an interesting phenomenon and was caused by the difference of the average reaction rate. In the continuous exposure, the curing rate of resin keep increasing to the maximum until all initiators were activated, but in discontinues exposure, the curing rate dropped once illumination was blocked. Therefore, in the same exposure time, the resin cured continuously showed relatively larger thickness and lead to a lower reflection. This phenomenon also proves the necessity of fast measurement since the operation of blocking the exposure and waiting measurement will influence the fabrication process.

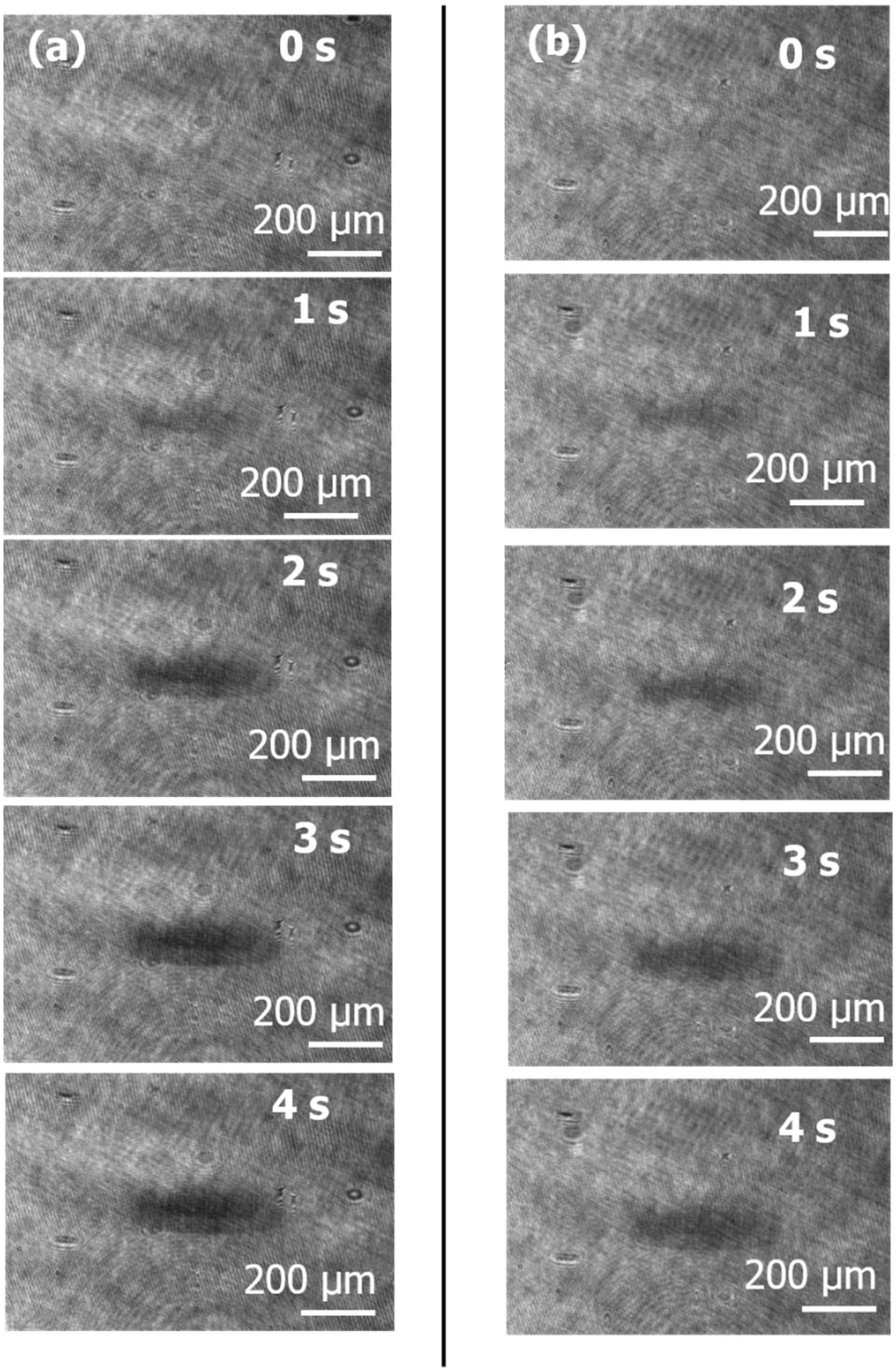

Figure 6-19 Original grey distribution for (a) Continuous exposure and (b) Discontinuous exposure.

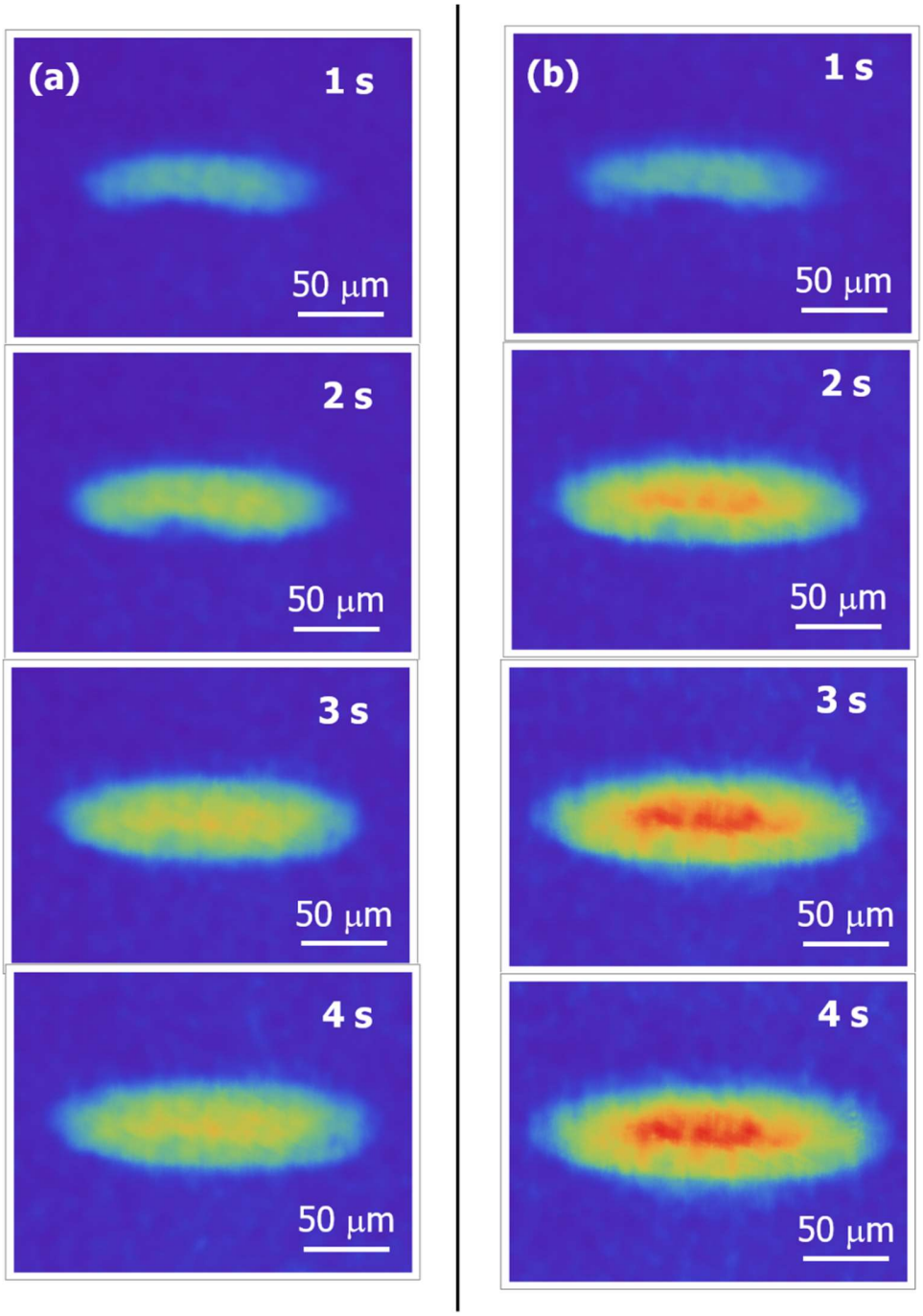

Figure 6-20 Processed image for (a) Continuous exposure and (b) Disontinuous exposure.

The image processing techniques were applied to remove the uneven distribution of measurement light. It was achieved by the subtraction between the reflection distribution before and after exposure. The imaging filter was adopted after subtraction to remove the

background noise. The processed images are shown in **Figure 6-19**, representing the continuous and discontinuous exposure condition corresponding to **Figure 6-20**. In the processed image, the variation of shape and reflectivity drop of cured resin in the curing process is more obvious than the original image; the difference between continuous and discontinuous exposure as discussed above can also be clearly observed. Obviously, imaging process benefits the in-process measurement at lot, however, the usage of filter results in some loss of image information and impact the measurement.

Figure 6-21 (a) and (b) show images of cured resin observed by optical microscopy after the etching and drying treatment when the resin was given 4 seconds continuous and discontinuous exposure. The profile marked by white lines were measured by AFM. The measurement results are plotted with the thickness obtained by in-process measurement, as shown in **Figure 6-22**.

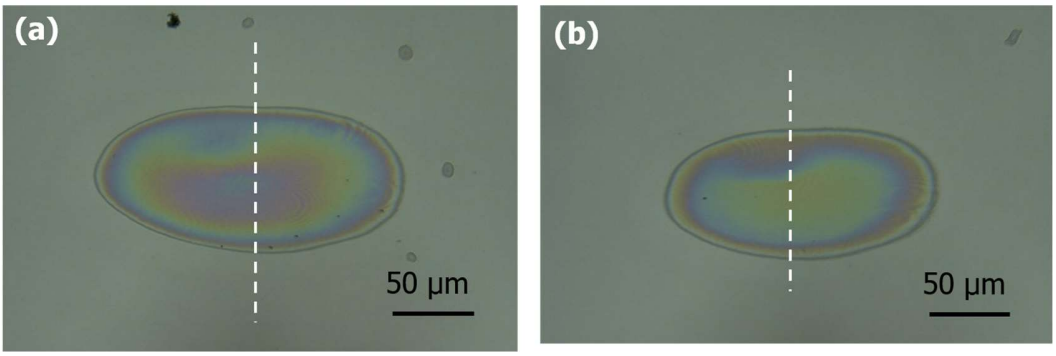

Figure 6-21 Image observed by microscopy after etching and drying process for (a) Continuous exposure and (c) Discontinuous exposure.

The blue point shows the raw data of thickness calculated from the reflectivity after subtraction. The grey line shows the processed date by applying bilateral and median filter to remove noise. Red line shows the thickness of cured resin measured by AFM after washing and drying treatment. Compared with the absolute thickness measured by AFM,

thicknesses measured by proposed method were close to the absolute thickness, especially in the center of cured resin, where the difference was smaller than 20 nm. However, in the two sides of cured resin, effective thickness were larger and changed more steeply than the absolute thicknesses.

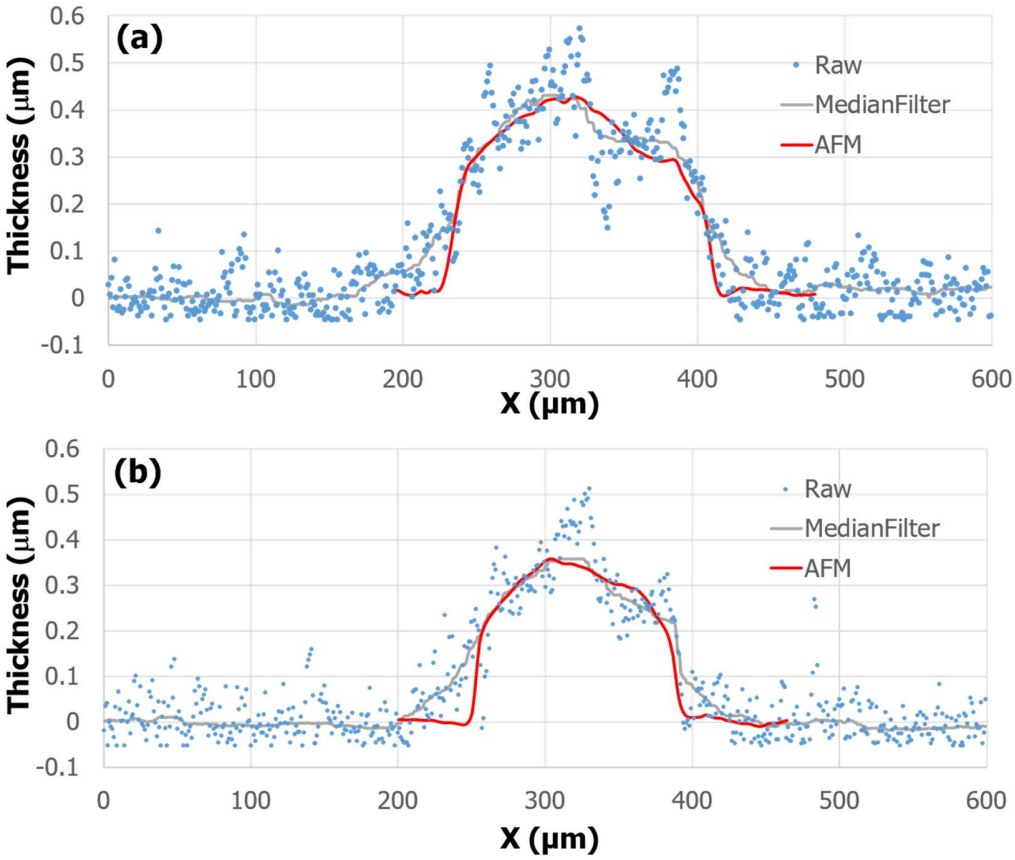

Figure 6-22 Thickness of cross-section measured by proposed method and AFM after etching and drying process for (b) Continuous exposure and (d) Discontinuous exposure. The blue point is in-process measured thickness. Median filter was used to reduce the noise and the processed results in plotted in the grey line.

The maximum difference between the effective and the absolute thickness reached 150 nm. The reason for this difference might cause by many factors. Most probably, the steepness of cured resin impact the relationship between reflectivity and thickness, which results in the linear relation is not applicable to the following experiment. In addition, the

etching and drying process influence the absolute thickness largely. To repeat a previous point, the absolute thickness appears after the etching and drying treatment and therefore, in-process measurement is applied to predict thickness in the fabrication process, which means I cannot provide a totally right measurement on thickness but can only give a tendency of thickness. According to the above results, the maximum thickness and rough size of cured resin were successfully measured.

6.6 Determine the exposure time and thickness of the cured layer

In Section 6.5, I proved that the thickness of the cured resin can be effectively measured by detecting the reflectivity of critical-angle reflection and using the numerical relationship of the reflectivity with the thickness of the cured resin. However, the final goal of this research topic is not just to measure the thickness but also determine the proper exposure duration (energy) to control the thickness of the cured layer. Based on this requirement, this section demonstrates how I control the thickness of each layer by applying the critical-angle reflection method.

It is known that when the resin is exposed by light in different exposure intensity, the curing rate of the resin will also be different and the resin exposed by a larger intensity has a larger thickness in certain exposure time. In this case, it is difficult to fabricate the resin in the same thickness even the total exposure energy is the same. For example, when the resin is exposed by light in an intensity of 2 μW in 4 seconds and 4 μW in 2 seconds, the total exposure energy of both conditions are in the same value of 8 μJ. However, the

thicknesses of the cured resin in these two exposure conditions are different. **Figure 6-23** illustrates this phenomenon using the exposure conditions described in the example.

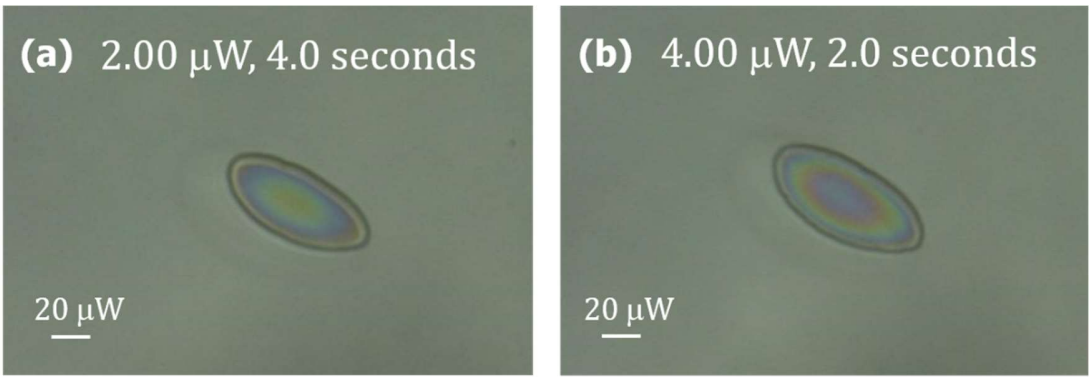

Figure 6-23 Resin cured by evanescent wave when exposure was in (a) 2 μW and 4 seconds and (b) 4 μW and 2 seconds.

Figure 6-23 (a) is the resin cured by the evanescent wave in an exposure intensity of 2 μW in 4 seconds and **Figure 6-23** (b) shows the resin exposed by light with 4 μW in 2 seconds. The total energy of both conditions are 8 μJ. By comparing these two images of the sample, the size of them is slightly different. The thickness of the cured resin can be directly estimated according to the color since the samples generated thin-film interference effect. It is obvious that the color in the center of the resin is different, and therefore, I can conclude that the thicknesses of the two resin are different even in the same exposure energy.

In order to determine the proper exposure duration when the resin was exposed by different intensity, the curing process of resin in these two exposure conditions are in-process measured by the proposed critical-angle reflection method. The reflection distribution was recorded as an image per 0.5 seconds, as shown in **Figure 6-24** and **6-25**.

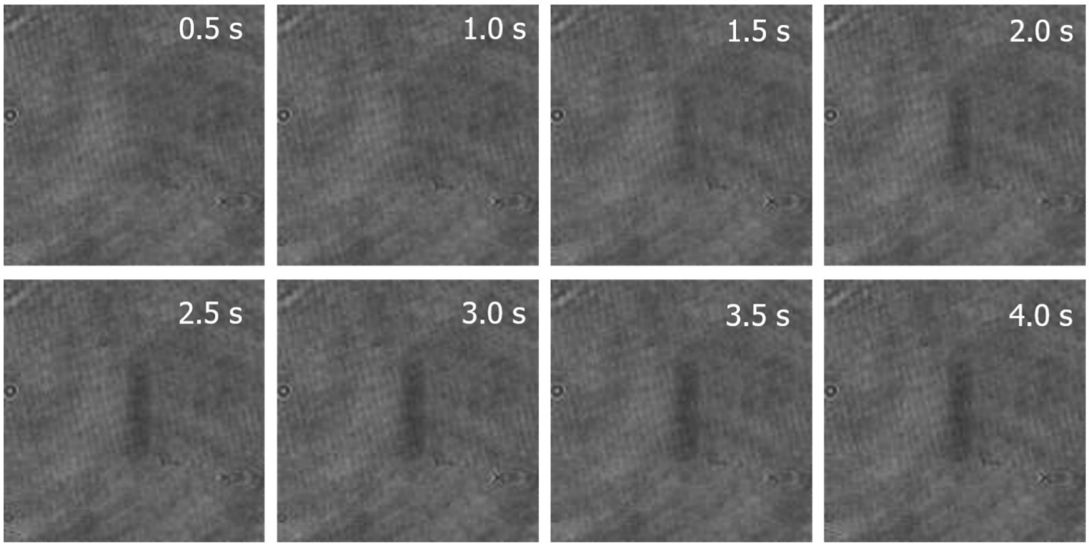

Figure 6-24 Reflection distribution of resin exposure by evanescent wave in 2 μW and 4 seconds

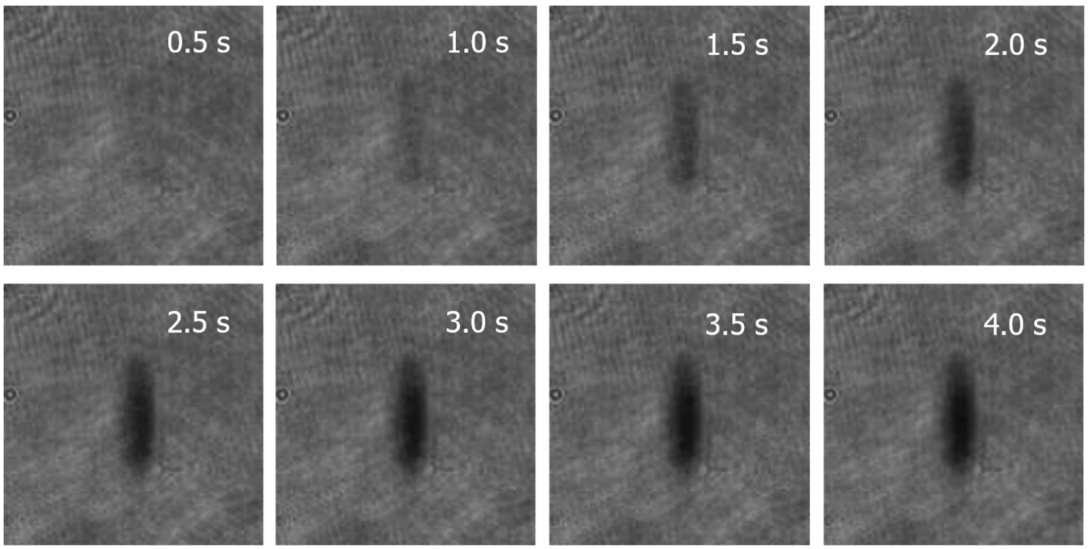

Figure 6-25 Reflection distribution of resin exposure by evanescent wave in 4 μW and 4 seconds

According to the original data in the **Figure 6-24** and **6-25**. The reflectivity change (reflectivity decrease) in the center of the cured resin as a function of the exposure duration in the above two exposure intensity is plotted in **Figure 6-26**.

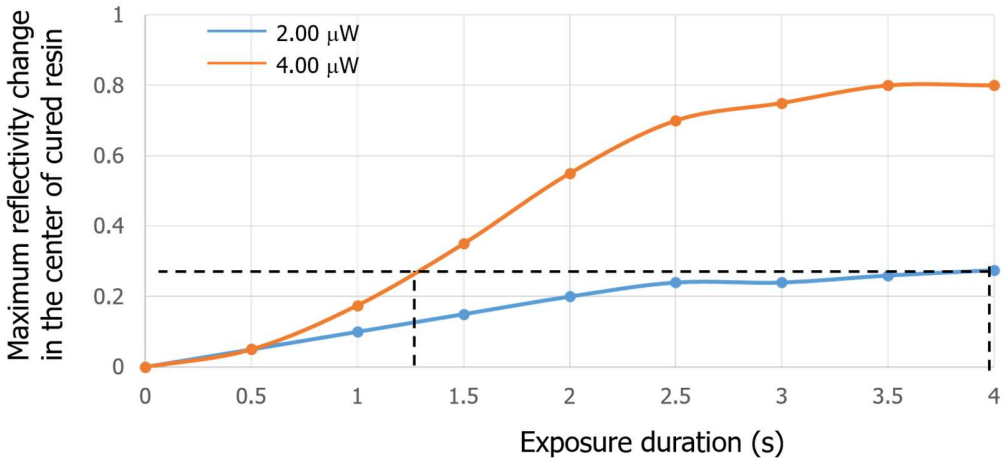

Figure 6-26 Reflectivity change (reflectivity decrease) in centre of cured resin as a function of the exposure duration in when resin was cured in an intensity of 2 and 4 μW.

As shown in this figure, in both exposure intensity, the change of the reflectivity keep increase with the exposure duration increase, but obviously, the reflectivity of resin cured by light in an intensity of 4 μW changes faster than that of 2 μW. Based on the fact that reflectivity shows a one-to-one correspondence with the thickness in a certain range, the resin shows the same reflectivity of the in-process measurement should be in the same thickness. Therefore, resin exposed by 2 μW in 4 seconds should be in the same thickness with the resin exposed by 4 μW in 1.24 seconds. In order to confirm this assumption, the resin was also cured in 4 μW and 1.24 seconds.

Figure 6-27 shows the reflection distribution of the resin exposed in the above three conditions. After imaging processing, the reflection variations were extracted and shown in **Figure 6-28**. The resin exposed in the condition of 2 μW and 4 seconds shows similar reflection with 4 μW and 1.24 seconds rather than 4 μW and 4 seconds that have same total exposure energy with the previous condition.

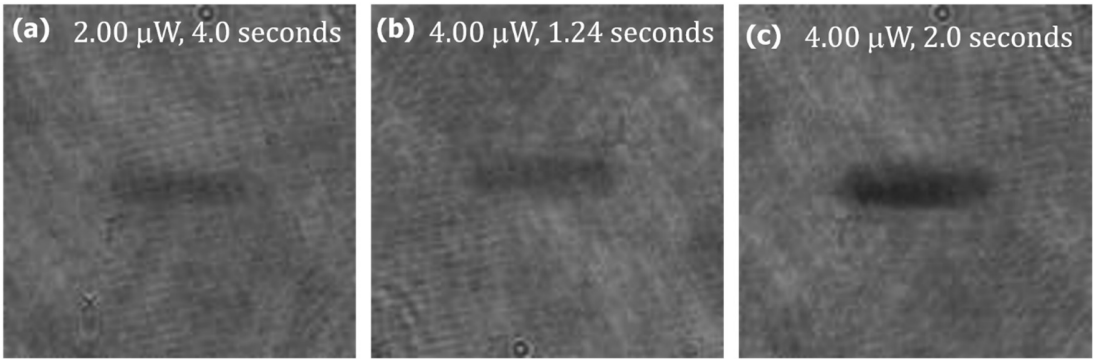

Figure 6-27 Reflection distribution of resin exposure by evanescent wave in exposure condition of (a) 2 μW and 4 seconds, (b) 4 μW and 1.24 seconds, and (c) 4 μW and 2 seconds, respectively.

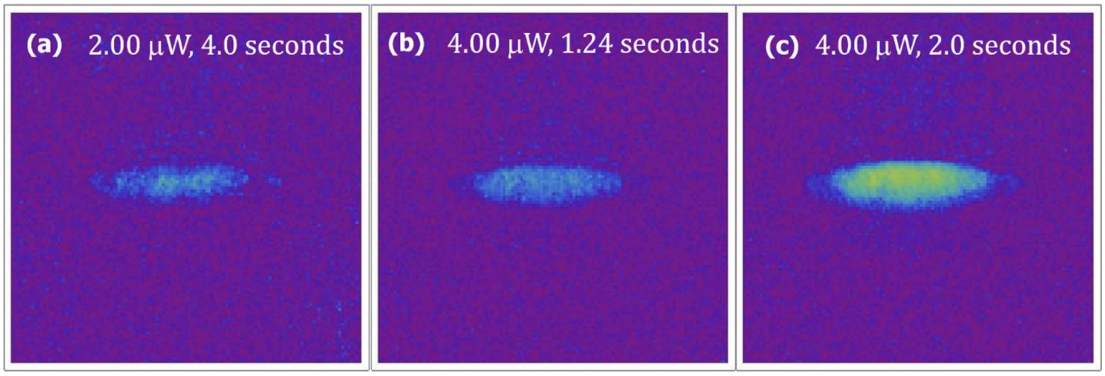

Figure 6-28 Variation of reflectivity of resin exposure by evanescent wave in exposure condition of (a) 2 μW and 4 seconds, (b) 4 μW and 1.24 seconds, and (c) 4 μW and 2 seconds, respectively.

The resin products in above three exposure conditions were also measured after the etching and drying process by using commercial optical microscopy and AFM to obtain the image and the profile of thickness of the cured resin. The measurement results of the resin samples are shown in **Figure 6-29** and **Figure 6-30**. The white dash lines in **Figure 6-29** mark the cross section where thickness of resin measured by AFM shown in **Figure 6-30**.

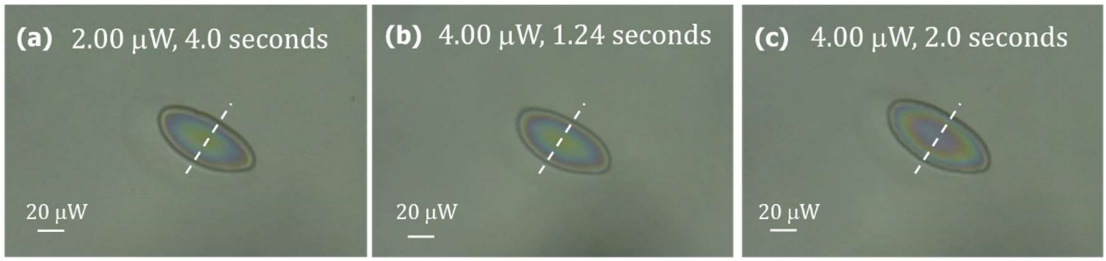

Figure 6-29 Resin cured by evanescent wave when exposure was in (a) 2 μW and 4 seconds, (b) 4 μW and 1.24 seconds, and (c) 4 μW and 2 seconds. The white dash lines mark the cross section where height of resin measured by AFM

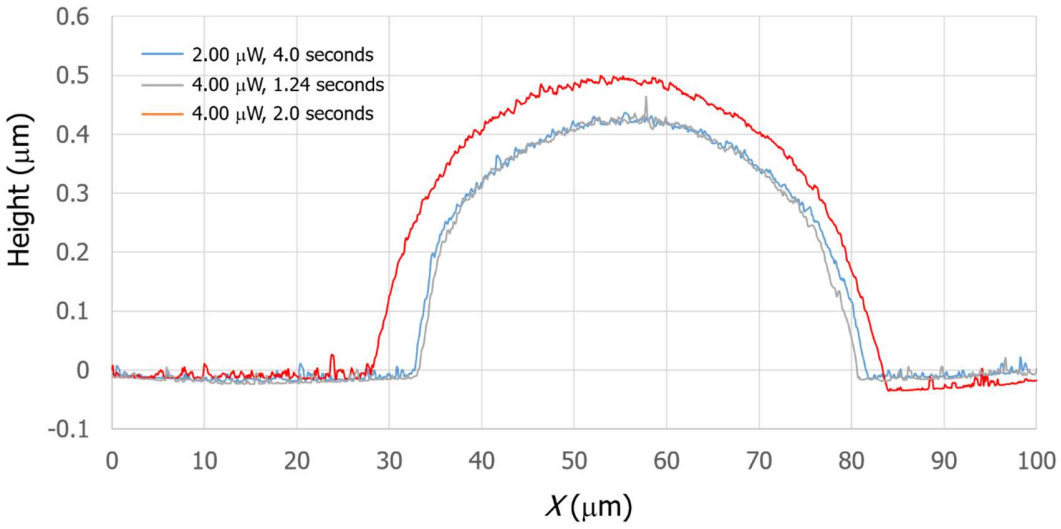

Figure 6-30 Thickness of resin measured by AFM when exposure was in 2 μW and 4 seconds, 4 μW and 1.24 seconds, and 4 μW and 2 seconds. Measurement of the gradient boundary using various incident angle

It is obvious that the resin exposed in 2 μW and 4 seconds shows same thickness with 2 μW and 1.24 seconds. This result proves that even in the different exposure intensity, after applying in-process measurement and determining the proper exposure duration, the thickness of the resin can be well controlled in the same value. It also directly proves that it is possible to control the thickness of cured resin using in-process measurement based on critical-angle reflection.

6.7 Measurement of the gradient boundary using various incident angle

The interfaces between the cured and the uncured resin are made up of half-cured resin in a state of the uncompleted polymerization. Due to the gradient boundary directly determines the thickness of each fabrication layer and greatly influences the quality of products, it is of great significance to study the gradient boundary in the fabrication process. I proposed the in-process measurement of gradient boundary using the reflection interference technique to monitor the formation of cured resin and investigate the gradient boundary.

6.7.1 Experiment Motivations

One of the biggest problems of EWNSL is the gradient boundary between the cured and uncured resin made by the half-cured resin. This is caused by the exponential intensity decay of the evanescent wave. Resin exposed by light in different intensity has different curing speed. The gradient boundary is made by the half-cured resin in a state of uncompleted polymerization and nonuniform curing degree; its physical characteristic is a medium between liquid and solid like gel; it can be removed by solvent or further cured in the exposure condition [76,77]. The existence of half-cured resin largely influences the shape and quality of cured resin. In order to improve the fabrication accuracy and further study of the curing process in EWNSL, the investigation of the gradient boundary shows great significance. To date, I only theoretically know the existence of the gradient boundary; however, the gradient boundary in EWNSL has never been measured. The difficulties on this work are mainly on, first of all, the spans of gradient boundary in EWNSL is in sub-micron scale. In addition, the gradient boundary has the gradient physical

and chemical characteristic. The gradient boundary is not totally in the solid state and therefore, it can be easily disturbed by contacting measurement. Based on the above demands and difficulties I proposed a measurement method utilizing the reflection interference at the critical angle of total internal reflection to measure the span of gradient boundary.

6.7.2 Theoritical backgound

My measurement method is still based on the total internal reflection at the critical angle. But I developed a simplified model to calculate the curing thickness. When the cured resin in a higher refractive index destroy the total internal reflection between the interface of substrate and resin, the light will transmit into the cured resin. Due to the measurement light is transmitted from the substrate to the uncured resin at the critical angle of these two mediums, the total internal reflection occurs when the light transmitted to the uncured resin. Therefore, all the light that transmitted into cured resin will be reflected from the top end of the gradient boundary. The reflections from the bottom side (r_1) and the top side (r_2) of resin generate the reflection interference. The curing thickness, that directly determines the length difference of optical path, largely influences the interference conditions and the reflection intensity. Therefore, is possible to obtain the curing thickness by detecting the intensity of reflection. However, not only the depth of the gradient boundary but also the refractive index of the cured resin determines the length of the optical path and therefore, the refractive index should be introduced into the calculation. It is known that the refractive index of the resin increases with its curing degree, and resin's curing degree decreases with

its distance to the substrate due to the special field distribution of the evanescent wave. It can be reasonably inferred that resin's refractive index decreases with its distance to the substrate. In these investigations, based on the facts that the spans of the gradient boundary are in sub-micrometer, I used the effective refractive index as an averaged refractive index of the cured resin. By this way, the prism, cured resin with gradient boundary, and uncured resin were treated as a three-layer-reflection model. The effective refractive index of cured resin was measured by changing the incident angle of the measurement light and finding the critical angle of the cured resin. The relationship between refractive index and critical angle can be simply calculated by Snell's equation. Once the effective refractive index of cured resin is measured, the reflectivity from the bottom side of cured resin (r_1) can be calculated according to the following equation.

$$I_{RI} = r_1^2 + (1-r_1)^2 + 2r_1(1-r_1)\cos(2\pi\Delta\varphi + \frac{\pi}{2}) \tag{6-7}$$

where r_1 can be calculated by Fresnel's equation, $\Delta\varphi$ is the phase difference generated by two different optical paths of. It can be expressed by the following equation.

$$\Delta\varphi = L_{Op1} - L_{Op2} = \frac{d_R n_{Eff}}{\lambda\cos(\theta_T)} - \frac{d_R \sin(\theta_I)\tan(\theta_T) n_P}{\lambda} \tag{6-8}$$

where θ_I is the incident angle and θ_T is the refractive angle calculated by Fresnel equations. Above equation shows the relation between the reflection depth (d_R) and the reflection intensity, which means it possible to obtain the value of reflection depth by measuring the reflection intensity in fabrication process.

6.7.3 Experiment and discussions

The experiment setup is shown in **Figure 6-31**. The setup and the experiment conditions are same with the in-process measurement in the previous experiment but the incident angle of two arms can be dynamically changed in this experiment.

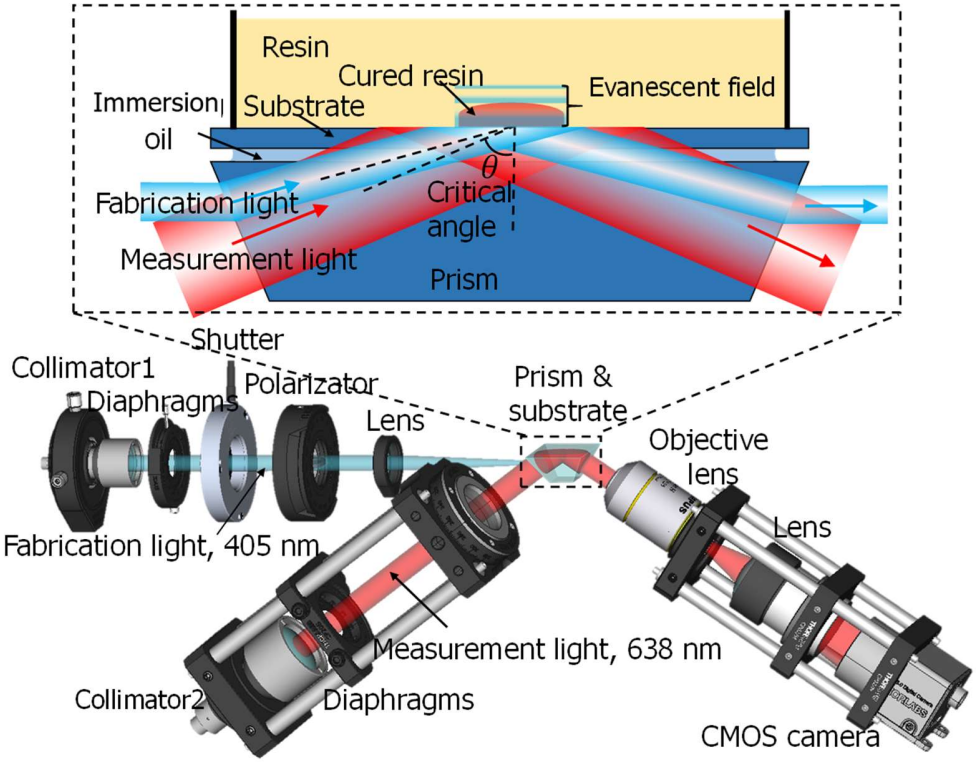

Figure 6-31 Experiment setup for measurement of cured resin in various in incident angle

After exposed by the light, the resin in the exposure filed was cured. **Figure 6-32** shows the experiment and calculation results. The intensity distributions of reflection were measured when a beam of measurement light was incident at 55.10°, 56.19° 56.24° and 56.13°. The refractive index of cured resin that corresponds to the critical angle in these degrees is 1.478, 1.479, 1.480 and 1.481, respectively.

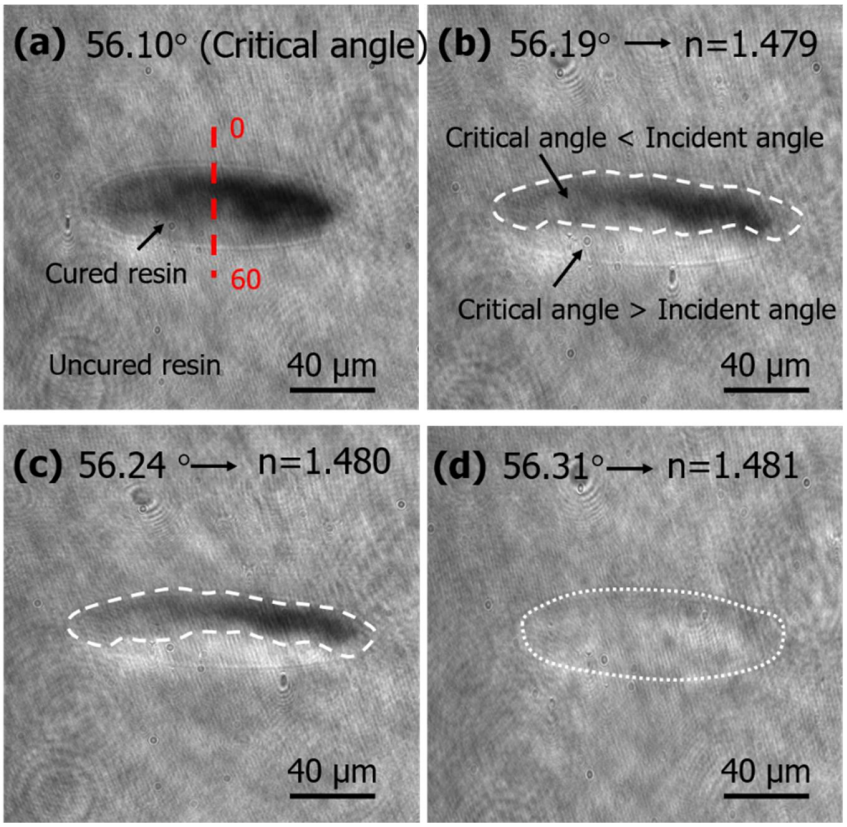

Figure 6-32 Experiment results. Reflection distribution when measured light was incident in angle of (a) 56.10, (b) 56.19, (c) 56.24 and (d) 56.31.

In **Figure 6-32** (a), the incident angle of the measurement light is equal to the critical angle of uncured resin. In this case, the total internal reflection occurred at the boundary between the uncured resin and the substrate, which leads the highest intensity of reflected light from uncured resin; while cured resin in a relatively higher refractive index destroyed the condition total internal reflection; and therefore, cured resin with a relatively lower reflectivity was clearly distinguished with the uncured resin.

In **Figure 6-32** (b), the incident angle was increased to 56.19°. The corresponding maximum refractive index of resin that meets the requirement of total internal reflection also increase from 1.478 to 1.479. In this case, the cured resin whose effective refractive

index smaller than 1.479 generates the total internal reflection. Therefore, in **Figure 6-32** (b), the bright area in cured resin means where resin's effective refractive index smaller 1.479. The dashed line that marks the range of the total internal reflection in the cured resin is the contour line of effective index 1.479.

By slightly changing the incident angle step-by-step, distribution of effective refractive index was measured. In this verification experiment, due to the oblique observation influences the quality of imaging (this problem can be solved by applying an immerging objective lens to control incident and observation angle), the distribution of effective refractive index was only roughly measured. **Figure 6-33** shows the cross-section of effective refractive index marked by the red line in **Figure 6-32** (a) measured various incident angles.

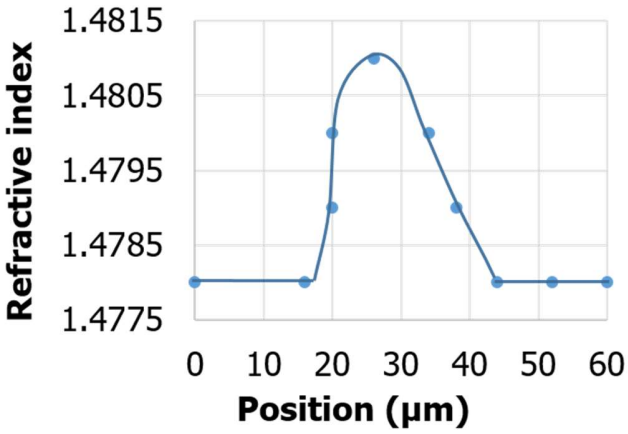

Figure 6-33 Cross-section of refractive counter map

Figure 6-34 shows the image of the cured resin after the etching and drying process measured by optical microscopy.

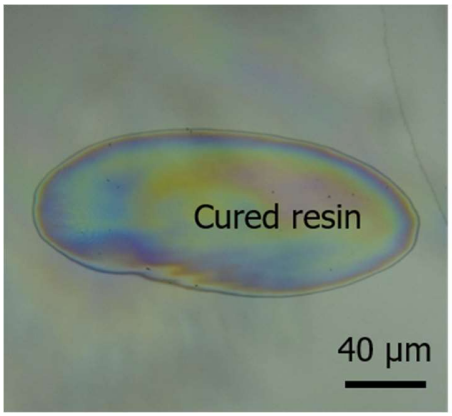

Figure 6-34 Cured resin measured by optical microscopy after etching and drying process.

The reflection depth, which calculated by using the effective refractive index and reflection distribution was plotted in **Figure 6-35**.

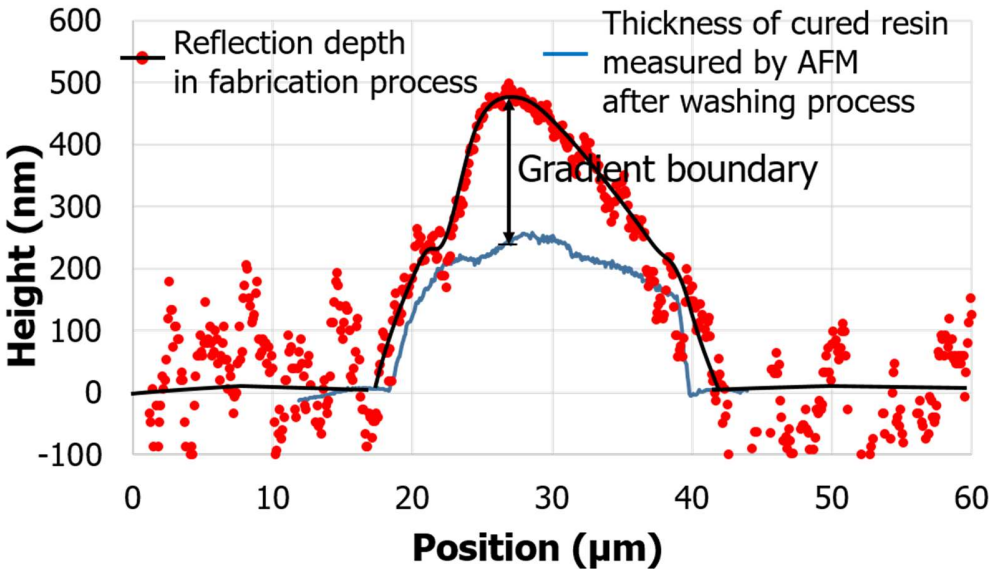

Figure 6-35 Calculated distribution of reflection depth measured by proposed method in fabrication, and thickness of cured resin measured by AFM after washing and drying process.

The red point is the raw data. The dark solid line is the processed results. In order to know the span of the gradient boundary, the thickness of cured resin after the washing and drying process was measured AFM as shown by the blue line. In the proposed method,

the measurement light was oblique incidence and inclined projection results in the distortion of the image, while **Figure 6-34** and AFM do not have this problem. In order to make subtraction to calculate the span of gradient boundary, the transverse span of AFM results was scaled down.

In **Figure 6-35**, the gradient boundary is slightly larger than the thickness of cured resin. The span of gradient boundary different with the position, and is a maximum value of around 250 nm in the center of the cured resin. In addition, comparing the shape and the tendency of reflection depth thickness of cured resin, I found that these two curves have better similarity in the left side. This is because the measurement light was the only incident from one side (from the left, and from the top side). The reflection distribution in another side might be influenced by the scattering and multi-reflection. This problem can also be solved by applying immersion objective lens in to experiment system, which can provide measurement at a particular incident angle from various directions. According to the above results, the gradient boundary of resin in EWNSL has been successfully measured. The problem is that it is hard to examine the rightness and accuracy of my measurement method.

6.8 Conclusions

Inclusion, in order to control the thickness of cured resin in EWNSL. In-process measurement using critical-angle reflection was applied in EWNSL to determine the proper exposure time. My investigation focus on the in-process measurement.

In the first verification experiment, I proved that the even resin was cured by the evanescent wave can still be clearly distinguished with the uncured resin in the fabrication process by using proposed critical-angle reflection.

In the second verification experiment, the curing process of the resin exposed by evanescent wave was observed. The successive decrease of the reflection of the cured resin confirmed that it is possible to measure the thickness of cured resin by detecting the reflection since a low reflectivity represents a larger thickness of the cured resin.

In the theoretical investigation, I simulated the curing process of the resin exposed by evanescent wave and obtained the conversion degree and refractive index profile. Based on the simulation results, I calculated the optical response of reflection interference and obtained the theoretical relationship between the reflectivity and turning depth of the cured resin. The results proved that the reflectivity changes apparently with the increase of curing thickness, which proves that it is possible to measure the thickness information by detecting the reflection using the proposed method.

In order to get the numerical relationship between reflectivity and the thickness, a calibration experiment was done to directly measure the relationship. Result showed that the reflectivity linearly decreased 0.51 as the thickness of the cured resin increase to 400 nm. This relationship was applied in the experiment of in-process measurement and the thickness measured in the curing process using the proposed method was proved in an accuracy better than 50 nm.

At last, when the reflectivity was used as the feedback to determine the exposure duration, the thicknesses of the cured resin were controlled within a difference of 10 nm

compared with the expected thickness. This proved that by usage of the in-process measurement, the thickness of the cured resin can be well controlled in EWNSL.

CHAPTER 7. EXPLORATION STUDY OF A NOVEL MULTI-LAYER SUBSTRATE FOR IN-PROCESS MEASUREMENT BASED ON SURFACE PLASMON RESONANCE WITH PLZT

In this chapter, the theoretical investigation of measurement using surface plasmon resonance is demonstrated. The simulation work that proves the feasibility is introduced in this chapter as well. This chapter also shows a novel SPR substrate with multi-layer that can provide fast scanning by change the applied voltage.

7.1 Motivation of applying SPR measurement in MSL/EWNSL

Surface plasmon resonance (SPR) measurement has been widely used in the refractive-index-based detection due to its high sensitivity on the refractive index. My in-process measurement in the MLS/EWNSL is based on the refractive-index increase of the resin and therefore, SPR measurement might provide higher sensitivity. In addition, the measurement system of SPR measurement is similar with the measurement system using the total internal reflection at the critical angle: both systems require large incident angle from the high refractive index substrate, measure the near-substrate resin, and detect the optical response. Therefore, the SPR measurement can be achieved by a slight change in the existing measurement system. Most importantly, SPR measurement avoids the problem the noise from the far-substrate resin, as shown in **Figure 7-1**. The left figure shows the measurement using critical-angle reflection. In this case, the measurement light propagates into the cured resin due to the total reflection is destroyed. A part of the light that propagates into the cured resin might be scattered or reflected, which generates the noise and

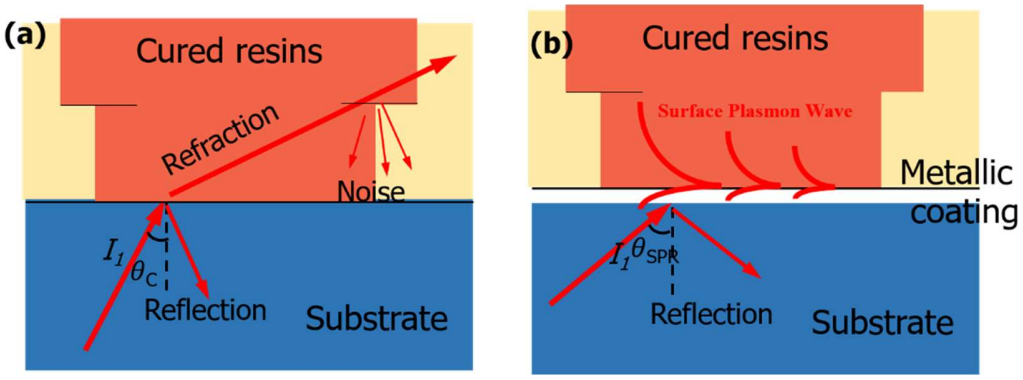

Figure 7-1 Optical response in (a) critical-angle reflection with noise problem (b) SPR measurement without noise problem.

influences the measurement largely since the detection is directly based on the intensity. For SPR measurement, no matter the SPR occurs or not, the measurement light will be reflected, propagate alone the metallic coating or be aborted, and there will be no light propagate into the resin, which avoids the noise from the resin.

7.2 Theoretical investigation of SPR

The use of SPR for measuring cured resin is based on the variation of the refractive index after solidified and the strong dependence of resonance conditions on the optical parameters of the medium in direct contact with the metal thin film. SPR occurs when propagating light strikes on and resonantly induces the free electrons of the metal to oscillate the metal/dielectric interface [93-95]. As a result, the radiant energy is absorbed by the metal at a certain incident angle, and rest of them, in a form of reflected light, whose reflectivity and phase shows extremely sensitive to the index of refractive index of the dielectric medium in contact with the metal surface.

A basic SPR substrate is made by coating 46-nm-thick Ag thin film on high index prism, as shown in **Figure 7-2**. When scanning the incident angle, an abrupt variation

reflectivity and phase occurs at a certain incident angle. A slight change on samples' optical characteristic (resin's refractive index) lead a shift on reflectivity-angle and phase-angle dependence curve and results in a variation of reflectivity and phase at a fixed incident angle.

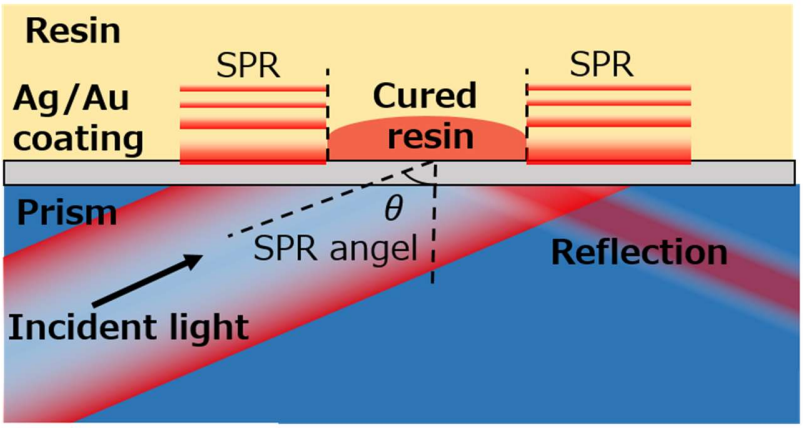

Figure 7-2 Diagram of in-process measurement of cured resin using SPR

The reflectivity-angle dependence curve is shown in **Figure 7-3** (a). In the case of the refractive index of the substrate is 1.78, when the refractive index of the cured resin increase from 1.49 to 1.50, it is obvious that the whole dependence curve shift to a larger angle. The angle of strongest SPR where reflectivity is almost zero increase from 64.6 to 65.5 degree. As a result, if the incident angle is fixed at the 64.6 degrees, the increase of refractive index (from 1.49 to 1.50) will make refractive index change around 0.35.

Therefore, similar to the measurement method based critical-angle reflection, in SPR measurement, the refractive index variation of the resin directly changes the reflection.

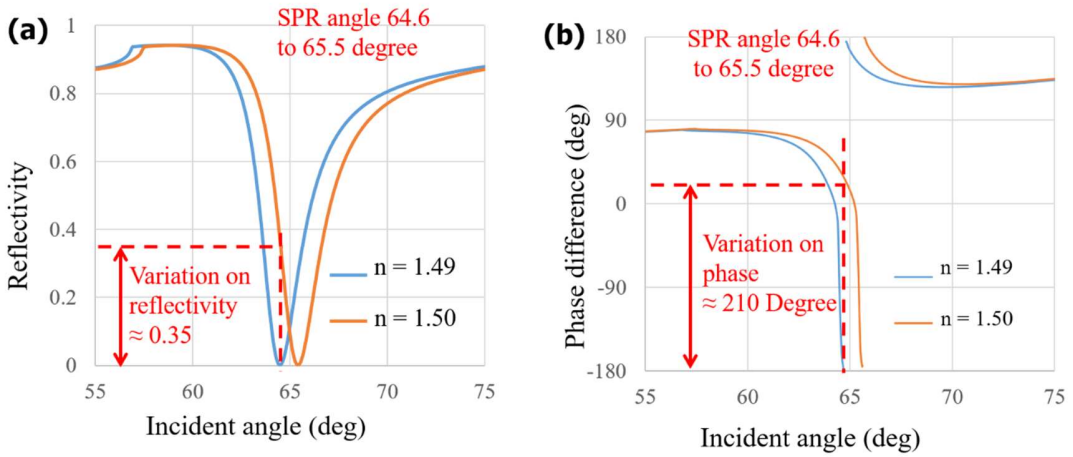

Figure 7-3 Optical response of SPR measurement when refractive index of resin is in 1.49 and 1.50. (a) Reflectivity and (b) phase as a function of indicent angle.

More significantly, the shift of SPR angle also generates a phase change. Due to there is a phase jump making phase-angle dependence curve changes drastically near the SPR angle, even a slight change of refractive index will lead a significant change of the phase, as shown in **Figure 7-3** (b). When the refractive index of the resin increase from 1.49 to 1.50, phase decrease as large as 210 degrees. This means phase-detection-based SPR measurement can provide much higher sensitivity than intensity-detection-based SPR as well as the measurement based on the critical-angle reflection.

In case of the phase-detection-based SPR measurement, one of the fatal shortcomings is that the steep jump of phase that generates high sensitivity phase detection only occurs at a small range of incident angle where strongest SPR obtained. In order to clearly illustrate this problem, the successive variation of reflectivity and phase when the refractive index of the resin increase from 1.49 to 1.53 is plotted in **Figure 7-4** (a) and (b), respectively. It shows that reflectivity changes with the refractive index in a wide range of refractive index; while phase only drastically changes with the refractive index in a narrow range near 1.49.

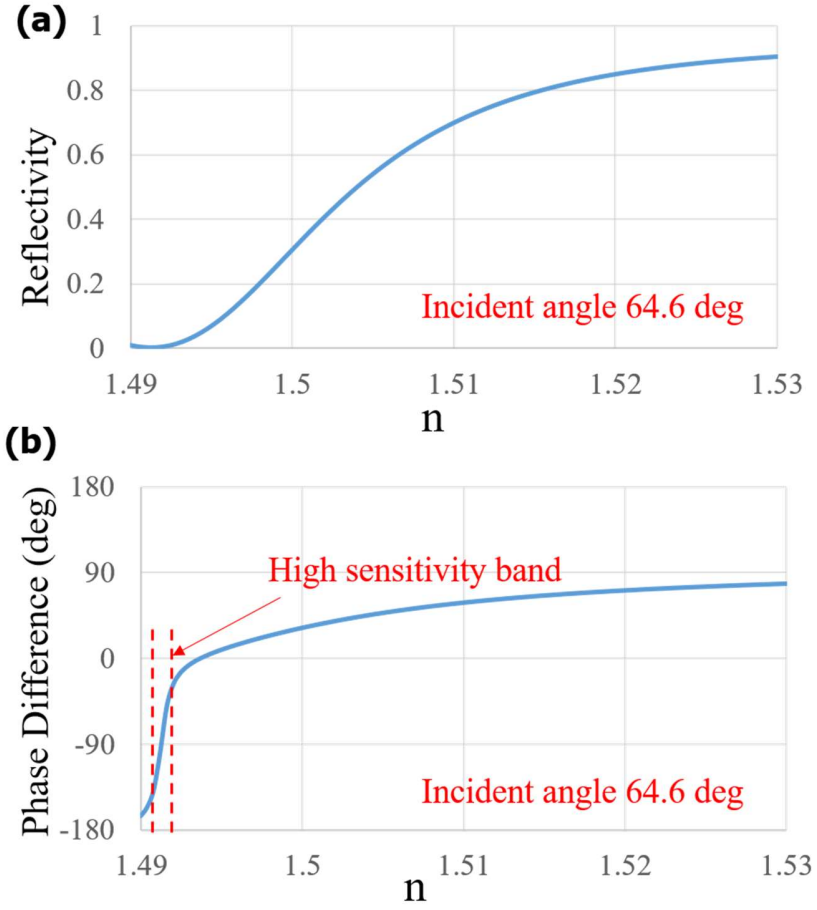

Figure 7-4 Optical response of SPR measurement when incident angle is fixed at 64.6 degree.(a) Reflectivity and (b) phase as a function of refractive index.

When the refractive index of the cured resin changes too much and is out of the highly sensitive range of phase-detection-based SPR measurement, the sensitivity of the variation of refractive index decrease a lot and might be even worse than intensity-detection-based SPR. This problem limits the application of phase-detection-based SPR measurement in MSL/EWNSL largely.

One way to adjust the high sensitivity range is to simply change the incident angle of the measurement light, as shown in **Figure 7-5**. When the incident angles are 66.4, 65.6, 66.6 and 66.7 degrees, the high sensitive ranges are near 1.491, 1.501, 1.512 and 1.522. It

is obvious that that changing the incident angle can effectively move the high sensitivity range, and indirectly widen the measurement range of phase-detection-based SPR measurement.

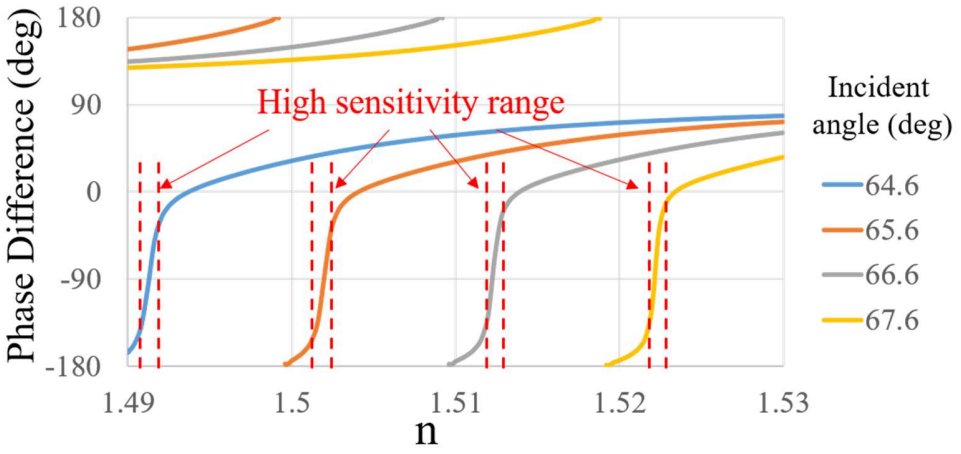

Figure 7-5 Phase response of SPR measurement as a function of refractive index in various incident angle of measurement light.

Considering the in-process measurement in MSL/NSL using SPR, it is hard to mechanically change the incident angle of the measurement light in the curing process, especially when 0.01-degree-precision control on the angle is required. In addition, in practical experiment or measurement, we have to adjust the incident angle for several times during once measurement in order to match the samples that have a large refractive index or thickness difference. Moreover, a gradual change and measure process might be required to investigate the gradual refractive index boundary between solidified and liquid resin, which will spend an extremely long time on calibrating and adjusting the incident angle.

Based on above facts, in order to apply phase-detection-based SPR in in-process detection, and in the meanwhile, achieve a more flexible way replacing incident angle

control I proposed a novel multi-layer SPR substrate with PLZT (a ceramic perovskite material that its refractive index changes with voltage on it).

7.3 Optimization of the multi-layer SPR substrate with PLZT

The proposed multi-layer SPR substrate is shown in **Figure 7-6**. It composed of a PLZT layer embedded between two metal thin films. The refractive index and thickness of each layer are marked in **Figure 7-6**. In the initial state of the substrate without an applied voltage, the reflectivity and phase of reflected light as a function of incident angle is calculated using the parameters marked in the figure, as shown in **Figure 7-7** (a) and (b), respectively.

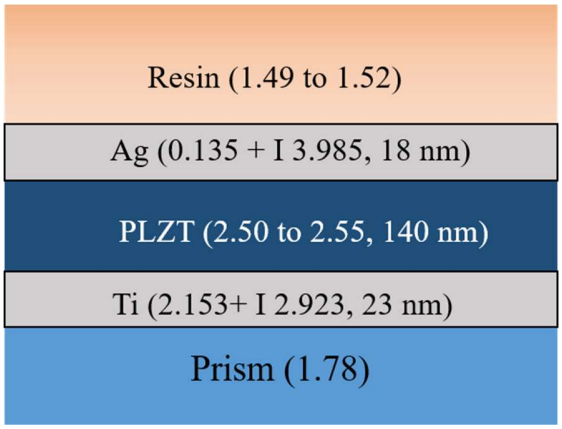

Figure 7-6 Diagram of multi-layer SPR substrate with PLZT

Compared with single layer substrate, PLZT based substrate provides a reflectivity curve with lower sensitivity, but its phase curve still has a quite steep change at a specific range of incident angle near strongest SPR angle, which proves the possibility of high-resolution detection using this substrate.

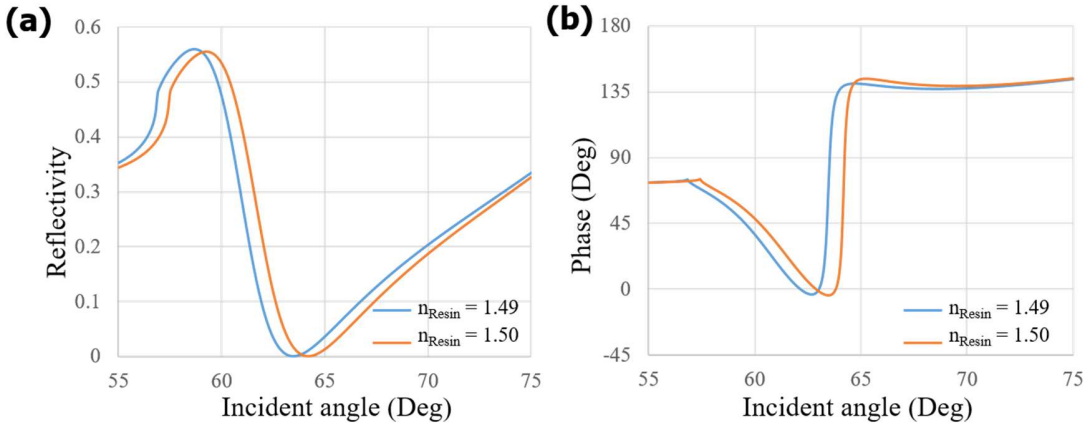

Figure 7-7 Optical response of SPR measurement using proposed multi-layer substrate when refractive index of resin is in 1.49 and 1.50. (a) Reflectivity and (b) phase as a function of incident angle.

PLZT based multi-layer SPR substrate was proposed to dynamically shift high-sensitive-detection range in a much more convincing way. It bypasses the high accuracy angle control by providing a variation of refractive index of PLZT realized by changing the applied voltage on it, and effectively influence the high-sensitive-detection range in a fixed incident angle. **Figure 7-8** clearly shows this feature.

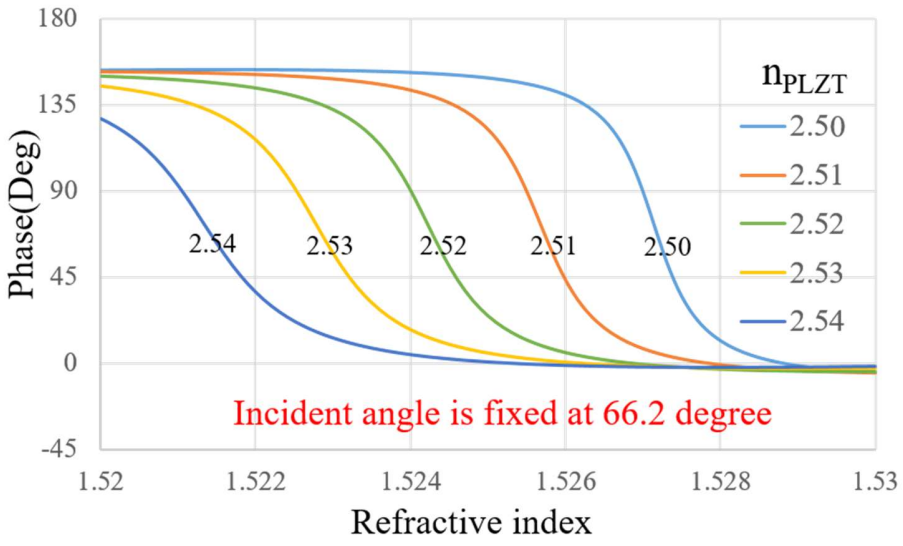

Figure 7-8 Phase response of SPR measurement as a function of refractive index in various refractive of PLZT controlled by applied voltage

High-sensitive-detection range shifts from 1.521-1.522 to 1.526-1.527 with the refractive index of PLZT changing from 2.5 to 2.54. Also according to **Figure 7-8**, 0.001 variations on resin's reflectivity index causes phase of reflected light linearly increase about 40 degrees. In case of resolution of the phase detector is 1 degree, the resolution of refractive index is 2.5×10^{-5}.

Besides, since the PLZT layer is extremely thin in my investigation (in a thickness of 140 nm), a slight change on the applied voltage is enough to cause a required variation on refractive index. The refractive index change as a function of voltage is approximately expressed by

$$\Delta \mathrm{n} = \frac{1}{2} n^3 r \frac{V}{t} \tag{7-1}$$

where n is reflectivity of PLZT and about 2.5 in my simulation; r is the electro-optic coefficient and value as 30 pm/V; V is the applied voltage; and t is the thickness of PLZT films. This proves the possibility of adjusting fixed incident angle into high sensitivity range by using voltage control rather than mechanically changing incident angle.

Due to the proposed SPR substrate is based on a multi-layer structure, the thickness of each layer influences the performance of the substrate largely. Therefore, it is necessary to make optimization of the thickness of each layer. In my investigation, I discussed a condition that uses Ti and Ag as the inner and outer metal thin film; and considering about the practical fabrication, the thickness of each layer relies on integer during calculation. According to my calculation and simulation on the multi-layer substrate, increasing the thickness of PLZT layer will weaken the influence on sensitivity near the strongest SPR

angle caused by the variation of refractive index of PLZT, and in the meanwhile, decrease the phase shift caused by the sample. As a result, the thickness of the PLZT has been limited between 110 and 150 nm. **Figure 7-9** plots the optical thickness of the outer metal thin film (t_{Outer}) corresponding to the thickness of the inner metal thin film (t_{Inner}) where maximal phase-detection sensitivity (steepest phase-angle curve) is obtained.

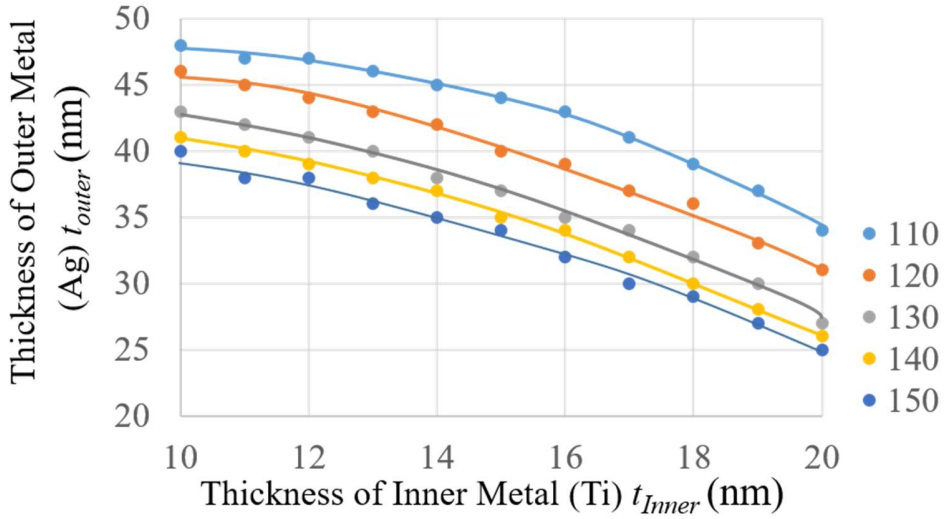

Figure 7-9 Optimal t_{Outer} where highest sensitivity is obtained as a function of t_{Inner} in various t_{PLZT}.

When maximal phase-detection sensitivity occurs, a slight increase on t_{Outer} will lead the steep jump of phase change from decreasing to increasing, as shown in **Figure7-10**. Phase-angle curve becomes rise to near 64 degrees when t_{Outer} change from 24 nm to 25 nm, in case of t_{Inner} = 20 nm. This phenomenon was utilized to find the optimal t_{Outer}. Besides, for t_{Inner} = 20 nm, even though 25 nm-thick t_{Outer} provides a steeper curve than it equals to 24 nm, optimal t_{Outer} has been chosen as 24 nm since in this case phase will keep decrease with incident angle increasing, and more important, trend of phase will not change direction when there are variations on refractive index of resin and PLZT, both of which benefit to measurement to a great extent. In addition, as I mention that PLZT layer is used

to provide a phase shift, in case of a larger t_{Inner}, a larger phase shift is caused by the same variation on n_{PLZT}; and as a trade-off, the sensitivity undertakes large influence by n_{PLZT}.

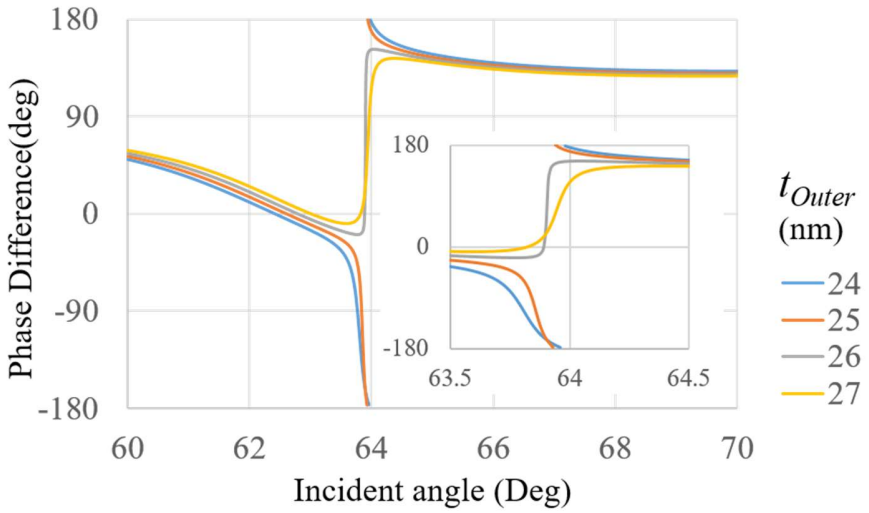

Figure 7-10 Optimal t_{Outer} where highest sensitivity is obtained as a function of t_{Inner} in various t_{PLZT}.

It is a remarkable fact that attempt other metal to generate SPR and slight vary the thickness of each layer in sub-nanometer scale might further increase the sensitivity. In addition, the multi-layer SPR substrate with PZLT layer is suitable for but not limited to the in-process measurement in MSL/NSL. For other field that requires a high sensitive measurement in a wide measurement range, proposed multi-layer PLZT-based substrate is a good option as well.

7.4 Conclusions

In this chapter, SPR measurement was theoretically investigated for applying as the in-process measurement in MSL/EWNSL due to its advantage of high sensitivity to refractive index and confinement of optical field. In order to utilize the phase-detection-

based SPR measurement. The measurement strategy and system were demonstrated in a similar way with the critical-angle-reflection method. Moreover, a novel multi-layer SPR substrate with PLZT was proposed to achieve the dynamical control of the high-sensitive detection range. By using this multi-layer substrate, the resolution of refractive index can be achieved in a value of 2.5×10^{-5} when the resolution of phase detection is 1 degree. Moreover, the high sensitive band of measurement can be shifted in a range of 0.04 refractive index by simply controlling load voltage on two side of PLZT in a range of 0 to 20 V. In addition, the optimized thicknesses relation among PLZT and two metal coating layers are demonstrated to ensure the existence of SPR and provide a maximum sensitivity. The investigation of SPR in this chapter proved the possibility to replace the critical-angle-reflection measurement by SPR measurement as the in-process measurement in MSL/EWNSL.

CHAPTER 8. CONCLUSIONS

In this chapter, important results of each chapter are summarized and conclusions are presented. Recommendation about how to achieve the in-process measurement in MSL/EWNSL is demonstrated. Finally, the future research based on the investigation in this thesis is illustrated.

8.1 Conclusions

In this thesis, the resin cured in fixable thickness by MSL and in ultra-thin thickness by EWNSL were proposed to be fabricate in an assistant of the in-process measurement based on the variation of refractive index of the resin near the substrate. The measurement method for the in-process measurement was achieved by detecting the reflection from the near-substrate resin when the measurement light was incident at the critical angle of the internal reflection. The optical response in MSL and EWSNL using the proposed critical-angle-reflection method were different and therefore, investigated as two topics. The feasibility of in-process measurement in MSL and EWNSL was experimentally confirmed, respectively. In addition, SPR measurement as an alternative method was also proposed to be applied as the in-process measurement in MSL/EWNSL. The possibility of SPR measurement was theoretically confirmed.

In chapter 1, the existing MSL and NSL techniques were summarized and classified according to the exposure strategies. Among them, the fixed-surface type MSL was expected to flexibly cure each layer in different thicknesses, and EWNSL shows the

strong demands on preciously controlling the thickness of the resin. In order to meet above requirements, the in-process measurement was proposed to be applied in MSL and EWNSL.

In chapter 2, based on the difficulties of the in-process measurement in MSL and EWNSL, the potential methods of the in-process measurement were discussed and the limitations of them were indicated as well. As a result, I proposed the measurement method using the refractive index change of the resin in the curing process and the optical response of the internal reflection at the critical angle from the near-substrate resin.

In chapter 3, the curing process of the resin was literature surveyed, including the curing rate, heat transfer and oxygen inhibition. The existence of gradient boundary of the cured resin in the curing process was claimed and its influences on MSL and EWNSL were discussed as well. Due to the measurement difficulties cased by the gradient boundary, in MSL, the distribution of conversion degree of the resin was used as the measurement target for the in-process measurement to determine the proper exposure duration; while in EWNSL, the thickness of the cured resin was directly measured to determine the exposure duration and control the thickness.

In chapter 4, the proposed measurement method based on the reflectivity change of the measurement light incident at the critical angle was detailed explained. The optical response using the proposed measurement in MSL and EWNSL was analysed respectively.

In chapter 5, I experimentally realized and proved the feasibility of in-process measurement of conversion degree in MSL using the critical-angle reflection method. The relationship between the refractive index and the conversion degree was experimentally measured. The results showed that the reflectivity linearly decreased 0.03 as the conversion

degree increase to 60%. In the in-process measurement calibrated by above relationship, the distribution of conversion degree was measured in resolutions around 1% with a lateral resolution of 2.6 μm, which can ensure a lateral resolution of width in several micron meters according to the measurement results. In a condition of knowing critical etching degree, my investigations powerfully indicate the feasibility to in-process measure the width of the cured resin, and determine the proper exposure duration in MSL.

In chapter 6, I confirmed the feasibility of the in-process measurement of the thickness in EWNSL. First of all, the mechanism of optical response from the cured resin in EWNSL was proposed in reflection-phase-contrast interference with gradient changed refractive index. According to the proposed mechanism, the theoretical variation of reflectivity in the curing process was calculated by using heat/mass-transfer model to simulate the profile of refractive index of the cured resin, fiber theory to obtain the optical path of light in the gradient refractive index, and the interference between light reflected from the bottom and top of the cured resin. The calculated results were well agree with the practical results in verification experiment. In addition, the relationship between the reflectivity change and the thickness of the cured resin was calibrated by comparing the in-process measurement with the thickness measured by AFM after the curing process. Result showed that the reflectivity linearly decreased 0.51 as the thickness of the cured resin increase to 400 nm. This relationship was applied in the experiment of in-process measurement and the thickness measured in the curing process using the proposed method was proved in an accuracy better than 50 nm. At last, when the reflectivity was used as the feedback to determine the exposure duration, the thicknesses of the cured resin were controlled within a difference of 10 nm compared with the expected thickness. This proved

that by usage of the in-process measurement, the thickness of the cured resin can be well controlled in EWNSL.

In chapter 7, SPR measurement was theoretically investigated for applying as the in-process measurement in MSL/EWNSL. The measurement strategy and system were demonstrated in a similar way with the critical-angle-reflection method. Moreover, a novel multi-layer SPR substrate with PLZT was proposed to achieve the dynamical control of the high-sensitive detection range. The resolution of refractive index can be achieved in a value of 2.5×10^{-5} when the resolution of phase detection is 1 degree using this multi-layer substrate. Moreover, the high sensitive band of measurement can be shifted in a range of 0.04 refractive index by simply controlling load voltage on two side of PLZT in a range of 0 to 20 V. The investigation of SPR in this chapter proved the possibility to use SPR measurement as the in-process measurement in MSL/EWNSL.

This research used a very concise method to achieve the in-process measurement of distribution of conversion degree and thickness of the cured resin in MSL and EWNSL respectively. The requirement of high sampling rate and existence of gradient boundary make in-process measurement extremely difficult, as a result, no suitable measured method has been proposed yet. In addition, due to the conversion degree is one of the chemical properties, the refractive index change of the resin that can be measured by optical method in a high accuracy was utilized in my method. Although the photo-polymerization influenced by many factors is a complex reaction, the model of the curing process and optical response were analysed to make it possible to obtain the variation of chemical reaction by directly detecting the optical response. In order to obtain an optical response sensitive to the refractive index, the critical-angle-reflection method was proposed. The

measurement system was concise enough to be simply and compactly integrated into the fabrication system. The feasibility of the proposed method was confirmed in the experiment where the thickness of the cured resin was well controlled within a different of 10 nm using the in-process measurement as the feedback. MSL and EWNSL with the in-process measurement that can flexibly and exactly control the thickness of the cured resin have a huge potential to become the next-generation fabrication techniques.

8.2 Recommendations

Based on my research experience, some notable problems and recommendations for repeating this experiment are introduced in this section.

The investigations of in-process measurement in MSL and EWNSL are exploratory work. My efforts were mainly on the verification of the mechanism and the feasibility of the proposed measurement method rather than the performance of the measurement. Therefore, the performance of experiment setup as well as the measurement system have a large potential to be improved by using optimized lens systems and a camera with a smaller pixel size, a higher resolution of intensity and a higher sampling rate.

It is worthy notable that the measurement light was incident in a large incident angle, which means the imaging surface was tilted from the object plane (the near-substrate resin). The distance between the near-substrate resin and detector in camera changed with the lateral position. As a result, only a small range of the cured resin can be clearly imaged. Regarding to this problem, it can be solved by titling the lens before the camera in particular

angle that can be calculated by Scheimpflug principle, or replacing the prism by an immersion objection with an annulus filter to control incident angle.

Regrading to the measurement light, laser in a wavelength of 638 nm was used, which provides strong interference and generated noises degrading the reflection distribution. Although a part of noise was removed by imaging subtracting, I highly recommend to use low coherence light source to further reduce the influence of noise.

I experimentally proved that the measurement light does not change the conversion degree of the resin even in a long-time exposure, however, it generates heat and speeds up the polymerization process when resin is exposed by the fabrication light (405 nm). Therefore, measurement light should be in low intensity. In addition, based on the fact that the resolution of reflectivity decreases with the reduction of exposure intensity, it is necessary to found a suitable value of the intensity of measurement light according to the trade-off.

8.3 Future work

This thesis established the in-process measurement in MSL and EWNSL. Based on this work, several topics that are worth pursuing are demonstrated in the following contexts.

The simulation of the curing process still needs further investigations. About this topic, there are some simulation models can be referred to; however, there is no uniform and widely recognized model for this kind of simulation and the simulation results differs with the models. In my simulation work, a mass/heat transfer model was used to simulate the curing process, which can effectively calculated the conversion degree in an increasing

exposure duration but still ignored some points including the oxygen inhibition and maximum conversion degree, which slight influences the accuracy of simulation results. In order to quantitatively analyse the theoretical relationship between curing condition and optical response, it is necessary to develop a more complex and accuracy simulation model.

The optical response in EWNSL was explained by the reflection-phase-contrast interference but ignored the multi-reflection in the cured resin. The order of multi-reflection also influences the calculation results. In the future work, it is necessary to develop a more detailed calculation model including analyzation of multi-reflection. This calculation should be compared with the simulation using FDTD or RCWA algorism.

The critical etching degree is still unknown. It is necessary to experimentally measure it to complete this research. The etching process is influenced by a lot of factors including the concentration of cleaning agent, temperature, etching duration, as well as the resin itself. Once the critical etching degree is determined, these influence factors in the in-process measurement should be strict same with the determination experiment.

The thickness measured in EWNSL is the etching thickness of a single layer that is different from the thickness after stacking process. Therefore, it is necessary to investigate the difference between etching thickness and stacking thickness. It is known that if the stacking process is in the same pressure, both etching thickness and thickness after stacking depend on the profile of conversion degree. A larger etching thickness corresponds to a larger thickness after stacking. However, the exact relationship between them needs to be experimentally calibrated.

The SPR measurement should be experimentally confirmed. The experiment system of SPR measurement can be similar with the measurement system based on critical-angle reflection, as both of them require a large incident angle for measurement light. In addition, some improvements and modifications are need for the experiment system of SPR measurement. Based on the fact that SPR has a high requirement of the metal coating over the substrate, the quality of coating should be examined, especially for multi-layer SPR substrate. In addition, in order to achieve the phase-detection-based SPR measurement, measurement unit for detection of phase change should be investigated and supplemented into the measurement system.

The feedback system has not been finished yet and needs to be further investigated. Although I successfully controlled the thickness of the cured resin by using the feedback of the reflectivity, a completed system consisting fabrication and measurement systems, as well as the control unit of feedback should be developed in the future. The response time of feedback system largely influence the performance, and therefore, high performance hardware for control system should be designed and applied in the whole system.

APPENDIX A: MEASUEMENT OF ABSORPTION CONSTANT OF RESIN IN THE CURING PROCESS

In this research, I measured the absorption constant of the resin in the curing process. The motivation of this investigation, experiment setup and results are demonstrated in this section.

A.1 Research motivation

The absorption constant is an important parameter of the resin. It directly determines the exposure intensity and influences the curing process. In addition, I considered utilizing the variation of absorption of the cured resin to achieve the in-process measurement if it changes enough in the curing process. In order to clearly know how absorption constant changes in the curing process, I made a real-time measurement of the absorption constant in an exposure condition.

A.2 Experiment setup

The absorption constant was obtained by measuring the transmittance of a bulk resin sample and making a calculation involving the thickness of the cured resin. The experiment setup is shown in **Figure A-1**. The left part is the design drawing and the right part is the physical map. Measurement light in a wavelength of 638 nm was incident from the bottom of the cured resin and measured by the photodetector after transmitting through

the resin. The thickness of the cured resin was confined in 2 mm by a distance between to cover glasses. In order to measure the absorption constant of the resin in various conversion degree, irradiation of UV was used as the exposure. The intensity of transmitted light was continuously recorded in the exposure condition.

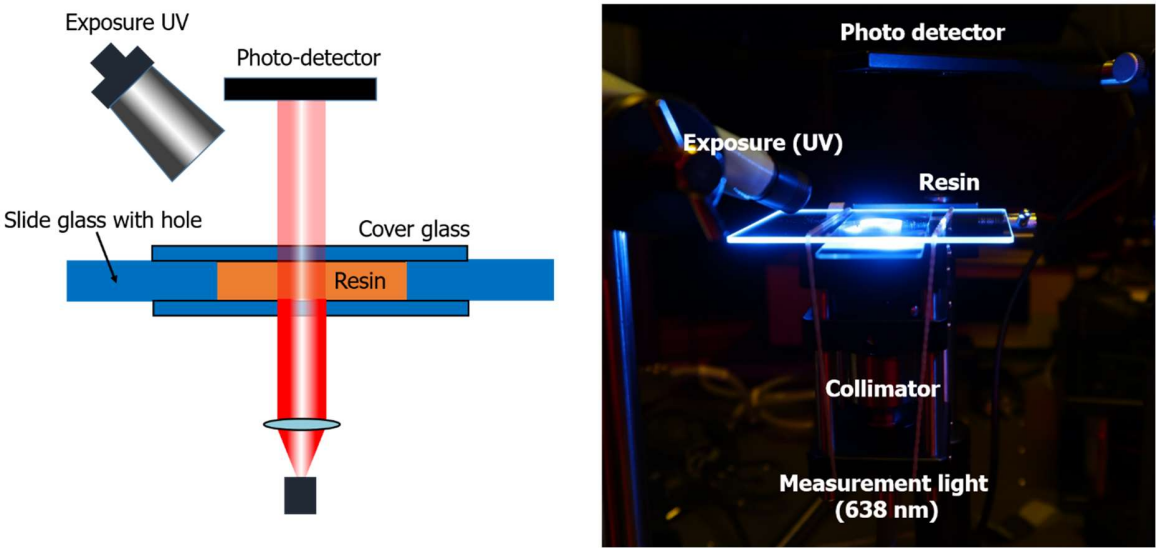

Figure A-1 Experiment setup for measurement of absorption constant of resin in the curing process

A.3 Experiment results

In order to confirm the irradiation of the measurement beam does not generate any influence of absorption constant or conversion degree. The intensity of transmitted light was first measured without the exposure of UV. The measurement results are shown in **Figure A-2**.

As we can see in **Figure A-2**, the intensity of transmitted light was almost constant in one hour, which means the measurement light itself did not change over time and did not generate any obvious influence on the absorption constant. Therefore, in the follow-up

experiment that using the exposure of UV, if the transmittance changes, the possibility of influence from measurement light can be excluded.

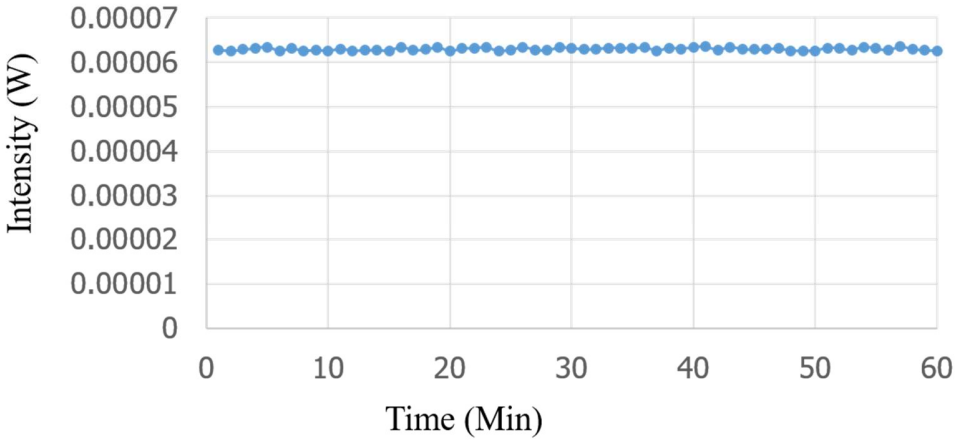

Figure A-2 Intensity of the transmitted light as a function of time in one hour

The intensity of transmitted light was also measured under the exposure of UV that excites the curing process of the resin. The measurement results are plotted in **Figure A-3**. In this case, there is a drastic decrease in intensity. This means the quick increase of absorption constant.

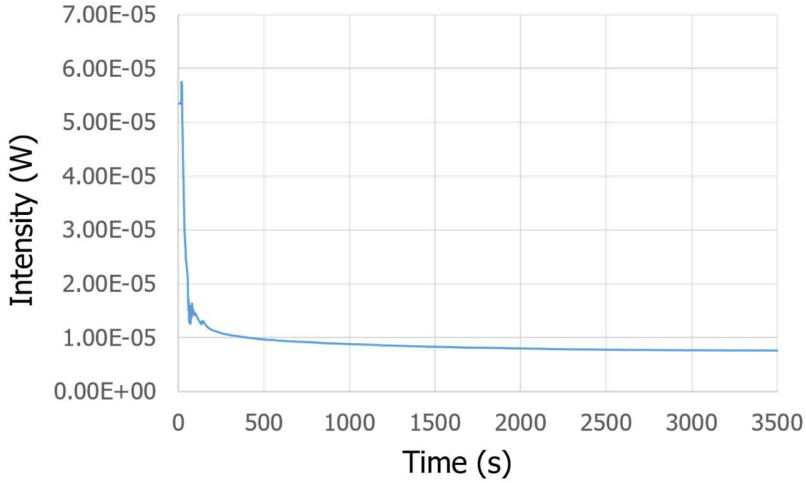

Figure A-3 Intensity of transmitted light in an increasing exposure time

Due to the apparent change of the intensity occurs at the beginning of the exposure. The first 300 seconds of the measurement was extracted and shown in **Figure A-4**.

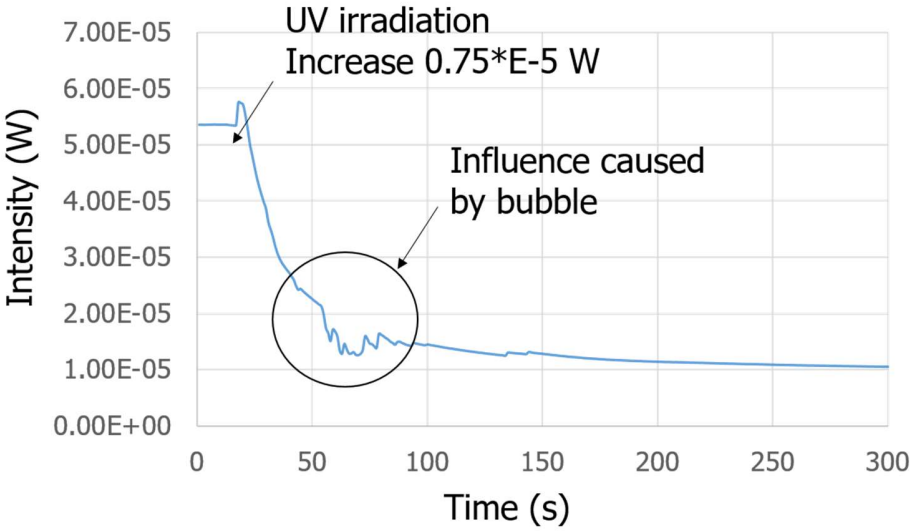

Figure A-4 Intensity of transmitted light in an increasing exposure time within 300 seconds

Figure A-4 clearly illustrates the variation of intensity in the beginning 300 seconds of the measurement. At first, the UV exposure was in a closed state, and therefore, the intensity of transmitted light keep in a constant value until 15 seconds. Then the UV exposure was in an open position, we can see a slight increase in the intensity which is due to the irradiation of UV was detected by the photo-detector. In the exposure condition of UV, the resin was being cured. It is obvious that the transmittance of the cured resin decreases to almost 20% after exposure in 300 seconds. This means the absorption of the resin increased in the curing process.

The absorption constant (α) can be calculated by

$$A = -\mathrm{Log}_{10}(I_t / I_0) / t \qquad \text{(A-1)}$$

where I_t is the intensity of transmitted light, I_0 the intensity of the light on the surface of the resin, and t the thickness of the resin. I_0 was measured in a value of 6.15×10^{-4} W when there was no resin filled between the cover glass. Therefore, the absorption constant of the uncured and cured resin (exposed in 3500 second) was calculated in a value of 0.943 mm^{-1} and 0.5284 mm^{-1} respectively. According to the absorption constant, we can calculate the intensity decrease of resin in any thickness. Based on the fact that the thickness of the cured resin fabricated by MSL is normally in a range of 10 μm to 100 μm. In these two thicknesses, when the resin becomes the cured resin, the transmittance (I_t/ I_0) changes 0.94% and 8.6% respectively. It is apparent that the variation of absorption of the resin in the curing process generates a certain influence of on exposure intensity. However, when the thickness of the resin reach or is smaller than 10 μm, the influence becomes negligible, especially in EWNSL where the thickness of each layer is on a submicron scale. In addition, regarding using the variation of absorption of the resin to make an in-process measurement, compared with the significant change of optical response in proposed critical-angle reflection or SPR measurement method, the measurement based on the variation of absorption is not an idea measurement way.

APPENDIX B: DISCRETIZATION OF PED-ODE FOR SIMULATION OF CURING PROCESS

In order to solve the PDE-ODE equation, initially, I tried to use FEM method since it is one of widely used method to solve the PDE. However, during the calculation, I found that FEM cannot solve the equation set including PDE with non-linear ODE. As a result, I made discretization on the PDE-ODE and calculated the curing process cell-by-cell and step-by-step. The discretization method was inspired so-called central in-space difference and forward-in-time Euler's method. The boundary condition is shown in Figure 94 and the procedure of discretization is shown in the following context.

1D model

$$\rho_R \frac{\partial}{\partial t} T(z,t) = \frac{\partial}{\partial z}(k_R \frac{\partial}{\partial z} T(z,t)) + \nu_R \rho_R \Delta H_R \frac{\partial}{\partial t} \alpha(z,t)$$

$$\frac{\partial}{\partial t} \alpha(z,t) = \phi S I_0 Exp(-\beta z) Exp(-E / R_{Gas}) \alpha^m(t,z)(1-\alpha(t,z))^n$$

Simplify equation, for confirming the possibility of solving.

$$\frac{\partial}{\partial t} T(t,z) = \frac{\partial^2}{\partial z^2} T(t,z) - \frac{\partial}{\partial t} \alpha(t,z)$$

$$\frac{\partial}{\partial t} \alpha(t,z) = e^{-2z} \cdot \alpha^{\frac{3}{2}}(t,z) \cdot \frac{1}{T(t,z)}$$

Coupled PDE and nonlinear ODE equation.
FEM: cannot solve the nonlinear ODE.

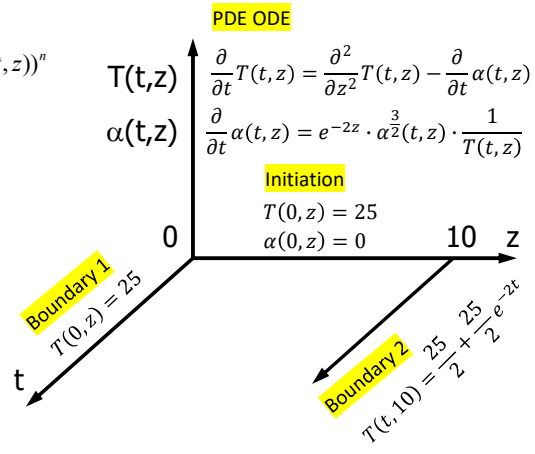

This equation is being solved by central in-space finite difference and forward-in-time Euler's method.

Figure B-1 boundary conditions

PDE ODE

$$\frac{\partial}{\partial t}T(t,z) = \frac{\partial^2}{\partial z^2}T(t,z) - \frac{\partial}{\partial t}\alpha(t,z)$$

$$\frac{\partial}{\partial t}\alpha(t,z) = e^{-2z} \cdot \alpha^{\frac{3}{2}}(t,z) \cdot \frac{1}{T(t,z)}$$

Boundary

$$\frac{\partial}{\partial t}T(t,0) = 25 - T(t,0)$$

->

$$T(0,z) = 25$$

$$\frac{\partial}{\partial t}T(t,10) = 25 - 2 * T(t,10)$$

->

$$T(t,10) = \frac{25}{2} + \frac{25}{2}e^{-2t}$$

Initiation

$$T(0,z) = 25$$

$$\alpha(0,z) = 0$$

Boundary z=0

$$\frac{\partial}{\partial t}T(t,0) = 25 - T(t,0)$$

PDE->ODE

$$\frac{d}{dt}T(t) = 25 - T(t)$$

$$T(t) = Ce^{-t} + 25$$

Add initiation,

$$T(0,z) = 25$$

For all the z ,

$$T(0,0) = 25$$

Therefore

$$T(t,0) = 25$$

Boundary z = 10,

$$\frac{\partial}{\partial t}T(t,10) = 25 - 2 * T(t,10)$$

Add initiation,

$$T(0,z) = 25$$

For all the z ,

$$T(0,10) = 25$$

Therefore

$$T(t,10) = \frac{25}{2} + \frac{25}{2}e^{-2t}$$

PDE discretization

$$\frac{\partial}{\partial t}T(t,z) = \frac{\partial^2}{\partial z^2}T(t,z) - \frac{\partial}{\partial t}\alpha(t,z)$$

$$\frac{\partial}{\partial t}T(t,z) = \frac{1}{\Delta t}\big(T(t+\Delta t,z) - T(t,z)\big)$$

$$\frac{\partial^2}{\partial z^2}T(t,z) = \frac{1}{(\Delta z)^2}\big(T(t,z+\Delta z) - 2\cdot T(t,z) + T(t,z-\Delta z)\big)$$

$$\frac{\partial}{\partial t}\alpha(t,z) = \frac{1}{\Delta t}\big(\alpha(t+\Delta t,z) - \alpha(t,z)\big)$$

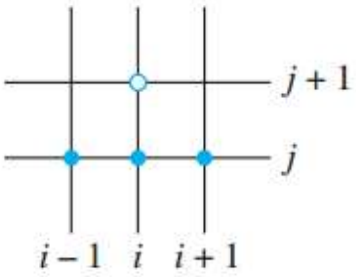

Figure B-2 Cells in discretization

Coordinate point division, x->z, y->t。

therefore,

$$z = \Delta z \cdot i, i = 1..M$$

$$\Delta z = \frac{10}{M}$$

$$t = \Delta t \cdot j, j = 1..N$$

$$\Delta t = \frac{10}{N}$$

PDE1：

$$\frac{1}{\Delta t}\big(T(i,j+1) - T(i,j)\big) = \frac{1}{(\Delta z)^2}\big(T(i+1,j) - 2\cdot T(i,j) + T(i-1,j)\big) - \frac{1}{\Delta t}\big(\alpha(i,j+1) - \alpha(i,j)\big)$$

PDE2：

$$\frac{\partial}{\partial \mathrm{t}}\alpha(\mathrm{t},\mathrm{z}) = \mathrm{e}^{-2\mathrm{z}} \cdot \alpha^{\frac{3}{2}}(\mathrm{t},\mathrm{z}) \cdot \frac{1}{\mathrm{T}(\mathrm{t},\mathrm{z})}$$

$$\frac{1}{\Delta t}\big(\alpha(i,j+1) - \alpha(i,j)\big) = e^{-2\Delta z \cdot i} \cdot \alpha^{\frac{3}{2}}(i,j) \cdot \frac{1}{T(i,j)}$$

If j=0,

$$\alpha(i,0) = 0$$

then,

$$\alpha(i,1) = 0$$

$$\alpha(i,j) == 0$$

Avoiding trivial solution

$$\alpha(t = 0, z) = 0.0001$$

REFERENCES

[1] Jacobs, P. F., Stereolithography and other RP&M technologies: from rapid prototyping to rapid tooling. Society of Manufacturing Engineers, (1995).

[2] Powers, D. B., Edgin, W. A., & Tabatchnick, L. Stereolithography: a historical review and indications for use in the management of trauma. The Journal of cranio-maxillofacial trauma, 4(3), (1998), 16-23.

[3] Wong, K. V., & Hernandez, A. A review of additive manufacturing. ISRN Mechanical Engineering, (2012).

[4] Stansbury, J. W. Curing dental resins and composites by photopolymerization. Journal of esthetic and restorative dentistry, 12(6), (2000), 300-308.

[5] Kumagai, T., Fusejima, F., Takada, M., Kobayashi, A., & Yamaguchi, K.. U.S. Patent Application No. 10/365,440, (2004).

[6] Fuchs, Y., Soppera, O., & Haupt, K.. Photopolymerization and photostructuring of molecularly imprinted polymers for sensor applications—A review. Analytica chimica acta, 717, 7-20, (2012).

[7] Vaezi, M., Seitz, H., & Yang, S.. A review on 3D micro-additive manufacturing technologies. The International Journal of Advanced Manufacturing Technology, 67(5-8), (2013), 1721-1754.

[8] Bertsch, A., Jiguet, S., Bernhard, P., & Renaud, P.. Microstereolithography: a review. MRS Online Proceedings Library Archive, 758, (2002)..

[9] JW. Lee, PX. Lan, B. Kim, G. Lim, DW. Cho, Fabrication and characteristic analysis of a poly(propylene fumarate) scaffold using micro-stereolithography technology, J. Biomed Mater Res. B Appl. Biomater, 87(1), (2008), 1-9.

[10] KS. Lee, RH. Kim, DY. Yang, SH. Park, (2008), Advances in 3D nano/microfabrication using two-photon initiated polymerization, Prog Polym Sci, 33(6), 631-681.

[11] MN. Cooke, JP. Fisher, D. Dean, C. Rimnac, AG. Mikos, Use of stereolithography to manufacture critical-sized 3D biodegradable scaffolds for bone ingrowth, J. Biomed Mater Res. B Appl. Biomater 64(2), (2003) 65-69.

[12] KW. Lee, SF. Wang, BC. Fox, EL. Ritman, MJ. Yaszemski, LC. Lu, Poly(propylene fumarate) bone tissue engineering scaffold fabrication using stereolithography:effects of resin formulations and laser parameters, Biomacromolecules 8(4), (2007), 1077-1084.

[13] Griffith, M. L., & Halloran, J. W.. Freeform fabrication of ceramics via stereolithography. Journal of the American Ceramic Society, 79(10), (1996), 2601-2608.

[14] V. K. Popov, A. V. Evseev, A. L. Ivanov, V. V Roginski, A. I. Volozhin, S. M. Howdle, Laser stereolithography and supercritical fluid processing for custom-designed implant fabrication, J. of Materials Science, Materials in Medicine 15(2), (2004), 123-128.

[15] T. M. Hsieh, C. W. B. Ng, K. Narayanan, A. C. Wan, J. Y. Ying, Three-dimensional microstructured tissue scaffolds fabricated by two-photon laser scanning photolithography, Biomaterials, 31(30), (2010), 7648-7652.

[16] C. Sun, N. Fang, D. M. Wu, X. Zhang, Projection micro-stereolithography using digital micro-mirror dynamic mask. Sensors and Actuators A: Physical, 121(1), (2005), 113-120.

[17] JW. Choi, R. Wicker, SH. Lee, KH. Choi, CS. Ha, I. Chung, Fabrication of 3D biocompatible/biodegradable micro-scaffolds using dynamic mask projection microstereolithography, J. Mater Process Tech. 209(15), (2009) 5494-5503.

[18] C. Zhou, Y. Chen, Z. Yang, B. Khoshnevis,. Digital material fabrication using mask-image-projection-based stereolithography. Rapid Prototyping Journal, 19(3), (2013), 153-165.

[19] C. Ecoffet, A. Espanet, D. J. Lougnot, Photopolymerization by evanescent waves: a new method to obtain nanoparts. Advanced Materials, 10(5), (1998), 411-414.

[20] S.Takahashi, Y. Kajihara, K. Takamasu, Submicrometer thickness layer fabrication for layer-by-layer microstereolithography using evanescent light. CIRP Annals-Manufacturing Technology, 61(1), (2012), 219-222.

[21] Y. Suzuki, H.Tahara, M. Michihata, K. Takamasu, S. Takahashi, Evanescent Light Exposing System under Nitrogen Purge for Nano-Stereolithography, Procedia CIRP 42 (2016), 77-80.

[22] Ikuta, K., & Hirowatari, K.. Real three dimensional micro fabrication using stereo lithography and metal molding. In Micro Electro Mechanical Systems, MEMS'93, Proceedings An Investigation of Micro Structures, Sensors, Actuators, Machines and Systems. (1993, February).

[23] Takagi T, Nakajima N Photoforming applied to fine machining. In: Proceedings of 4th International Symposium on Micro Machine and Human Science (MHS‘93). (1993), 173–178.

[24] Cumpston, B. H., Ananthavel, S. P., Barlow, S., Dyer, D. L., Ehrlich, J. E., Erskine, L. L., & Qin, J.. Two-photon polymerization initiators for three-dimensional optical data storage and microfabrication. Nature, 398(6722), (1999), 51.

[25] Ostendorf, A., & Chichkov, B. N.. Two-photon polymerization: a new approach to micromachining. Photonics spectra, 40(10), (2006), 72.

[26] Maruo S, Kawata S (1998) Two-photon-absorbed near-infraredphotopolymerization for three-dimensional microfabrication.IEEE ASME J Microelectromech Syst 7:411–415

[27] Kawata, S., Sun, H. B., Tanaka, T., & Takada, K. Finer features for functional microdevices. Nature, 412(6848), (2001), 697.

[28] Anthony S. Kewitsch and Amnon Yariv, "Self-focusing and self-trapping of optical beams upon photopolymerization," Opt. Lett. 21, (1996), 24-26

[29] Kagami, M., Yamashita, T., & Ito, H.. Light-induced self-written three-dimensional optical waveguide. Applied Physics Letters, 79(8), (2001), 1079-1081.

[30] Jacobsen, A. J., Barvosa‐Carter, W., & Nutt, S.. Micro‐scale truss structures formed from self-propagating photopolymer waveguides. Advanced Materials, 19(22), (2007), 3892-3896.

[31] Jacobsen, A. J., Kolodziejska, J. A., Doty, R., Fink, K. D., Zhou, C., Roper, C. S., & Carter, W. B.. In Twenty first annual international solid freeform fabrication symposium-an additive manufacturing conference (2010, August).

[32] Hatashi T. Direct 3D forming using TFT LCD mask. In: Proceedings of the 8th International Conference on Rapid Prototyping, Tokyo, Japan. pp. 172–177, (2000)

[33] Huang YM, Jeng JY, Jiang, CP, Wang JC Computer supported force analysis and layer imagine for masked rapid prototyping system. In: Proceedings of the 6th International Conference on Computer Supported Cooperative Work in Design, Ontario, Canada. pp. 562–567, (2001).

[34] Hadipoespito G, Yang Y, Choi H, Ning G, Li X, Digital micromirror device based microstereolithography for micro structures of transparent photopolymer and nanocomposites. In: Proceedings of the 14th Solid Freeform Fabrication Symposium, Austin, TX. pp. 13–24, (2003).

[35] Melchels, F. P., Feijen, J., & Grijpma, D. W.. A review on stereolithography and its applications in biomedical engineering. Biomaterials, 31(24), (2010), 6121-6130.

[36] Zhou, C., Chen, Y., Yang, Z. G., & Khoshnevis, B.. Development of multi-material mask-image-projection-based stereolithography for the fabrication of digital materials. In Annual solid freeform fabrication symposium, Austin, TX (2011).

[37] Wu, X., Lian, Q., Li, D., & Jin, Z. Tilting separation analysis of bottom-up mask projection stereolithography based on cohesive zone model. Journal of Materials Processing Technology, 243, (2017), 184-196.

[38] Maruo, S., & Ikuta, K.. New microstereolithography (Super-IH process) to create 3D freely movable micromechanism without sacrificial layer technique. In Micromechatronics and Human Science, 1998. MHS'98. Proceedings of the 1998 International Symposium on (pp. 115-120). IEEE (1998, November).

[39] Bertsch, A., Jiguet, S., Renaud, P., "Microfabrication of ceramic components by micro-stereolithography," J. Micromech Microeng. 14, (2004), 197–203.

[40] Tan, B, Sivakumar, N. and Venkatakrishnan, K., "Direct grating writing using femtosecond laser interference fringes formed at the focal point," J. Opt. A: Pure Appl. Opt. 7, (2005), 169–174.

[41] Kondo, T., Matsuo, S., Juodkazis, S., Mizeikis, V., "Multiphoton fabrication of periodic structures by multi beam interference of femtosecond pulses," Appl Phys. Lett. 82, (2003), 2758–2760.

[42] Lasagni, A., Holzapfel, C., Mücklich, F., "Periodic pattern formation of intermetallic phases with long range order by Laser Interference Metallurgy," Adv. Eng. Mater. 7, 6, (2005), 487-492.

[43] Müller-Meskamp, L., Kim, Y.H., Roch, T., Hofmann, S., Scholz, R. Eckhardt, S., Leo, K., Lasagni, A. F., "Efficiency enhancement of organic solar cells by fabricating periodic surface textures using direct laser interference patterning," Adv. Mater. 24, (2012), 906 – 910.

[44] Suzuki, Y., Suzuki, K., Michihata, M., Takamasu, K., & Takahashi, S.. One-shot stereolithography for biomimetic micro hemisphere covered with relief structure. Precision Engineering, 54, (2018), 353-360.

[45] Hafkamp, T., van Baars, G., de Jager, B., & Etman, P.. A feasibility study on process monitoring and control in vat photopolymerization of ceramics. Mechatronics, (2018).

[46] Scherzer, T., & Decker, U.. Real-time FTIR–ATR spectroscopy to study the kinetics of ultrafast photopolymerization reactions induced by monochromatic UV light. Vibrational Spectroscopy, 19(2), (1999), 385-398.

[47] Osaka, K., Kasai, A., Kosaka, T., & Sawada, Y.. Cure monitoring of UV Polymers by Raman spectroscopy. In Proceedings of the 16th International Conference on Composite Materials, Kyoto, (2007).

[48] Hoyle C.E. Calorimetric Analysis of Photopolymerization. In: Pappas S.P. (eds) Radiation Curing. Topics in Applied Chemistry. Springer, Boston, MA, (1992).

[49] Höhne, G. W. H., Breuer, K. H., & Eysel, W.. Differential scanning calorimetry: comparison of power compensated and heat flux instruments. Thermochimica Acta, 69(1-2), (1983), 145-151.

[50] Falk, B. (2004). Optical Pyrometry: A New Method for Monitoring Photopolymerizations Benjamin Falk, Santiago M Vallinas, Michael R. Zonca, Jr. and James V. Crivello New York State Center for Polymer Synthesis, Department of Chemistry Rensselaer Polytechnic Institute.

[51] Zahouily, K., Decker, C., Kaisersberger, E., & Gruener, M.. Real-time UV cure monitoring. European coatings journal, (11), (2003), 14-34.

[52] Lee, S. S., Luciani, A., & Månson, J. A. E.. A rheological characterisation technique for fast UV-curable systems. Progress in organic coatings, 38(3-4), (2000), 193-197.

[53] Hunston, D.. Assessment of the State-of-the-art for Process Monitoring Sensors for Polymer Composites. DIANE Publishing, (1992).

[54] Fomitchov, P. A., Kim, Y. K., Kromine, A. K., & Krishnaswamy, S.. Laser ultrasonic array system for real-time cure monitoring of polymer-matrix composites. Journal of composite materials, 36(15), (2002), 1889-1901.

[55] De Boer, J., Visser, R. J., & Melis, G. P.. Time-resolved determination of volume shrinkage and refractive index change of thin polymer films during

photopolymerization. Polymer, 33(6), (1992), 1123-1126.

[56] I. Kostylev, D. Labrie, and R. B. T. Price, "Time-resolved 2D shrinkage field of dental resins using laser interferometry," Appl. Opt. 54, (2015), 1852-1860.

[57] HOWARD, Benjamin. Acta biomaterialia, 2010, 6.6: 2053-2059.

[58] COLTHUP, Norman. Introduction to infrared and Raman spectroscopy. Elsevier, 2012.

[59] Li, J. F., Huang, Y. F., Ding, Y., Yang, Z. L., Li, S. B., Zhou, X. S., ... & Wang, Z. L.. Shell-isolated nanoparticle-enhanced Raman spectroscopy. nature, 464(7287), (2010), 392.

[60] Kneipp, K., Kneipp, H., Itzkan, I., Dasari, R. R., & Feld, M. S.. Ultrasensitive chemical analysis by Raman spectroscopy. Chemical reviews, 99(10), (1999), 2957-2976.

[61] Chittur, K. K.. FTIR/ATR for protein adsorption to biomaterial surfaces. Biomaterials, 19(4-5), (1998), 357-369.

[62] Mansur, H. S., Sadahira, C. M., Souza, A. N., & Mansur, A. A.. FTIR spectroscopy characterization of poly (vinyl alcohol) hydrogel with different hydrolysis degree and chemically crosslinked with glutaraldehyde. Materials Science and Engineering: C, 28(4), (2008), 539-548.

[63] González, M. G., Cabanelas, J. C., & Baselga, J.. Applications of FTIR on epoxy resins-identification, monitoring the curing process, phase separation and water uptake. In Infrared Spectroscopy-Materials Science, Engineering and Technology. InTech (2012).

[64] Trovati, G., Sanches, E. A., Neto, S. C., Mascarenhas, Y. P., & Chierice, G. O.. Characterization of polyurethane resins by FTIR, TGA, and XRD. Journal of Applied Polymer Science, 115(1), (2010), 263-268.

[65] Stansbury, J. W.. Curing dental resins and composites by photopolymerization. Journal of esthetic and restorative dentistry, 12(6), (2000), 300-308.

[66] Cho, J. D., & Hong, J. W.. Photo-curing kinetics for the UV-initiated cationic polymerization of a cycloaliphatic diepoxide system photosensitized by thioxanthone. European Polymer Journal, 41(2), (2005), 367-374.

[67] Wang, J. S., & Matyjaszewski, K.. Controlled/" living" radical polymerization. Atom transfer radical polymerization in the presence of transition-metal complexes. Journal of the American Chemical Society, 117(20), (1995) 5614-5615.

[68] Candau, F., Leong, Y. S., & Fitch, R. M.. Kinetic study of the polymerization of acrylamide in inverse microemulsion. Journal of Polymer Science: Polymer Chemistry Edition, 23(1), (1985)1, 93-214.

[69] Andrzejewska, E.. Photopolymerization kinetics of multifunctional monomers. Progress in polymer science, 26(4), (2001), 605-665.

[70] Hafkamp, T., van Baars, G., de Jager, B., & Etman, P.. A feasibility study on process monitoring and control in vat photopolymerization of ceramics. Mechatronics, (2018).

[71] Ferracane, J. L., & Greener, E. H.. The effect of resin formulation on the degree of conversion and mechanical properties of dental restorative resins. Journal of biomedical materials research, 20(1), (1986), 121-131.

[72] Silikas, N., Eliades, G., & Watts, D. C.. Light intensity effects on resin-composite degree of conversion and shrinkage strain. Dental Materials, 16(4), (2000), 292-296.

[73] Knežević, A., Tarle, Z., Meniga, A., Šutalo, J., Pichler, G., & Ristić, M.. Degree of conversion and temperature rise during polymerization of composite resin samples with blue diodes. Journal of Oral Rehabilitation, 28(6), (2001), 586-591.

[74] Uchiyama, H., & Shiota, T. U.S. Patent No. 6,746,938. Washington, DC: U.S. Patent and Trademark Office, (2004).

[75] Hanabata, M., & Yasuda, T. U.S. Patent No. 6,534,235. Washington, DC: U.S. Patent and Trademark Office, (2003).

[76] Odian, G. Principles of polymerization. John Wiley & Sons, (2004).

[77] Tang, Y.. Stereolithography cure process modeling(Doctoral dissertation, Georgia Institute of Technology), (2005)

[78] Goodner, M. D., & Bowman, C. N.. Development of a comprehensive free radical photopolymerization model incorporating heat and mass transfer effects in thick films. Chemical Engineering Science, 57(5), (2002), 887-900.

[79] Yebi, A., & Ayalew, B.. Optimal layering time control for stepped-concurrent radiative curing process. Journal of Manufacturing Science and Engineering, 137(1), (2015), 11020.

[80] Yebi, A., & Ayalew, B. PDE-based Process Control for UV Curing of Thick Film Resins.

[81] Ligon, S. C., Husar, B., Wutzel, H., Holman, R., & Liska, R.. Strategies to reduce oxygen inhibition in photoinduced polymerization. Chemical reviews, 114(1), (2013), 557-589.

[82] Ligon, S. C., Husar, B., Wutzel, H., Holman, R., & Liska, R.. Strategies to reduce oxygen inhibition in photoinduced polymerization. Chemical reviews, 114(1), (2013), 557-589.

[83] Suzuki, Y., Tahara, H., Michihata, M., Takamasu, K., & Takahashi, S.. Evanescent light exposing system under nitrogen purge for nano-stereolithography. Procedia CIRP, 42, (2016), 77-80.

[84] Tumbleston, J. R., Shirvanyants, D., Ermoshkin, N., Janusziewicz, R., Johnson, A. R., Kelly, D. & Samulski, E. T.. Continuous liquid interface production of 3D objects. Science ,a2397, (2015).

[85] FUJITA, K., NISHIYAMA, N., NEMOTO, K., OKADA, T., & IKEMI, T.. Effect of base monomer's refractive index on curing depth and polymerization conversion of photo-cured resin composites. Dental materials journal, 24(3), (2005), 403-408.

[86] Howard, B., Wilson, N. D., Newman, S. M., Pfeifer, C. S., & Stansbury, J. W.. Relationships between conversion, temperature and optical properties during composite photopolymerization. Acta biomaterialia, 6(6), (2010), 2053-2059.

[87] Goodner, M. D., & Bowman, C. N.. Modeling and experimental investigation o flight intensity and initiator effects on solvent-free photo polymerizations. In T. E. Long, & M. O. Hunt (Eds.), Solvent-free polymerizations and processes: Minimization of conventional organic solvents. 713, (1998), 220 –231.Washington, DC: American Chemical Society.

[88] Goodner, M. D., & Bowman, C. N.. Modeling primary radical termination and its effects on auto acceleration in photopolymerization kinetics. Macromolecules, 32, (1999), 6552–6559.

[89] Goodner, M. D., Lee, H. R., & Bowman, C. N.. Method for determining the kinetic parameters in difusion-controlled free-radical homopolymerizations. Industrial and Engineering Chemistry Research,36, (1997) 1247–1252.

[90] Gao, J., & Penlidis, A.. A comprehensive simulator/database package for reviewing free-radical homopolymerizations. Journal of Macromolecular Science, Part C: Polymer Reviews, 36(2), (1996), 199-404.

[91] Haynes, W. M. (2014). CRC handbook of chemistry and physics. CRC press.

[92] Riedel, T., Majek, P., Rodriguez-Emmenegger, C., & Brynda, E.. Surface plasmon resonance: advances of label-free approaches in the analysis of biological samples. Bioanalysis, 6(24), (2014), 3325-3336.

[93] Liang, D., & Cao, Z.. Study on the measurement ways of SPR Sensor. In Optical Technology and Image Processing for Fluids and Solids Diagnostics 2002 (5058), (2003), 563-569. International Society for Optics and Photonics.

[94] Iwasaki, Y., Horiuchi, T., & Niwa, O.. Detection of electrochemical enzymatic reactions by surface plasmon resonance measurement. Analytical chemistry, 73(7), (2001) 1595-1598.

[95] Budd, K., Dey, S. K., & Payne, D. A.. SOL-GEL PROCESSING OF PbTiO//3, PbZrO//3, PZT, AND PLZT THIN FILMS. In British Ceramic Proceedings. Inst of Ceramics, (1985).

[96] Haertling, G. H.. PLZT electrooptic materials and applications—a review. Ferroelectrics, 75(1), (1987), 25-55.

ACHIEVEMENTS

1. Journal

[1-1] Satoru Takahashi, Deqing Kong, Masaki Michihata and Kiyoshi Takamasu, “In-process measurement for cure depth control of nano stereolithography using evanescent light”, CIRP AnnalsManufacturing Technology (Submitted).

[1-2] Deqing Kong, Masaki Michihata. Kiyoshi Takamasu and Satoru Takahashi, "In-process measurement of gradient boundary of resin in evanescent-wave-based nano-stereolithography using reflection interference near critical angle", Journal of Photopolymer Science and Technology, 31(3), 441-446, 2018.

[1-3] Deqing Kong, Masaki Michihata. Kiyoshi Takamasu and Satoru Takahashi, "In-Process Measurement of Thickness of Cured Resin in Evanescent-Wave-Based Nano-stereolithography Using Critical Angle Reflection", Nanomanufacturing and Metrology, 1(2), 112-124, 2018.

[1-4] Masaki Michihata, Deqing Kong, Kiyoshi Takamasu and Satoru Takahashi, “A simulation study of plasmonic substrate for in-process measurement of refractive index in nano-stereolithography”, International Journal of Automation Technology, 11(5), 772-780, 2017

2. International conference

[2-1] ○Deqing Kong, Masaki Michihata, Kiyoshi Takamasu, Satoru Takahashi, “In-process measurement of resin’s curing degree in micro -stereolithography using internal reflection at critical angle”, IMEKO 2018, Belfast, UK, 2018/9.

[2-2] ○Deqing Kong, Masaki Michihata, Kiyoshi Takamasu, Satoru Takahashi, “In-process measurement of gradient boundary of resin in evanescent-wave-based nano-stereolithography using reflection interference near critical angle”, SPST-35, Tokyo, Japan, 2018/6.

[2-3] ○ Deqing Kong, Masaki Michihata, Kiyoshi Takamasu, Satoru Takahashi, “Monitor resin’s curing degree for in-process measurement in micro-stereolithography”, ASPEN 2017, Seoul, Korea, 2017/11.

[2-4] ○Deqing Kong, Masaki Michihata, Kiyoshi Takamasu and Satoru Takahashi, “In-process measurement on the thickness of photosensitive resin in evanescent wave-based

nano-stereolithography”, The 13th ISMTII, Xi'an, China, 0017 , 2017/8. [Best Paper Award]

[2-5] ○Deqing Kong, Masaki Michihata, Kiyoshi Takamasu, Satoru Takahashi, “A tunable surface-plasmon- resonance substrate for in-process measurement of micro-stereolithography”, ISOT, Tokyo, Japan, B6-5-1, 2016/9. [Best Student Award]

3. Domestic conference

[3-1] ○ 道畑正岐，孔 徳卿，高増 潔，高橋 哲，臨界角照明を用いたナノ光造形硬化樹脂のインプロセス計測 −基本原理の検証−”，日本機械学会 2018 年度年次大会講演論文集，関西大学（2018）

[3-2] ○Deqing Kong, Masaki Michihata, Kiyoshi Takamasu, Satoru Takahashi, “In-process measurement of the resin's conversion degree in micro-stereolithography using near-critical-angle reflection”, 2018 年度精密工学会春季大会, K16, 東京, 2018/3.

[3-3] ○Deqing Kong, Masaki Michihata, Kiyoshi Takamasu, Satoru Takahashi, “In-process measurement of evanescent wave based nano- stereolithography using critical angle shift”, 2017 年度精密工学会春季大会, D39, 東京, 2017/3.

[3-4] ○ Deqing Kong, Masaki Michihata, Kiyoshi Takamasu, Satoru Takahashi, “Optimization on a PLZT based multi-layer surface plasmon resonance substrate used in in-process measurement of nano-stereolithography”, 日本光学会学術講演会, 東京, 2016/10.

[3-5] ○ Deqing Kong, Masaki Michihata, Kiyoshi Takamasu, Satoru Takahashi, “表面プラズモン共鳴を用いたマイクロ光造形のインプロセス計測”, 日本機械学会 第 11 回生産加工・工作機械部門講演会, D05, 名古屋, 2016/9.

4. Award

[4-1] 三豊科学技術振興協会, 海外渡航助成金受給, 2018/09

[4-2] The 13th International Symposium on Measurement Technology and Intelligent Instruments (ISMTII), Best Paper Award, 2017/09

[4-3] 村田学術振興財団, 海外渡航助成金受給, 2017/06

[4-4] International Symposium of Optmechatronic Technology (ISOT) 2016, Best Student Award, 2016/9